UNIVERSITÀ POLITECNICA DELLE MARCHE

FACOLTÀ DI INGEGNERIA

Corso di Laurea Magistrale in Ingegneria Meccanica Progettuale Costruttivo

MECHANICAL CHARACTERIZATION OF FIELD JOINT INFILL MATERIAL OF AN OFFSHORE PIPELINE BY MEANS OF A FEM SIMULATION OF A FULL SCALE IMPACT TEST

CARATTERIZZAZIONE MECCANICA DEL RIVESTIMENTO ESTERNO DELL'AREA DI GIUNZIONE DELLE CONDOTTE SOTTOMARINE MEDIANTE SIMULAZIONE FEM DI UN TEST DI IMPATTO SU SCALA REALE

Supervisor:
Chiar.mo Prof. Ing. Marco Rossi

Author:
Mattia Carnaroli

Co-supervisor:
Ing. Angelo Ferrulli, Saipem S.p.A.

Academic Year 2018-2019

To my mother

PREFACE

The work exhibited in this master's degree thesis was developed within Saipem Fano, in the offshore division.

Saipem is the world leader in drilling, engineering, procurement, construction and installation of pipelines and large plants in the offshore and onshore oil & gas sector, with a strong focus on activities in difficult environments, remote areas and in deep waters.

My most sincere thanks to Saipem Fano who allowed me to train twice in the offshore division and for having proposed me a job position in the Fano offshore division.

In particular, the thesis was carried out at the FAWEL (FAno WELding) office in the ECA (Engineering Critical Assessment) section which has the Eng. Enrico Torselletti as Manager. My sincerest thanks to him for his inclusion in his team, for his professionalism and competence which he passed on to me.

My corporate tutor and co-supervisor Eng. Angelo Ferrulli has provided to direct the work towards the objectives to be pursued. I want to thank him strongly for having trained me and increased my engineering skills and competences, I will never forget him.

I thank my supervisor Prof. Eng. Marco Rossi for giving me the opportunity to train in Saipem and for supporting me in developing my thesis. Thanks again for encouraging me to write my thesis in English, I will never forget it (see the opportunity and not just the negative side!).

I want to thank my parents for giving me the opportunity to study.

I dedicate this thesis to my mother who fought against the disease to be with me on this important day.

I want to thank all the people I knowing during my university career, in particular Sonia Carradorini, Luca Cerioni, Davide Durastanti, Mario Francolini, Michele Giaccaglia and Alessandro Paci.

Mattia Carnaroli,
San Costanzo, 19 December 2019.

ABSTRACT

The subsea pipelines are designed to withstand the impacts due to fishing devices, in fact, the pipeline design includes external protection systems (coating and field joint coating) to adequately withstand these dynamic loads.

In particular, the analyzed offshore pipeline has a Concrete Weight Coating (CWC) applied on external anticorrosive coating in Three-Layer Polyethylene (3LPE) and the ends of the uncoated and welded pipe joints have been applied a field joint coating system with infill material. The infill material used is Solid Polyurethane (Solid PU), mixture of polyol and isocyanate. This material is specifically designed for offshore application and is subject to full scale impact testing to characterize its mechanical behavior, in accordance with the DNV-RP-F111.

The aim of this thesis is:

1) Simulate the full scale impact test using finite element analysis;
2) Define the model of material that best represents the real infill material used.

During the finite element model development, two models of the infill material have been investigated, i.e. elastic-plastic and hyperelastic-plastic models. To define the hyperelastic-plastic behaviour of solid PU, compressive material test results have been considered, in accordance with the ASTM D695-15. The finite element analysis shows that the hyperelastic-plastic model is the most appropriate to simulate the permanent deformation generating during the impact. This model of material, which includes the strain energy potential of Marlow model, required the calibration of the plastic curve, using an elastic strain limit of 42.2% to extend the finite element analysis scenarios and then to analyze the behavior under operational load of the offshore pipelines that is not easy to test in the laboratory.

ABSTRACT

Le condotte sottomarine per il trasporto di olio o gas sono realizzate saldando giunti di tubo di lunghezza pari a circa 12.2 m e l'area risultante, chiamata field joint, necessita di essere rivestita con materiali opportunamente concepiti per applicazioni offshore.
In particolare, dopo aver preparato la superficie risultante dall'unione di due giunti di tubo, viene applicato il materiale di riempimento, detto infill material, che nel caso specifico è il poliuretano solido, ovvero una miscela di poliolo e isocianato: tale materiale viene iniettato utilizzando uno stampo che verrà rimosso solo successivamente. La caratterizzazione meccanica del poliuretano solido è molto complessa, infatti, questo materiale è progettato per assorbire l'energia d'impatto minimizzandone il trasferimento energetico alla tubazione sottostante. Tale materiale deve superare un severo test d'impatto, definito dalla normativa DNV-RP-F111, poiché durante la vita operativa le condotte sottomarine possono sperimentare carichi dinamici provocati dai dispositivi da pesca.
L'obiettivo di questa tesi è:

1) Definire il corretto modello di materiale che meglio rappresenta il poliuretano solido;
2) Riprodurre agli elementi finiti il test d'impatto su scala reale.

La calibrazione del modello agli elementi finiti avviene analizzando due modelli costitutivi del materiale di riempimento, ovvero il modello elasto-plastico e il modello iperelastico-plastico, utilizzando le curve a compressione del poliuretano solido, ottenute in accordo alla ASTM-D695-15.
Le numerose simulazioni eseguite con il modello elasto-plastico, dimostrano che il poliuretano solido non ha comportamento elastico lineare, poiché anche se incrementassimo le proprietà meccaniche del materiale nel range osservato dal test di

compressione non si ottiene la medesima profondità d'impronta rilevata dal test d'impatto su scala reale.

Successivamente si è adottato il modello iperelastico-plastico, con potenziale di energia di deformazione per unità di volume Marlow, che richiede la definizione del limite elastico di deformazione per la singola curva testata poiché, rispetto al precedente modello, si ha un comportamento elastico non lineare.

Con questo modello si è osservato che, variando il limite elastico di deformazione o fissando il limite elastico di deformazione e variando le proprietà meccaniche nel range osservato dal test di compressione, si ottiene la stessa profondità d'impronta rilevata dal test d'impatto su scala reale, pertanto il modello iperelastico-plastico è rappresentativo del poliuretano solido.

Una volta validato il modello agli elementi finiti vengono eseguite delle analisi energetiche che evidenziano come il poliuretano solido sia un'ottima barriera per la protezione della tubazione sottostante, poiché solo una modesta percentuale del carico è trasferita ad essa.

In conclusione, il modello agli elementi finiti riproduce fedelmente il test d'impatto su scala reale e, tale modello, può essere adottato per estendere gli scenari di analisi sulle condotte sottomarine sotto carico operativo, poiché il test in laboratorio non è di facile esecuzione.

INDEX

INDEX OF FIGURES

INDEX OF TABLES

ABBREVIATIONS

ERW	Electric Resistance Welding
DC	Direct Current
TIG	Tungsten Inert Gas
AC	Alternating Current
SAW	Submerged Arc Welding
SMAW	Shielded Metal Arc Welding
GMAW	Gas Metal Arc Welding
MIG	Metal Inert Gas
MAG	Metal Active Gas
GTAW	Gas Tungsten Arc Welding
CRAs	Corrosion-Resistant Alloys
CP	Cathodic Protection
FBE	Fusion Bonded Epoxy
3LPE	Three-Layer Polyethylene
3LPP	Three-Layer Polypropylene
LAT	Low Application Temperature
PE	Polyethylene
LDPE	Low Density Polyethylene
MDPE	Medium Density Polyethylene
HDPE	High Density Polyethylene
PP	Polypropylene
CWC	Concrete Weight Coating
FJC	Field Joint Coating

HSS	Heat-Shrink Sleeve
PU	Polyurethane
HDPF	High Density Polyurethane Foam
ID	Inner Diameter
SAWL	Longitudinally Submerged Arc Welded
WT	Wall Thickness
FEA	Finite Element Analysis
OD	Outer Diameter
SMYS	Specified Minimum Yield Strength
SMTS	Specific Minimum Tensile Strength
FEM	Finite Element Model
FE	Finite Element
C3D8R	Continuum, 3-D, 8-node, Reduced integration
U1	Translation in the x-direction
U2	Translation in the y-direction
U3	Translation in the z-direction
UR1	Rotation about the x-direction
UR2	Rotation about the y-direction
UR3	Rotation about the z-direction

INTRODUCTION

During the operating life, the subsea pipelines is subjected to dynamic loads from the fishing devices, therefore, they are adequately designed with specific external coatings. In particular, the concrete weight coating is applied over external anticorrosion coating provides anti-buoyancy and/or mechanical protection.

At the welding joints of the pipe joints a filed joint coating system is applied with infill material. This infilling material is designed for the offshore application that requires advanced mechanical behavior, i.e. to absorb and adequately release the impact energy transferring as little as possible to the pipe. For resistance checks it is subject to full scale impact test which reproduces the same load scenario, as for fishing devices.

The engineering challenge addressed in this thesis is:

1) Reproduce the full scale impact test with finite element analysis;
2) Define the correct infill material model.

The implementation of the finite element model of the full scale impact test is possible thanks to its results, therefore is adopted the Abaqus software.

For define the correct behaviour of the infill material are investigated two different constitutive models, elastic-plastic and hyperelastic-plastic respectively.

The thesis is divided into nine chapters: the first chapter exposes the offshore pipelaying technologies. The second chapter exposes the welding technologies and the preparation of the ends of the pipe joint to be weld.

The third chapter shows the main external anticorrosion coatings, the application of concrete and the main field joint coating systems. The fourth chapter shows infill material for offshore applications. The fifth chapter shows the difference between the elastic and hyperelastic material and the classification of hyperelastic constitutive

models as a function of the strain energy potential. The sixth chapter shows the types of fishing devices and the full scale impact test.

The seventh chapter shows the basic data, assumptions and all the steps necessary for the implementation of the full scale impact test using finite element analysis. The eighth chapter shows the finite element analysis results. The ninth chapter exposes the conclusion of the master's thesis work.

In particular, the finite element analysis shows that the hyperelastic-plastic constitutive model for the infill material is most appropriate to simulate the permanent deformation generating during the impact.

For more detailed results, see the conclusions.

1 OFFSHORE PIPELAYING

1.1 INTRODUCTION

The installation of pipelines and flowlines and their connection to platforms constitute some of the most challenging offshore operations. This chapter provides the reader with basic knowledge of the objectives, challenges, methods and background for offshore pipelaying. The major milestones are presented in the development of offshore pipelaying as a discipline, along with the current methods and equipment used in offshore pipeline construction [1].

1.2 MAIN PIPELAYING TECHNOLOGIES

The pipelaying technologies can be divided in two groups:

1) Onshore welded pipeline: The pipe segments are assembled onshore in strings of suitable length and then carried with different methods in place for installation.
2) Offshore welded pipeline: The pipelaying barge carries short pipe segments, which are then assembled during laying operations. This method is the only one suited for practical installation of very long pipelines [1].

1.2.1 ONSHORE WELDED PIPELINE

This group includes towing and reeling methods: both imply the welding and the control of the joints onshore, while the transportation method is different. The towing methods envisage the pipe strings being transported to the offshore location of installation by means of one or more tug boats, while being kept in a suitable configuration by a combination of pull cables, floaters and ballast weights.
In Figure 1–1 the surface-tow method is depicted. The pipe string is kept in tension between two tug boats to guarantee to be able to control its configuration against lateral bending, while the floaters control the pipe shape along the vertical plane. This way of operation forces the pipe to withstand the actions from waves, if present, and therefore cannot be used in situations where significant rough weather is expected [1].

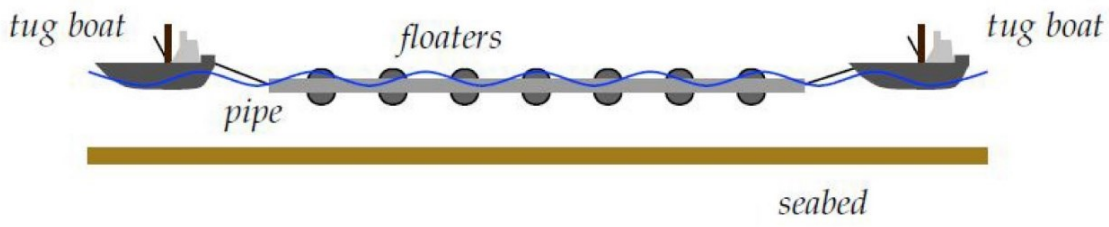

Figure 1–1 Surface tow method [1].

The mid-depth tow uses floaters or weights to make the pipe string nearly neutrally buoyant, such that the configuration can be controlled by the pull applied by the tug boats connected at the two ends, see Figure 1–2.

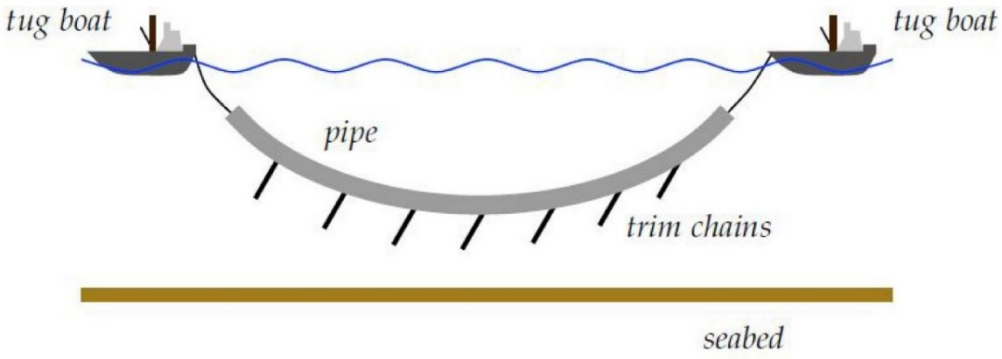

Figure 1–2 Mid-depth tow method [1].

The objective is to keep the pipe string sufficiently in depth not to be excited by the action of waves, should they be present somewhere during the route.

The bottom tow method is adopted when the pipe has sufficient specific gravity to guarantee stability on the seabed. A tow head is applied on a single end and the string is pulled while dragging the seabed, see Figure 1–3.

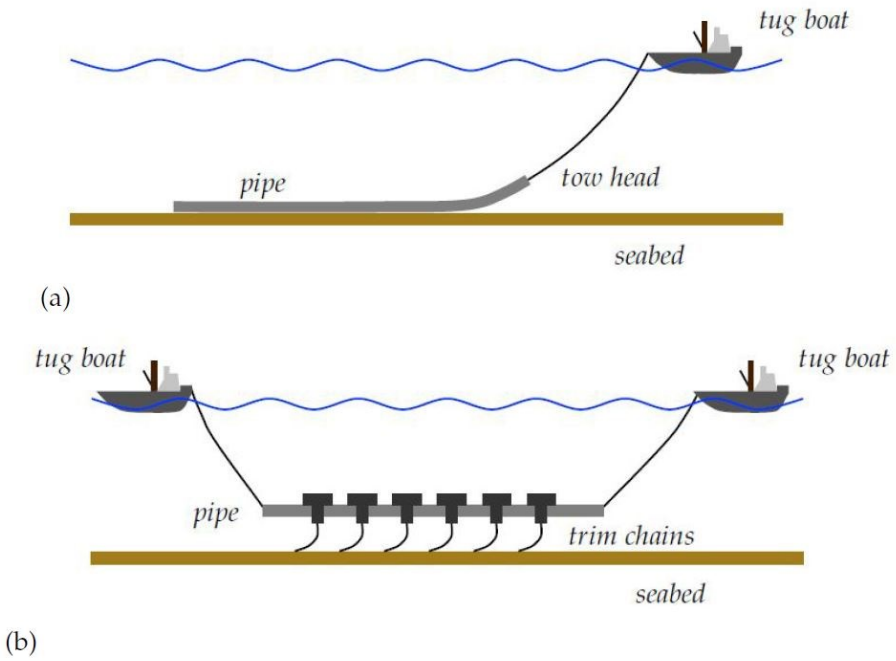

Figure 1–3 Bottom tow method [1].

The off-bottom method is slightly different, requiring two tug boats to guarantee alignment. Tow methods are only practical for short lines, often in remote areas where transit costs of conventional pipelayers could be overly expensive. The reeling technology is based on onshore bars assembling as well. The strings obtained away from the installation location are wrapped around a reel which is then mounted on the vessel deck, with horizontal or vertical rotational axis, see Figure 1–4.

The laying operations are very rapid because there is not any welding and controlling cycle, but the method is limited to small diameter pipelines: the bending radius is the parameter which determines the stress envisaged during reeling and straightening, and of course limited by the reel size to be fitted on-board [1].

Figure 1–4 Reeling technology [1].

1.2.2 OFFSHORE WELDED PIPELINE

This group of technologies is employed in most strategic trunklines, being able to lay linepipe along very long routes (currently even longer than 1000 km), with increasingly high diameters. Submarine pipelines are assembled then launched and laid on the seabed by dedicated mono-hull (keel or flat-bottom) or semisubmersible vessels [1].

On these vessels there is a firing line along which line pipe joints are brought, aligned and coupled, welded and controlled, then held and carefully released moving up the vessel for launching in the depths. The integrity of the pipeline during installation is a crucial task due to the intended operational targets, as far as the safe-life and leak-less carrying capacity of the pipeline over the design lifetime is concerned. Pipe laying technology for such strategic life-lines (20 in to 48 in diameter, 20 to 40 mm wall thickness) includes [1]:

- S-lay: The pipe is assembled along a horizontal welding or firing line, it leaves the lay vessel supported by a curved launching ramp that moves the configuration from horizontal to inclined to the depths, it crosses the water column to reach the seabed in a S shape, it is borne and kept within pipe curvature allowance limits by a lay pull applied by the tensioner placed at the end of the firing line, Figure 1–5.
- J-lay: The pipe is assembled in a vertical tower, it leaves the lay vessel vertically towards the depths, it crosses the water column and smoothly bends to reach the sea-bed due to a weak horizontal pull applied by the lay vessel, particularly by propellers, it is borne by the tensioning device placed on the tower after the welding station, usually on tracks, sometimes assisted by active clamps, Figure 1–5.

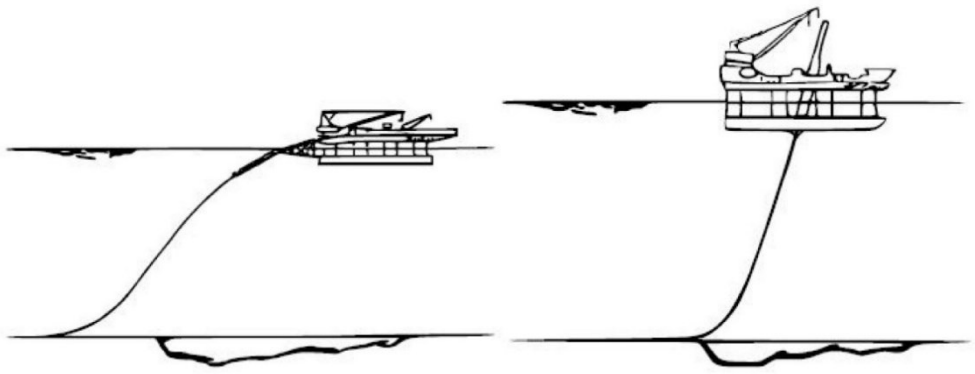

Figure 1–5 S-lay and J-lay [1].

In both pipe-lay modes, the horizontal lay pull is applied by mooring lines or/and propellers, which guarantee station keeping and regular pipe pay-out at the end of each welding cycle.

1.3 S-LAY

S-lay refers to an installation method in which the pipeline starts in a horizontal position on the vessel and acquires a characteristic S-shape on the way to the seabed, as shown in Figure 1–6.

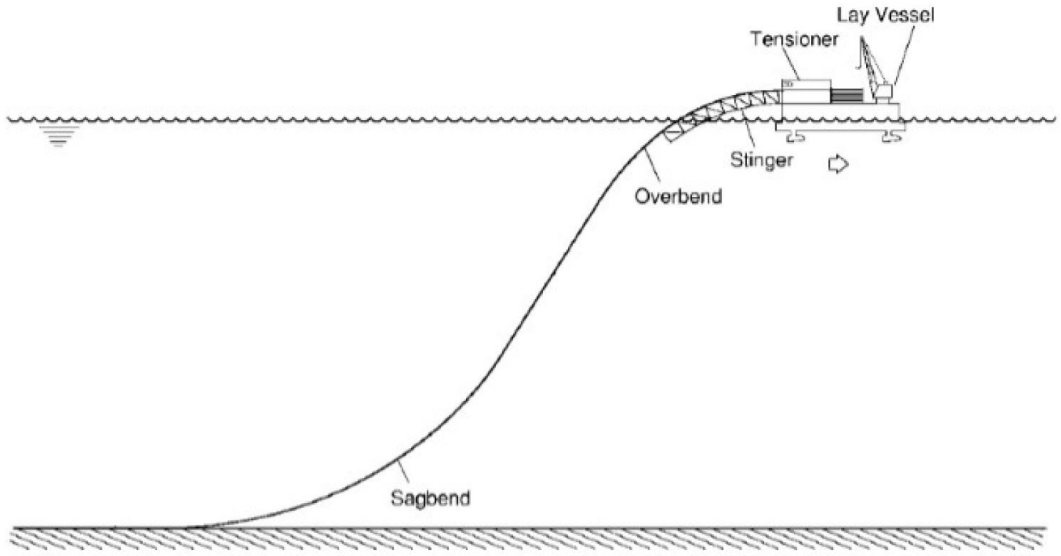

Figure 1–6 Schematic representation of S-lay pipeline installation and associated pipeline leadings [1].

The first role of the vessel is to act as a work platform to assemble the line and to store incoming pipe lengths. Usually, a linearly-arranged series of stations (firing line) weld 40 to 80 ft (12-24 m) lengths to the free end of the line. The welds are checked and coated and the vessel moves forward, paying the line into the sea [1].

The line leaves at the stern of the vessel via a sloping ramp (firing line). At the end of the ramp it comes in contact with a long boom-like curved structure known as the stinger. The stinger is an open-frame structure that supports the line on rollers, providing a controlled-shape transition from the horizontal to the inclined suspended section. Older stingers were rigid, whereas modern ones are articulated, involving several segments that are connected via hinges. The stinger shape is prescribed by setting the segments at chosen angles. Stinger lengths vary with water depth and the submerged weight of the line. The suspended length of pipeline is held by tensioners that are usually located on the ramp [1].

Most commonly these involve v-shaped Caterpillar tracks with rubber pads that press on to the surface of the pipe from the top and bottom (Figure 1–7).

Figure 1–7 Tensioning device [1].

The pipe is paid over the stinger by rotation of the tracks. In this setup, the section of pipeline on the stinger experiences bending combined with relatively high tension. Too short a stinger can result in excessive bending at the end of the stinger, which can buckle the pipeline. Such a buckle can in turn cause fracturing and flooding of the line. Flooding of the pipeline can make it too heavy to hold by the tensioners, which can result in loss of the line to the seabed. The upper curved part of the pipeline is known as overbend. The line leaves the stinger at a chosen angle called departure angle. Further down, it straightens and then gradually bends in the opposite direction, as shown in Figure 1–6. Often the maximum curvature occurs closer to the seabed in the sagbend region, which is nearly at the maximum water depth. Thus it must be ensured that the combined bending and pressure loads can be safely sustained. The curvature in the sagbend is controlled by the tension applied at the top. Sudden movement of the ship or loss of tension for whatever reason can result in excessive bending, local buckling and collapse. Local collapse, in turn, has the potential of initiating a propagating buckle. Soon after the sagbend, the line touches the seabed and conforms to its relief.

If the seabed is relatively flat, the pipeline can be considered to be under hydrostatic external pressure loading while empty. Its design is often based on avoiding collapse under this type of pressure loading.

One of the main roles of the lay-vessel is to provide the tension that holds the suspended line and controls its shape. In older lay barges, the tension is reacted by several long mooring lines connected to anchors. The mooring lines are attached to winches, and the barge moves forward by winding in the mooring lines. This is a delicate operation essential to keeping the position and direction of the lay barge in accordance with the planned route. The loss of a mooring anchor during such an operation can cause sudden yawing or drifting of the barge, which in turn can result in buckling of the pipe at the end of the stinger due to excessive bending. More modern S-lay vessels used in deeper waters use dynamic positioning to control their position.

This is achieved by thrusters (shrouded propellers that can be freely directed) that are computer-controlled using GPS [1].

Dynamic positioning significantly requires more power but it increases the efficiency of the lay operation.

The long suspended section of the pipeline behaves more like a cable rather than a beam, and thus its length as well as the sagbend curvature are mainly governed by the water depth, the submerged weight of the line and by the tension applied at the barge.

The philosophy of the installation design is first to avoid buckling failures either in the overbend or the sagbend, and second to keep the pipeline in the elastic regime.

The curvature in the sagbend is mainly controlled by tension.

However, excessive tension can be detrimental to the section over the stinger, perhaps plasticizing the pipe.

In some cases, high lay tension can also increase the cost of the operation by requiring a larger installation vessel.

In general, plastic deformation on either the stinger or the sagbend is avoided, as it can cause excessive ovalization to the pipe cross section and spiraling of the pipeline on the seabed.

Overall, the installation parameters are optimized to take all of these issues as well as material and installation costs into account. Traditionally, S-lay has been the main pipe installation method for water depths up to 3,300 ft (1,000 m).

More recently, S-lay water depth has been nearly doubled by the design and installation of longer articulated stingers on dynamically-positioned vessels with high tension capacities.

Figure 1–8 shows the Allseas vessel Solitaire, while Figure 1–9 shows his deep water stinger [1].

Figure 1–8 Allseas vessel Solitaire [1].

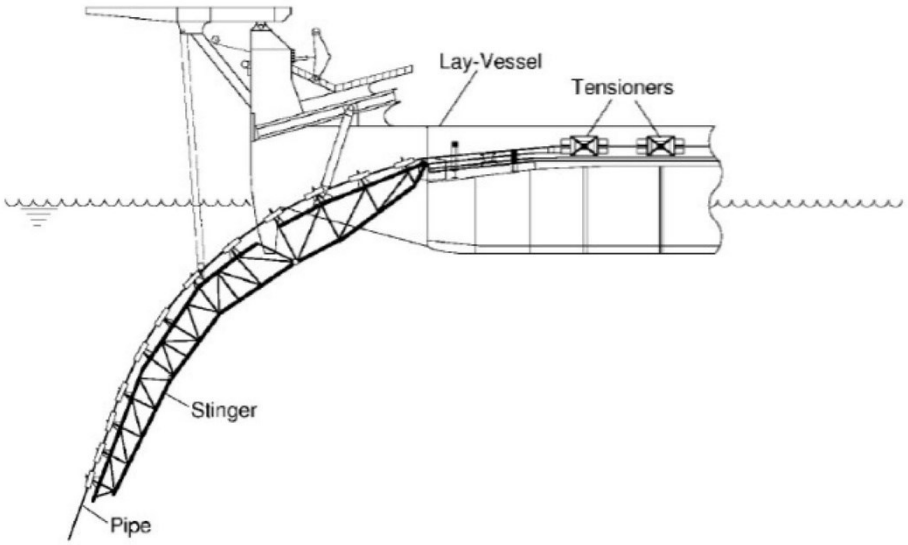

Figure 1–9 Schematic showing the Solitaire deepwater stinger [1].

1.4 J-LAY

As the water depth increases, the suspended length in conventional S-lay increases, and as a result the tension that must be applied by the lay vessel goes up. In addition, the required stinger length increases and its shape becomes more complex. These tough requirements are avoided by dropping the condition that the line starts in a horizontal position. J-lay is an alternative installation method in which the pipeline leaves the vessel from a nearly vertical position, as shown schematically in Figure 1–10 (actual tower angles vary between 0 deg and 15 deg from the vertical) [1].

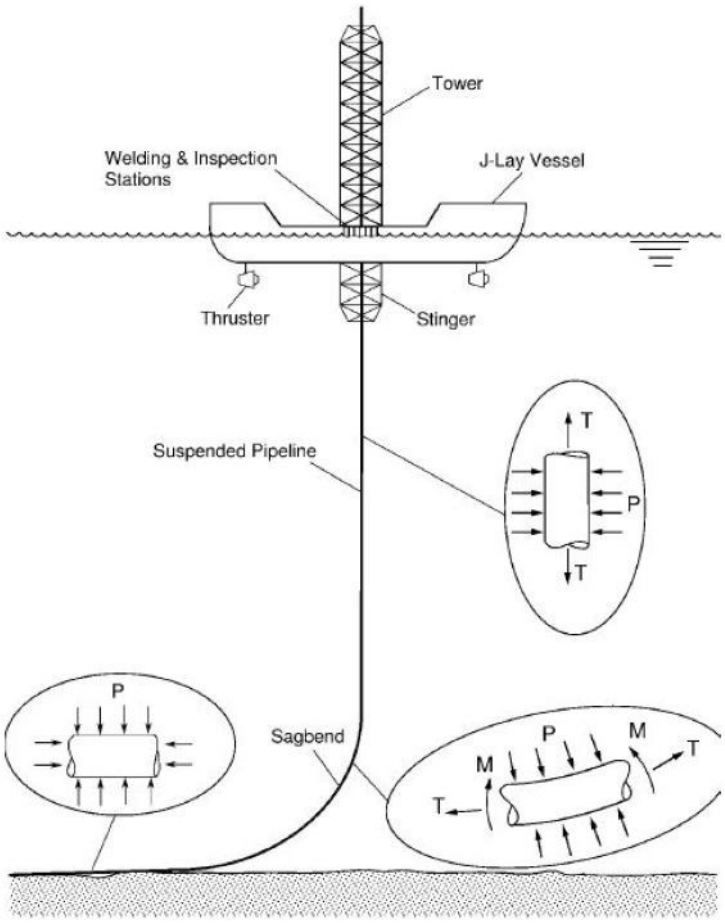

Figure 1–10 Schematic representation of J-lay pipeline installation and associated pipeline loading [1].

On the way down to the seabed, it acquires the characteristic J-shape from which the name J-lay is derived. The first effect of the J-configuration is that the suspended length is reduced by comparison to S-lay. In this case, the role of the tension is to support the shorter suspended length and to control the line curvature in the sagbend. A consequent second effect is a reduced tension requirement from the vessel and a significant reduction in the required thruster power. Each pipe section is raised to the tower, aligned with the suspended pipe, welded to it, inspected and coated. The long section is then lowered into the water while the vessel moves forward, installing a corresponding length to the seabed. A short support structure (stinger) below the holding point guides the direction of the line close to the water surface. Since the touchdown point is not that far behind the vessel, the positioning of the pipeline can be more precise.

Better vessel control also results from the fact that only a short length of the line close to the surface is exposed to wave motion. An additional advantage is that the lower tension in the line on the seabed translates into shorter free spans.

J-lay is somewhat slower than traditional S-lay, but it has been projected to be capable of installing pipelines down to 11,000 ft (3,350 m) of water.

The loads experienced by the pipe during such deepwater J-lay are illustrated schematically in Figure 1–10: high tension and relatively small external pressure close to the surface of the sea, progressively increasing pressure and decreasing tension further down the long suspended section, high external pressure and bending in the sagbend, and essentially hydrostatic pressure on a flat seabed. Each of these loadings must be designed for [1].

Figure 1–11 shows the Saipem vessel Saipem 7000.

Figure 1–11 Saipem 7000 owned by Saipem [1].

2 WELDING

2.1 INTRODUCTION

The welding procedures used are briefly described in this chapter. Submarine pipelines are constructed from lengths of pipe joined together by manual, semiautomatic, or automatic fusion welding. The selection of the welding method is determined by the contractor's capability, the pipe diameter, wall thickness, and, to a lesser extent, fabrication location. Pipelines constructed on land for installation by reeling or in a bundle as well as pullouts, and small-diameter S-lay lines are almost always welded by manual welding. However, for offshore fabrication by S-lay, the larger-diameter lines are more economically welded using semiautomatic or fully automatic welding. This division of techniques arises because of the cost associated with use of the lay barge.
Welding is the critical step in pipelaying because it dictates the length of time to construct the pipe and, for this reason, has a major impact on the cost of the project.
Welding is the critical step in pipelaying because it dictates the length of time to construct the pipe and, for this reason, has a major impact on the cost of the project.
Pipeline contractors are constantly researching for faster methods of welding to speed up the laying process and reduce the time the lay barge is required.
However, further large increases in the speed of conventional welding appear unlikely. Major advances will occur through the introduction of newer welding procedures such as flash butt welding. The requirement for a faster welding procedure results from the limitation in J-laying used for installation of pipelines in deep water. In J-lay, there is only one welding station; and, though multiple jointed pipes are used (up to six joints), the single weld station is the limiting factor because the complete weld must be produced at this one location [2].

2.2 WELDING PROCESS

Welding joins metal by inducing coalescence of the material, which is accomplished by heating to a suitable temperature with or without pressure and with or without the addition of filler metal. There are three critical parameters:

- Heat input: Sufficient energy must be provided to melt the metal and consumable (W/m^2).
- Heat input rate: The rate of energy input controls the rate of welding ($W/m^2/s$).
- Shielding from the atmosphere: Shielding is done to prevent oxidation of the molten melt, which would produce a weak weldment.

The heat for melting the metal may be provided by laser, burning acetylene gas with oxygen, or by an electrical process. Laser welding is not practicable at present for welding thick-wall pipeline material, but in the long term, future pipe joining using laser heating coupled with pressure is a possibility. Acetylene gas welding is not used for pipeline welding but may be used for cutting, though plasma-arc cutting is a more common procedure nowadays. The electrical methods produce heat by either resistance heating or by production of an arc between the welding torch and the pipe. Electric resistance welding (ERW) and flash butt welding are examples of resistance heating.

Manufacture of welded pipe requires rapid welding procedures, and two processes are used: submerged arc welding and electric resistance welding. The weld of pipe produced by submerged arc welding is generally made in two weld passes, one internal and one external. Electric resistance welding is a single-pass operation used for fabrication of modest-diameter pipe. At present, girth welds are made exclusively by a sequence of arc-welding processes in which the arc is a plasma discharge of high temperature, and typically four to seven passes are required. The electrical process to generate the plasma arc depends on the welding process. Direct current (DC) welding machines with drooping characteristics are used for manual arc welding with cellulosic-coated electrodes, and the voltages used are 80–100 V, whereas gas metal arc welding and tungsten inert gas (TIG) welding generally use pulsed alternating current (AC) [2].

Welding technology uses acronyms as shorthand for the processes. The terms commonly encountered in pipelining include [2]:

- SAW—Submerged arc welding is used for producing longitudinally welded pipe and also for producing double or triple jointed pipe (24- to 36-m lengths). The metal is joined by fusing with an electric arc or arcs struck between a bare metal wire electrode or electrodes and the pipe. A blanket of granular, fusible material spread in a deep layer over the weld area shields the arc and molten metal. The process is illustrated in Figure 2–1.
- SMAW—Shielded metal arc welding is the conventional, manual arc-welding process in which the heat for welding is supplied by an electrical arc struck between a consumable electrode and the pipe. The electrode, or stick, is covered with a basic or cellulosic coating that burns during use, releasing carbon dioxide that shields the molten weld metal. The process is illustrated in Figure 2–2. The cellulosic cover is a blend of organic fibers. Cellulosic electrodes are sensitive to temperature changes, which alters their moisture content. This type of electrode is supplied in sealed cans, which are baked to ensure that they are dry. The electrodes are kept warm in quivers. Rebaking of electrodes that have been allowed to cool should not be permitted.
- GMAW—Gas metal arc welding is a weld produced by heating with an arc struck between a bare metal electrode wire and the work. The electrode wire is fed continuously through the welding head. Shielding of the molten metal is provided by gas introduced through an annulus around the welding wire in the welding head. If the gas is inert, the procedure may be called metal inert gas welding (MIG); and if the gas is active, the procedure may be called metal active gas welding (MAG). For pipe welding, a mixture of argon and carbon dioxide is generally used. The process is illustrated in Figure 2–3. Modern automatic systems use twin (tandem) welding heads.
- GTAW—Gas tungsten arc welding, also known as tungsten inert gas (TIG) welding, is the process is which the arc is struck between an inert, nonconsumable electrode fabricated of tungsten, and the filler metal is

introduced as a wire consumable fed into the molten metal pool. The molten metal is shielded by an inert or active gas introduced through an annulus around the tungsten electrode in the welding head. In the past, helium was used as the shielding gas; and this process was termed heli-arc welding. GTAW is used for root passes and also for welding of corrosion-resistant alloys (CRAs) such as the duplex stainless steel with an argon shielding gas. TIG welding is slow because the heat input rate is limited. Welding using a hot wire feed into the weld pool is about 20% more rapid, but it is not a suitably robust process for offshore production welding. The procedure is illustrated in Figure 2–4.

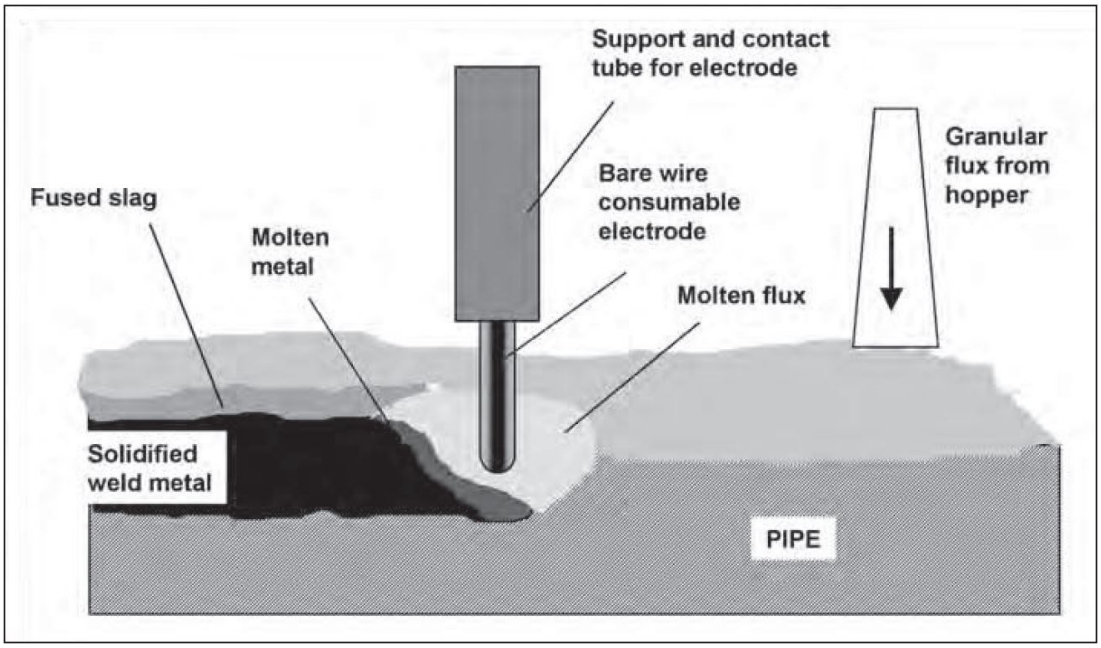

Figure 2–1 Submerged arc welding [2].

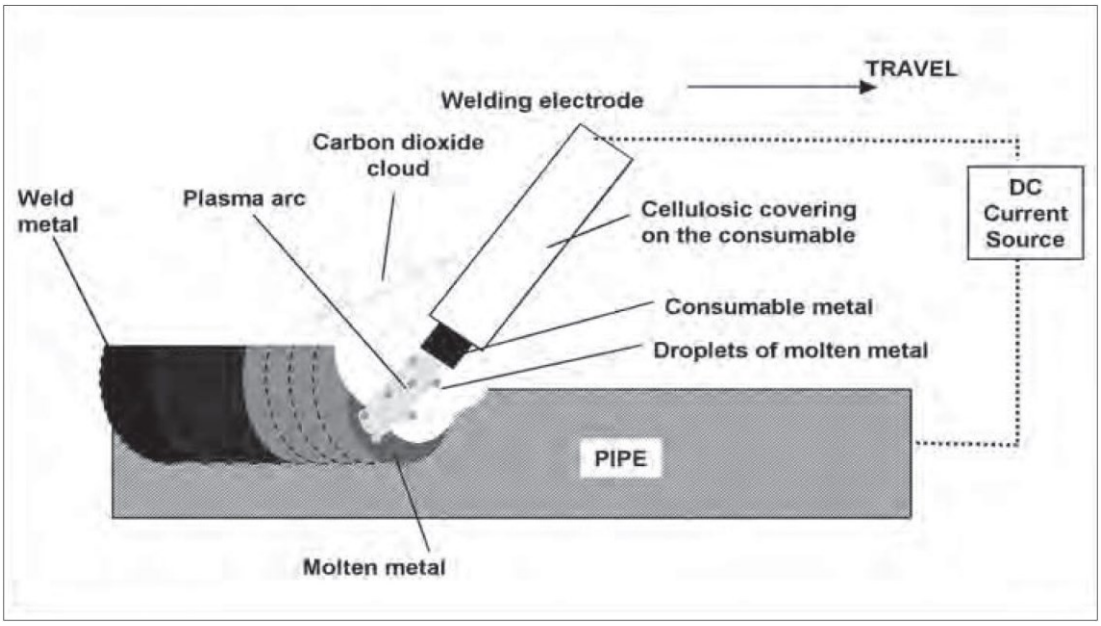

Figure 2–2 Manual metal arc welding [2].

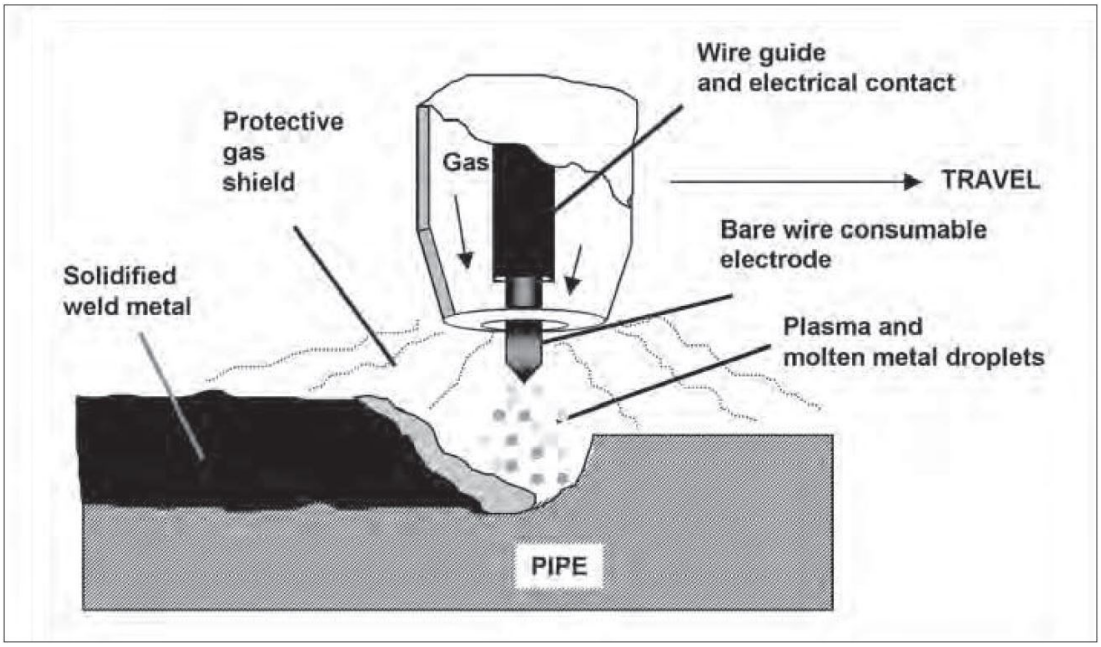

Figure 2–3 Gas metal arc welding [2].

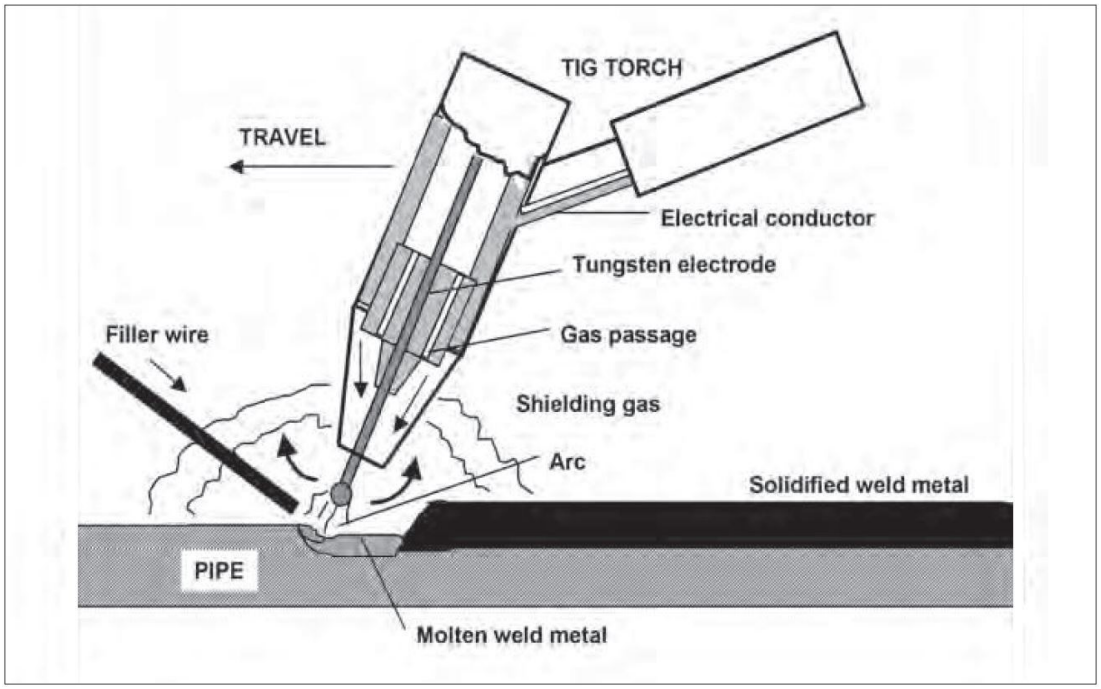

Figure 2–4 Tungsten inert gas welding [2].

2.3 WELDING BEVEL

The pipes to be welded must be prepared with a bevel at the ends of each pipe. The classic bevel preparation for most pipe is a straight angle cut of about 30° with a residual 1.5–2 mm left for the formation of the root pass. The bevel is necessary to ensure that the first weld completely fuses the inside ends of the pipe. The 30° angle was developed in the early days when all welding was with done with sticks, that is, SMAW. The typical stick electrode is quite thick, and this means that a large space has to be provided to allow the welder to reach into the joint and also to allow the shielding gas fumes to escape. The large bevel has to be filled subsequently with weld metal, and this takes time. Whenever wall thickness permits, it is advantageous to provide a slightly more acute bevel. With the advent of GMAW, using thin continuous metal wire of small diameter, the requirement for a large bevel on thick pipes was reduced, and narrower bevels were devised [2].

Examples of bevels are shown in Figure 2–5 and Figure 2–6.

The narrow bevels, however, do increase the risk of lack of side-wall penetration, creating a particular problem with automatic welding if the set traverse of the wire is inadequate. To avoid this problem, the gas mixture can be modified to a blend of argon and carbon dioxide. The addition of about 5% carbon dioxide enhances lateral spread of the plasma arc, thereby increasing side-wall penetration. The heat-input rate also needs careful control. If the root pass is to be made from the inside of the pipe, which is common for larger-diameter pipelines, then the bevel must be more complex with angle cuts from both sides. In all cases, the weld gap must be accurately set to ensure full root penetration [2].

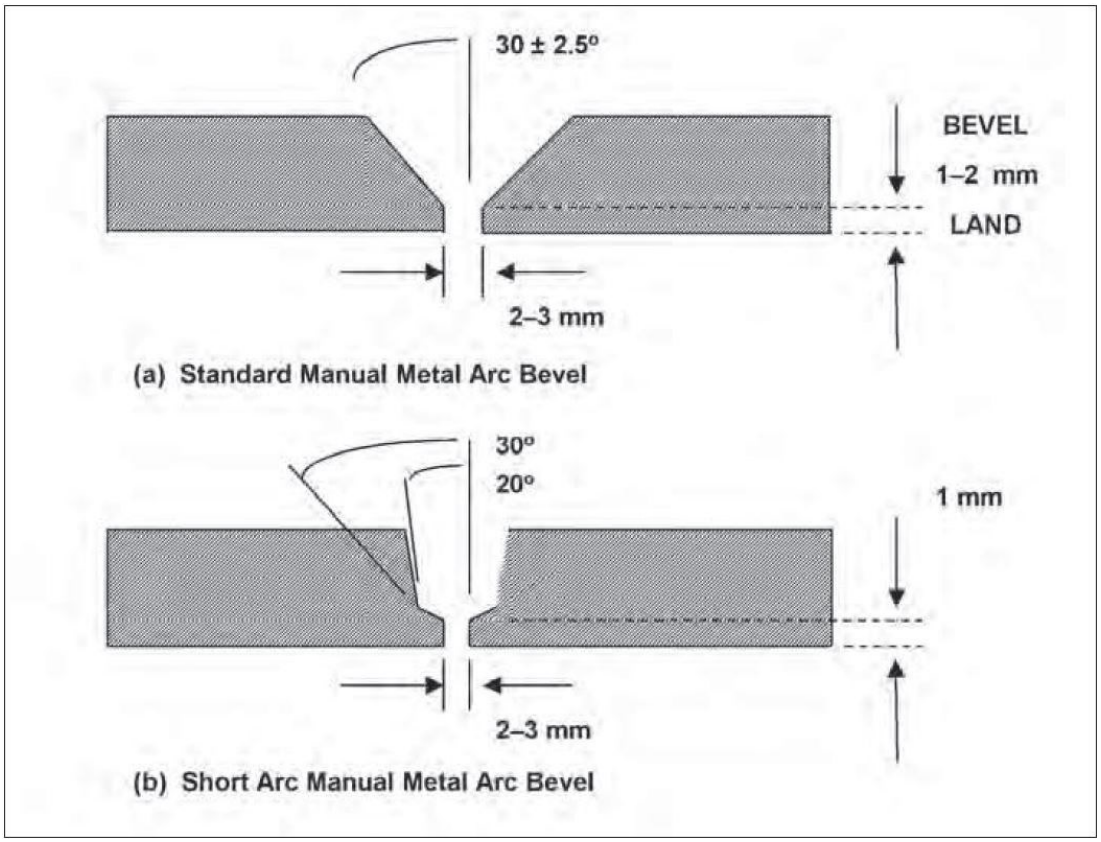

Figure 2–5 Bevels for manual arc welding [2].

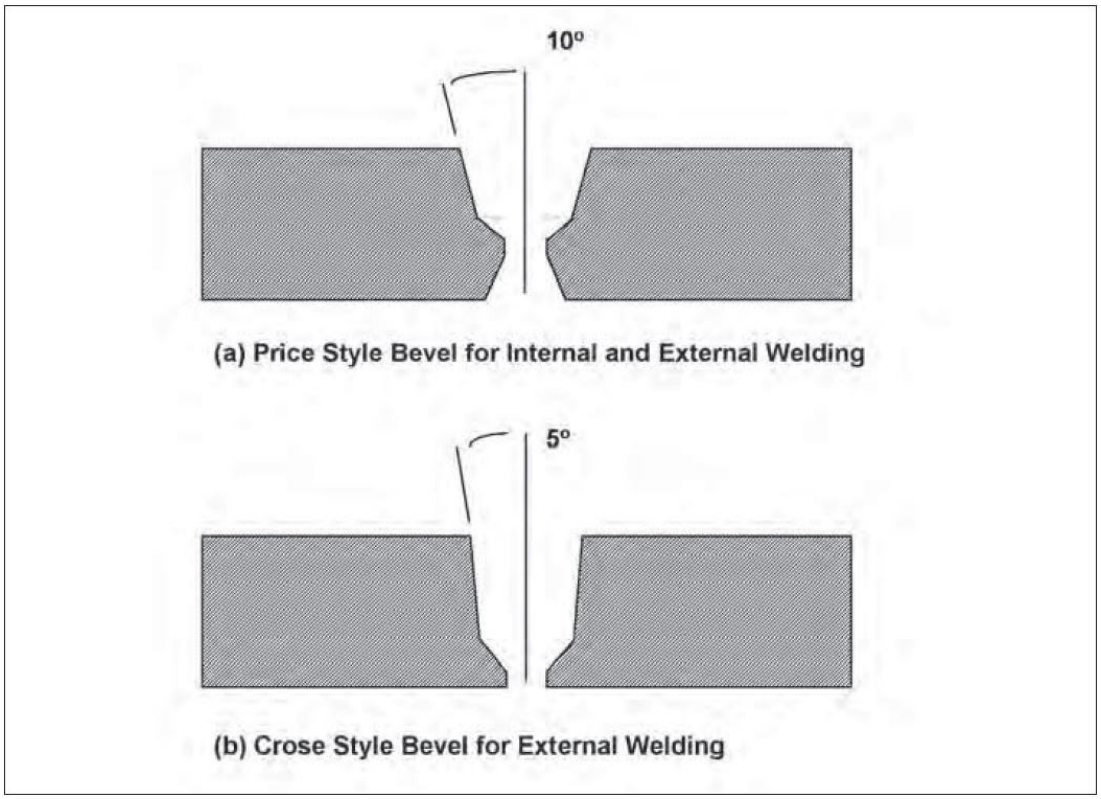

Figure 2–6 Bevels for semiautomatic and automatic welding [2].

Prior to moving the pipe into the firing line for welding, about 40 mm at each of the bevelled ends of each joint of pipe are thoroughly cleaned and inspected. Any pipe showing laminations requires cutting back, then rebevelling and reinspecting. Usually, to avoid wasting time, ultrasonic testing for laminations within the 25- to 40-mm zone is used. It is also usual for the pipe to be inspected by magnetic particle inspection to ensure that all the laminations have been removed from the new bevel. Laminations result in porosity, which would weaken the welds and result in a high risk of cracking, but may not show up in X-ray examination [2].

3 PIPELINE OFFSHORE SCENARIO

3.1 INTRODUCTION

In this chapter are exposed the main systems of external anticorrosive coating, without considering the internal coating.

An addition external coating is applied over anticorrosive coating, for guarantee stability on the seabed and protection from dynamic loads induced to the pipe by fishing devices. In particular, are exposed the main applications of concrete weight coating.

Pipeline offshore is obtained by welding the ends of the pipe joints (length 12.2 m) and the resulting area must be covered by a field joint coating system. Therefore, the most common field joint coating systems in the offshore sector are exposed.

3.2 PIPELINE COATING

A primary objective of external coatings on submarine pipelines is corrosion control. Coating systems can be designed also to provide mechanical protection during installation and operation. A corrosion protective coating (sometimes referred to as corrosion coating) may be combined with a concrete weight coating (for anti-buoyancy and/or mechanical protection) or a coating for thermal insulation.

Coatings for external corrosion control of pipelines are applied to individual pipe lengths at a dedicated coating plant. This coating is referred to as linepipe coating (sometimes also as factory coating, plant applied coating or parent coating). In order to facilitate girth welding, areas at each end of the individual pipe length are left uncoated.

These areas are normally coated after welding, by applying a field joint coating system (see DNVGL-RP-F102).

Submarine pipelines are almost invariably designed with a cathodic protection (CP) system, mostly based on galvanic (or sacrificial) anodes. The CP system serves as a back-up for any deficiencies of the pipeline coating, including defects during application and damage during transportation/installation, in addition to any assumed environmental degradation of coating properties and mechanical damage during operation. For submarine pipelines, maintenance of coating and cathodic protection systems is essential. This is reflected by high requirements to the quality control of coating application [3].

3.3 EXTERNAL COATING SYSTEM FOR OFFSHORE LINEPIPES

Offshore steel pipelines are normally designed for a life ranging from 20 years to 40 years. To enable the pipeline to last for the design life, the pipeline needs to be protected from corrosion both internally and externally. Internal coating will not be analyzed in this thesis.

This first external pipe coating layer is used to protect the pipe against corrosion. A single layer coating is used when the installed pipeline is always in a static, laterally stable condition lying on soils such as clay or sand. Additional layers of coating are used for additional protection, for weight to help the pipeline remain laterally stable on the seabed, or for providing insulation. A multi-layer coating is generally used in cases where the external environment tends to easily wear out the external coating (e.g. pipeline lying on top of rocky soil, calcareous material, etc.). Depending on the external environment and on the location or use of the pipeline, a single-layer coating or a multi-layer coating is required [4].

For application in Oil & Gas pipeline, there are three most common external anticorrosion coating systems:

1) Fusion Bonded Epoxy (FBE);
2) Three-Layer Polyethylene (3LPE);
3) Three-Layer Polypropylene (3LPP).

Primarily for use in combination with a concrete weight coating [3].

3.3.1 FUSION BONDED EPOXY

Fusion Bonded Epoxy (FBE, see Figure 3–1) is a thermosetting powder applied anti-corrosion coating that provides excellent protection for small to large diameter pipelines at up to moderate operating temperatures. Special grades of FBE are also available for higher operating temperatures, high strength steel pipes, or other specific applications.

This anticorrosion coating system provides the following advantages [5]:

- FBE has excellent adhesion to steel and provides superior long term corrosion resistance and protection of pipelines operating at moderate temperatures for the designed life;
- Superior adhesion properties provide excellent resistance to cathodic disbondment which reduces the total cost of cathodic protection during the operation of the pipeline;
- Special grades of FBE are available for use at higher operating temperatures, for coating of high strength steels and other specific applications;
- FBE can be applied as a dual-layer product which provides tough physical properties that minimize damage during handling, transportation, installation and operation;
- FBE has been designed for good chemical resistance under most soil conditions;
- FBE is flexible and allows bending of the pipe for installation.

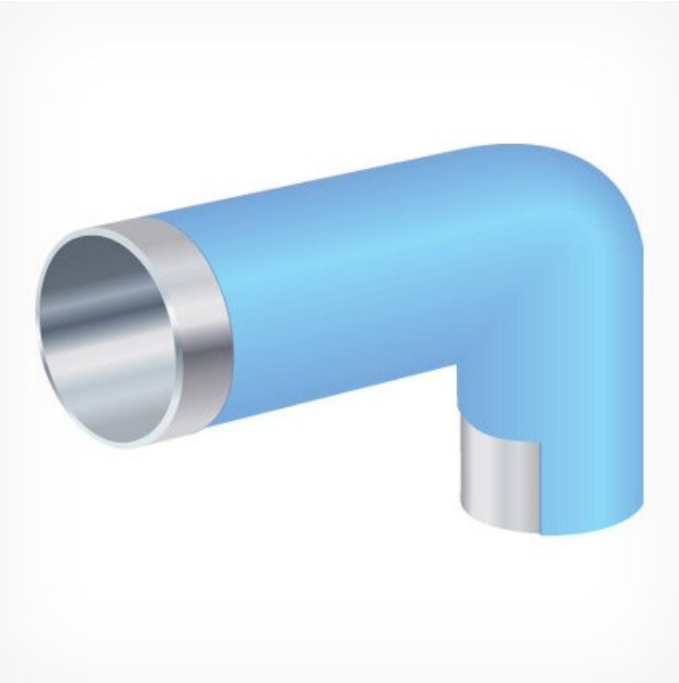

Figure 3–1 FBE anticorrosion coating system [5].

The nominal thickness of FBE varying from 350 μm to 500 μm (minimum thickness 300 μm), while design temperature varying from -30 °C to +110 °C, according to DNV-RP-F106 and ISO 21809-2 respectively [6].

3.3.2 THREE-LAYER POLYETHYLENE

3-Layer Polyethylene (3LPE, see Figure 3–2) is a multilayer coating composed of three functional components: A high performance Fusion Bonded Epoxy (FBE) primer, followed by a copolymer adhesive and an outer layer of polyethylene which provides tough, durable protection. 3LPE systems provide excellent pipeline protection for small and large diameter pipelines operating at up to moderately high temperatures [7].

This anticorrosion coating system provides the following advantages [7]:

- The FBE component provides excellent adhesion to steel, providing superior long-term corrosion resistance and protection of pipelines operating at moderate temperature;
- If required, Low Application Temperature (LAT) FBE can be selected as the primer to ensure low preheating conditions and long term integrity of high strength steels (X80 or higher);
- 3LPE systems offer excellent resistance to cathodic disbondment, reducing lifecycle costs of cathodic protection;
- The tough outer PE layer protects pipelines during transportation and installation thereby reducing costly repairs while also providing added in-ground protection against shear forces, chemicals and abrasive soil condition;
- By increasing the thickness of the PE outer layer, the 3LPE system can provide a high level of mechanical protection across a variety of difficult environments.

The total nominal thickness of 3LPE varying from 3.0 to 4.0 mm (minimum thickness 2.5 mm), while design temperature range depends on the type of polyethylene, as from DNV-RP-F106 and ISO 21809-1 respectively [8].

The cut-back length depend on project needs, usually equivalent to 150 mm with tolerance of +20 mm/-0 mm.

According to design temperature range the polyethylene may be:

- Low Density Polyethylene (LDPE, 918-935 Kg/m3);
- Medium/High Density Polyethylene (MDPE/HDPE, 940-950 Kg/m3).

The design temperature range of LDPE is -20 °C to +60 °C, while -40 °C +80 °C for MDPE/HDPE [8].

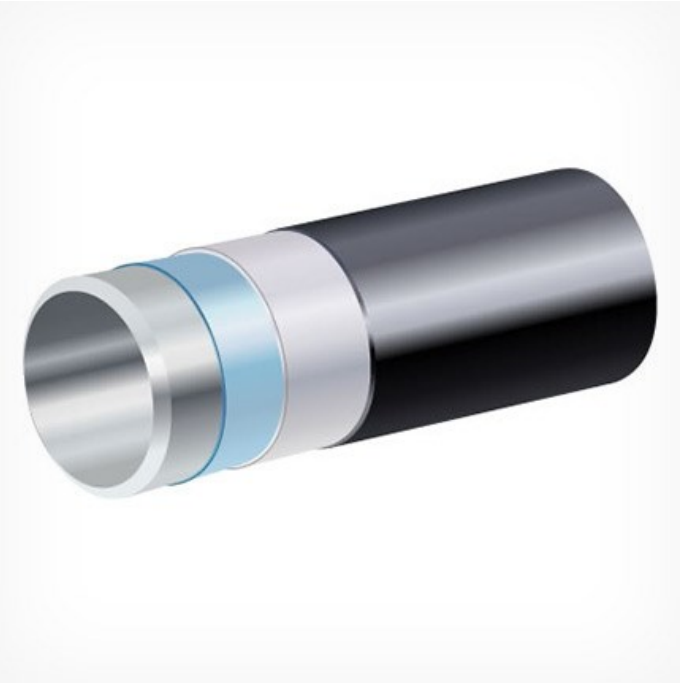

Figure 3–2 3LPE anticorrosion coating system [7].

3.3.3 THREE-LAYER POLYPROPYLENE

3-Layer Polypropylene (3LPP, see Figure 3–3) is a multilayer coating composed of three functional components, in which the first two layer are equal to 3LPE, while the third layer is in polypropylene with minimum density to 900 kg/m3.

The outer layer of polypropylene provides one of the toughest, most durable pipe coating solutions available. 3LPP systems provide excellent pipeline protection for small and large diameter pipelines at up to high operating temperatures [9].

This anticorrosion coating system provides the following advantages [9]:

- The FBE component of the 3LPP system provides excellent adhesion to steel, providing superior long term corrosion resistance and protection of pipelines operating at high temperatures;
- The superior adhesion properties of the FBE also results in excellent resistance to cathodic disbondment, reducing the total cost of cathodic protection during the life of the pipeline;

- The tough outer layer of polypropylene protects pipelines during transportation and installation thereby reducing costly repairs and providing added in-ground protection against shear forces, chemicals and abrasive soil conditions;
- By increasing the thickness of the polypropylene outer layer, 3LPP can provide the highest level of mechanical protection across many diverse environments.

The total nominal thickness and cut-back is the same as 3LPE, while the design temperature range is higher than 3LPE, varying from -20 °C to +110 °C, in according to DNV-RP-F106 and ISO 21809-1 respectively [8].

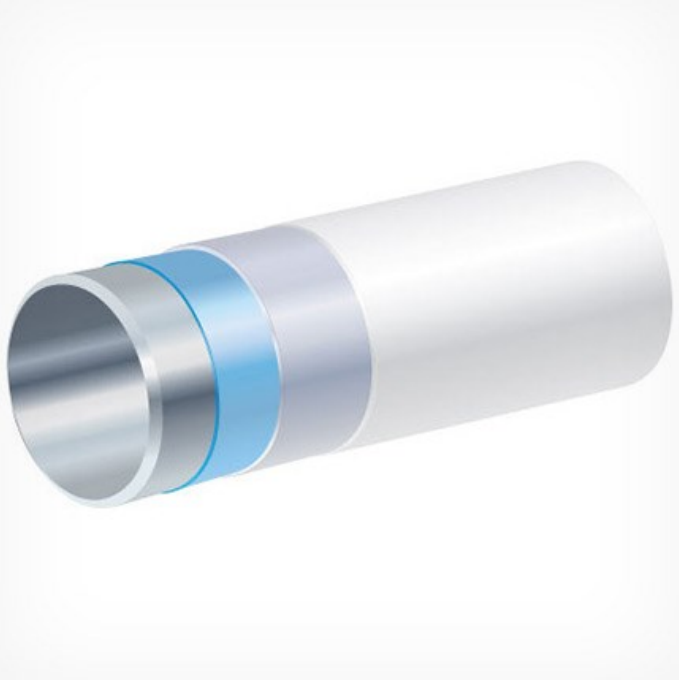

Figure 3–3 3LPP anticorrosion coating system [9].

3.4 CONCRETE WEIGHT COATING

Concrete weight coating (CWC) may be applied on top of the external anticorrosion coating system FBE, 3LPE and 3LPP. The objectives of a concrete weight coating are to provide negative buoyancy to the pipeline, and to provide mechanical protection of the corrosion coating and linepipe during installation and throughout the pipeline's operational life [10]. The concrete weight coating (thickness, strength, density, amount of reinforcement) shall be designed for the specific project. In addition, the actual installation, laying and operation conditions for the pipeline shall then be taken into consideration [10]. Concrete coating is a right mixture of cement, aggregates and water. Reinforced is used in form of wire mesh or steel cage.

Typical data on the concrete coating are:

- Minimum concrete thickness of 40 mm;
- Maximum concrete thickness of 150 mm;
- Minimum concrete density (dry) of 2240 kg/m3;
- Maximum concrete density (dry) of 3040 kg/m3;
- Minimum compressive strength shall not be less than 40 MPa;
- Increase the weight of 2% on bottom stability analysis and 5% laying analysis, due to the absorption of water from the concrete;
- Cut back length varying from 370 to 390 mm with tolerance +20 mm/-0 mm (depends on welding system used).

Concrete coatings can be applied in two ways:

1) Impingement;
2) Compression coat.

3.4.1 APPLICATION BY IMPINGEMENT

Impingement process in able to apply lightweight, normal weight and heavy weight concrete coatings, making it ideal for large diameter pipelines [11]. The product is available in various thicknesses and densities and can be applied over anti-corrosion and insulation coatings (see Figure 3–4). The main advantages of this coating are [11]:

- Can be applied in a wide range of densities and thicknesses to meet project requirements;
- Available in thicknesses up to 230 mm (9”) providing a high level of mechanical protection and stability;
- Depending on design requirements, concrete coating applied by impingement can be manufactured with a reinforcing wire cage, galvanized reinforcing wire mesh, or both;
- Can be applied over anti-corrosion and insulation coating systems, enabling project teams to choose the most appropriate weight and protection coating system without compromising the long term corrosion protection of the pipeline.

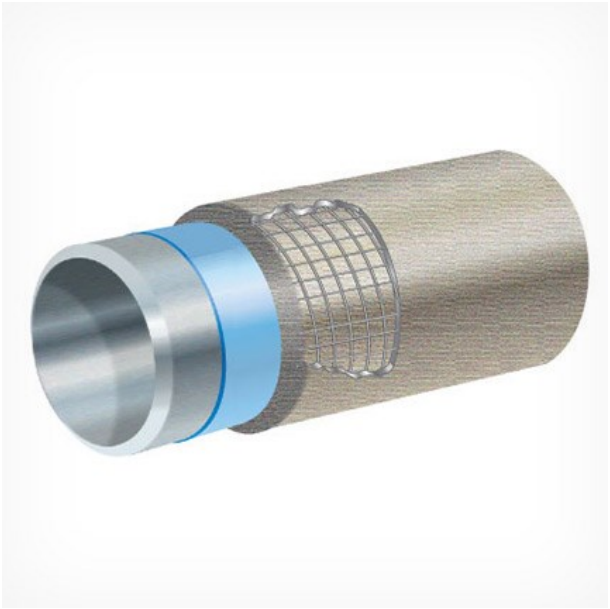

Figure 3–4 Concrete weight coating applied by impingement [11].

Capability/Property	Concrete Weight Coating
Density	1800-3450 Kg/m^3 (112-215 lbs/ft^3)
Compressive strength (28 days)	40-50 MPa (5800-7200 psi)
Minimum concrete thickness	25 mm (1″)
Maximum concrete thickness	230 mm (9″)
Minimum pipe diameter	150 mm (6″)
Maximum pipe diameter	1422 mm (56″)
Minimum pipe length	8.5 m (28′)
Maximum pipe length	18 m (60′)

Table 3–1 Typical concrete weight coating properties applied by impingement [11].

3.4.2 APPLICATION BY COMPRESSION COAT

Concrete coating applied by compression coat is also designed to provide negative buoyancy and mechanical protection for pipelines in subsea and wet environments . Compression coat uses a side-wrap application process making it ideal for both small and large diameter pipelines (see Figure 3–5). The product is available in various thicknesses and densities and can be applied over most anti-corrosion and insulation coatings [12]. The main advantages of this coating are [12]:

- Can be applied to a wide range of densities, thicknesses and strengths to meet project requirements;
- Available in thicknesses up to 150 mm (6″) providing a high level of mechanical protection and stability;
- Offers a more consistent thickness and smoother surface than concrete weight coatings applied by impingement;
- Can be applied over anti-corrosion and insulation coating systems;
- Gentle wrap application reduces potential for holidays in linepipe coating during coating;

- Can be enhanced with additional features including bendability slots and crack inducers as well as sacrificial anodes.

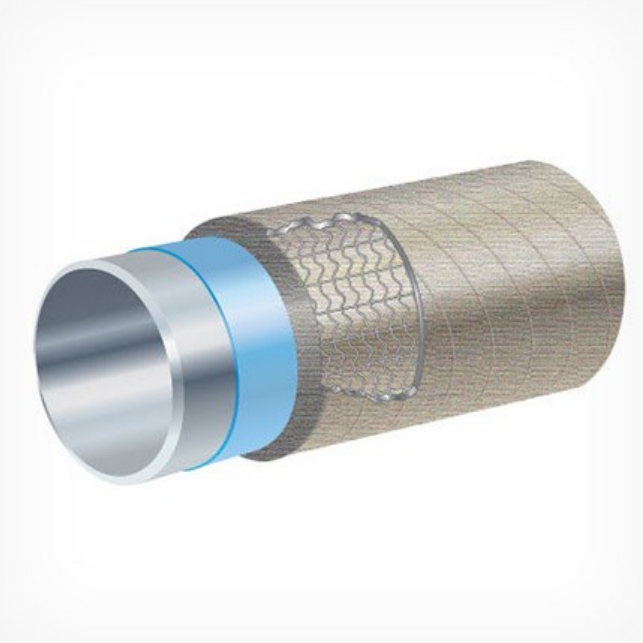

Figure 3–5 Concrete weight coating applied by compression coat [12].

Capability/Property	Concrete Weight Coating
Density	1800-3050 Kg/m^3 (112-190 lbs/ft^3)
Characteristic proctor cylinder compressive strength (28 days)	30-40 MPa (4350-5800 psi)
Characteristic cube compressive strength (28 days)	40-50 MPa (5800-7250 psi)
Minimum concrete thickness	25 mm (1″)
Maximum concrete thickness	150 mm (6″)
Maximum pipe diameter	1220 mm (48″)
Minimum pipe length	5.5 m (18′)
Maximum pipe length	19.8 m (65′)

Table 3–2 Typical concrete weight coating properties applied by compression coat [12].

3.5 FIELD JOINT COATING

In order to facilitate girth welding, areas at each end of the individual pipe length are left uncoated. These areas are normally coated after welding by applying a field joint coating (FJC) system [13]. The field joint area is defined as uncoated area that results when two pipe sections or a pipe section and a fitting with coating cutbacks are assembled, by welding, in the field [14].

Depending on the type of linepipe coating, the FJC may consist of one or more layers of coating materials applied for the purpose of corrosion control, mechanical protection and/or thermal insulation. FJC systems may also be designed to provide a smooth transition to a concrete weight coating of the linepipe, or to a thick-layer thermally insulating coating in order to facilitate offshore installation operations. This is typically achieved by application of a moulding compound, referred as infill. In some cases, prefabricated half shells are installed by strapping to the field joint.

The infill may further be designed to provide mechanical protection during installation (e.g. against trawl board damage) or thermal insulation [13].

For offshore pipelines, there are four main field joint coating systems [14]:

1) Heat-shrinkable materials, polyethylene-based (2A);
2) Heat-shrinkable materials, polyethylene-based, applied over a liquid or fusion-bonded epoxy layer (2B);
3) Heat-shrinkable materials, polypropylene-based, applied over a liquid or fusion-bonded epoxy layer (2C);
4) Cast polyurethane (4E).

3.5.1 HEAT-SHRINKABLE COATING

Heat-shrinkable materials consist of an external backing made of extruded and cross-linked polyolefin and an internal adhesive made of thermoplastic material. The shrinkage of the backing instils a level of circumferential compression in the coating that supplements the bonding of the sleeve to the pipe surface [14].

Heat-shrinkable materials are available in the following forms [14]:

- Tubular sleeve;
- Wrap-around sleeve;
- Pre-formed material (assembly for complex configuration parts);
- Tapes.

Type 2A coatings are cross-linked, heat-shrinkable materials based on polyethylene, applied without primer, which can be further subdivided into [14]:

- 2A-1: mastic-adhesive based, typically with a low design temperature of up to 50 °C;
- 2A-2: high shear-strength mastic adhesive, bitumen or butyl-based, with a design temperature of up to 80 °C;
- 2A-3: high shear-strength hybrid or hot-melt adhesive, with a design temperature of up to 120 °C.

4 FIELD JOINT COATING – INFILL SCENARIO

4.1 INTRODUCTION

In this chapter are exposed the most common infill materials of the field joint coating in the offshore sector. In particular, this materials are designed for withstand from dynamic loads induced by fishing devices, to protect the welded area of the offshore pipelines. Solid polyurethane is the infill material subject to investigation in this thesis. Furthermore, the equipment used, the mechanical and chemical characteristics of each infill material are exposed below.

4.2 INFILL MATERIAL

During offshore pipeline construction activities, the field joint between two concrete weight coated pipes shall be filled with a material that restore the overall outside diameter of the field joint in order to match the diameter of the concrete coated pipeline. Offshore pipelines may experience impact or abrasion after a FJC has been applied. These impact loads or abrasions may occur due to interference with trenching equipment, fishing activities, dropped objects etc. To reduce the risk of damage to the anti-corrosion coating, the infill material is added to the field joint to provide a second layer of mechanical protection.

The infill may further designed to provide mechanical protection on the field joint coating area during:

- Installation for protection to the weld joint area and to assist with pipe movement over the rollers;

- Operation (e.g. against trawl board damage);
- Thermal insulation.

Thermal insulation requirement will not be investigated in this thesis.

Usually polyurethane infill material is applied in three form:

1) Solid polyurethane infill;
2) Polyurethane foam infill;
3) Pre-fabricated polyurethane half shells.

Solid or foam polyurethane materials are applied by injection molding processes.

The polyurethane material is applied into a mold made to the welded joint area [15].

In this thesis the field joint coating system infill material analyzed is the solid polyurethane.

The Figure 4–1 below shows a typical application of the FJC and the infill material for offshore pipelines.

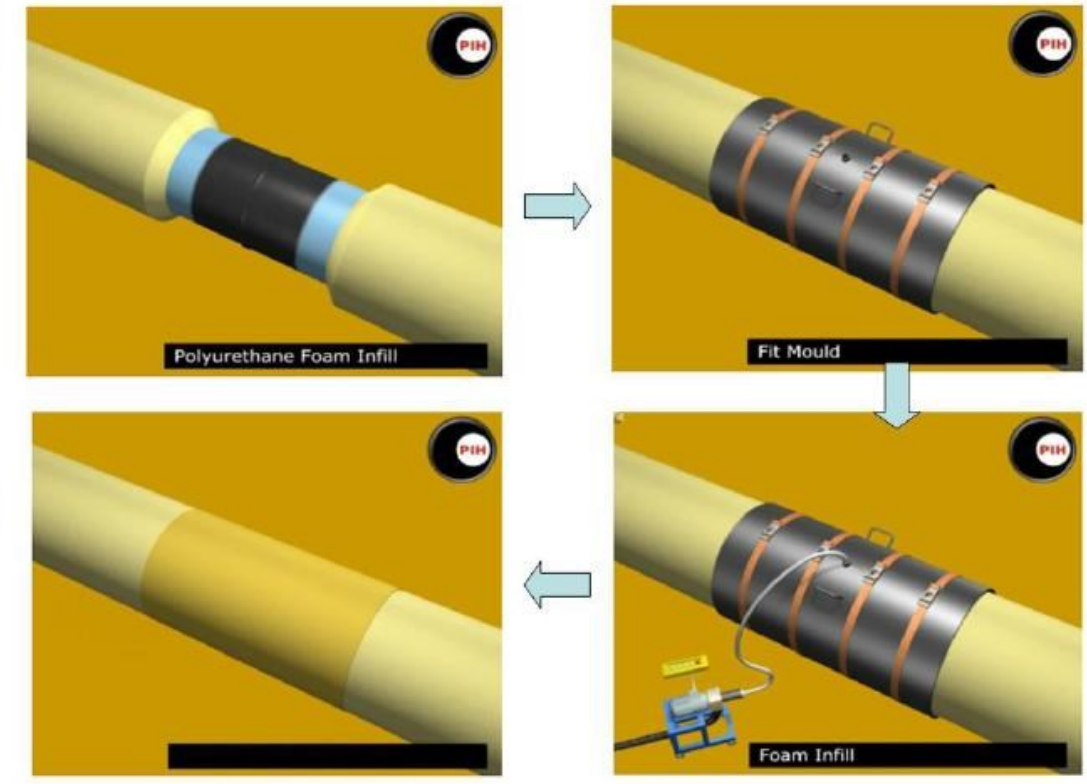

Figure 4–1 Pipeline field joint coating.

4.2.1 SOLID POLYURETHANE

Solid polyurethane (PU) consists of a two part liquid component (isocyanate and polyol). The blend is formulated to give high compressive strength, superior impact resistance, quick reaction and solidification time. The resultant field joint is a smooth, hard coating providing a flush transition from concrete coating, end-to-end.

The material most commonly used has a typical density between 1000 kg/m^3 and 1500 kg/m^3.

Infilling the field joint void on concrete weight coated pipe is performed by pouring or injecting solid polyurethane into a mould around the joint on top of the anti-corrosion layer. After the solid PU has cured, the mould is removed and utilized for another one (reusable mould).

With respect to PU Foam, solid PU provides the following advantages:

- Very high compressive strength;
- Very high shock and flexural resistance.

Solid thermoset polyurethane elastomers are widely used for off-shore pipe field joint infill due their properties to completely fill any cavity as liquid, followed by quick solidification (i.e. curing).

Polyurethane develops their final mechanical properties after a defined period of time that can take hours or days, depending on chemical composition (both isocyanate and polyol components) and curing conditions like temperature.

Generally, in order to minimize the damage to a molded part, the material must attain a suitable strength prior to subjecting it to any mechanical stress; the behavior of molded PU part to external solicitation depends on chemical composition of polymer and process conditions, and therefore should be evaluated accordingly.

Solid polyurethane elastomers used for field joint infill ensure high strength able to withstand the mechanical stresses developed during the laydown operations, meeting short cycle time and high productivity requirements.

Fully cures solid polyurethanes represents a validated solution to protect the joint also after pipe installation, and the large track record of construction pipeline projects proves the success in using polyurethane technology for field joint infilling [14].
Gravel-filled polyurethane materials provide additional impact resistance and compressive strength [15].
Key features solid PU field joint coating systems [15]:

- Compatible with thin-film and multi-layer polyethylene and polypropylene factory-applied line pipe coatings;
- Incompressible polyurethane materials suitable for deeper water applications;
- High-impact-resistant polyurethane material;
- Fast application and cure times, fast cycle times.

Scope of the activity is to better understand the behavior of solid polyurethane after curing, when the pipeline is laid on the sea bed.

4.2.2 FOAM POLYURETHANE

Polyurethane foam infill can be applied to the joint area of concrete weight coated pipes. Polyurethane foam material formulations are available to offer specific performance criteria.
The high density polyurethane foam (HDPF) system develops a rigid, open cell structure. Upon immersion, the open cells will absorb water, thereby increasing in overall density to approximately 1025 kg/m^3 (similar to seawater itself).
The low-viscosity product formulation of the HDPF system allows “free flow” of chemicals to ensure quick and complete filling of the mold, within the cycle times demanded by today’s offshore laybarge operations [16].
Infilling the field joint void on concrete weight coated pipe is performed by pouring or injecting polyurethane foam into a mould (often made by metal sheet) around the joint on top of the anti-corrosion layer.

The metal form is tightly banded and clipped onto the concrete coating ensuring an equal overlap on either side of the field joint. An injection hole is drilled by means of a milling cutter [16].

Adequate foam quantity shall be injected to ensure that foam is extruded from top window after filling all voids and the required density is achieved.

The mould is usually left in place: this system will allow the field joint to pass over the vessel rollers and stinger without damage. Disposable plastic or metal moulds can be used as required by environmental and operational demands.

Polyurethane foam infill features and benefits are [16]:

- Commercially attractive;
- Rapid cycle times;
- Reusable or expendable/disposable (metallic or plastic) mold systems;
- Compact, reliable application equipment;
- Compatibility with all conventional anti-corrosion field joint coating systems;
- No solvents required: all equipment is air-/water-purged;
- A range of foam densities is available.

5 INFILL MATERIAL CHARACTERIZATION

5.1 INTRODUCTION

In this chapter is presented an overview of non-linearity material with regard to solid mechanics. Initially, is introduced a general description of the constitutive relationship associated with non-linearity material in solid mechanics. Then is given a brief description of the most common cases of non-linearity material, with specific material example included where appropriate [17].

Finally, is showed a detailed description of all isotropic hyperelastic constitutive models implemented in Abaqus software.

Hyperelastic materials are described in terms of a "strain energy potential," $W(\varepsilon)$, which defines the strain energy stored in the material per unit of reference volume (volume in the initial configuration) as a function of the strain at that point in the material. There are several forms of strain energy potentials available in Abaqus to model approximately incompressible isotropic elastomers: the Arruda-Boyce form, the Marlow form, the Mooney-Rivlin form, the neo-Hookean form, the Ogden form, the polynomial form, the reduced polynomial form, the Yeoh form, and the Van der Waals form. As will be pointed out below, the reduced polynomial and Mooney-Rivlin models can be viewed as particular cases of the polynomial model; the Yeoh and neo-Hookean potentials, in turn, can be viewed as special cases of the reduced polynomial model [18]. Thus, we will occasionally refer collectively to these models as "polynomial models".

5.2 NON-LINEARITY MATERIAL

Non-linearities materials occur in solid mechanics when the relationship between stress and strain, otherwise known as the constitutive relationship of the material, is no longer linear. The direct proportionality of stress and strain can no longer be assumed, as it is in the simple linear elastic case.

The constitutive relationship may now be a function of the combined or individual stress, strain or strain rate and may also be path dependent with regard to the load history.

The variation of the constitutive relationship also causes the stiffness of the structure or component consisting of the non-linear material to vary also.

Thus the stiffness of the structure or component may vary as a function of the combined or individual load level and load history.

To describe a particular case of non-linear material behavior in solid mechanics must be adopted a suitable model.

Non-linear material models describe the macroscopic behavior of the material, hence they are approximations to the real behavior of the material as the real behavior is also related to micro-mechanical effects within the material.

It is possible to classify non-linear material behavior in solid mechanics into two categories, rate independent and rate dependent.

Rate independent materials non-linearity are assumed independent of time, while the rate dependent materials non-linearity are assumed dependent of time.

The rate dependence for same material under specific loading conditions is such that it can be neglected, without reasonable loss of accuracy.

A case of non-linearity material in solid mechanics for which rate independence is assumed is non-linear elastic behavior, where the stress is not linearly related to the strain. In this case the deformation is recoverable and no energy is lost from the system.

A particular case is the hyper-elastic behavior of materials such as rubber, where the stresses are a function of a strain dependent constitutive relationship.

A simple non-linear elastic relationship is illustrated in Figure 5–1, which indicates the conservative nature of the non-linear stress-strain relationship, as it follows the same path through loading and unloading [17].

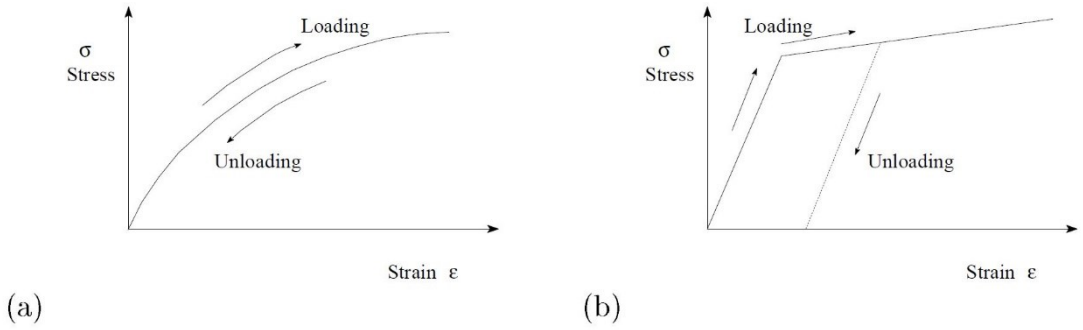

Figure 5–1 Non-linear stress-strain relationships. (a) Non-linear elasticity and (b) elasto-plasticity [17].

5.3 HYPERELASTIC CONSTITUTIVE MODEL

The hyperelastic constitutive models are mathematical models that attempt to simulate the behavior of materials whose stress strain relationship is non-linear.

This type of constitutive laws are used to model materials that respond elastically when subjected to very large strains, then to simulate the material properties a large displacement theory should be considered.

A hyperelastic material is still an elastic material, which means it returns to its original shape after the forces have been removed. It is also Cauchy-elastic, which means that the stress is determined by the current state of deformation and not history or path of deformation.

The difference between linear elastic and a hyperelastic material is the fact that, in the second one, the stress-strain relation derives from a strain energy density function and not a constant factor.

The concept of a strain energy function could be described with the example of a non-linear elastic bar [19]:

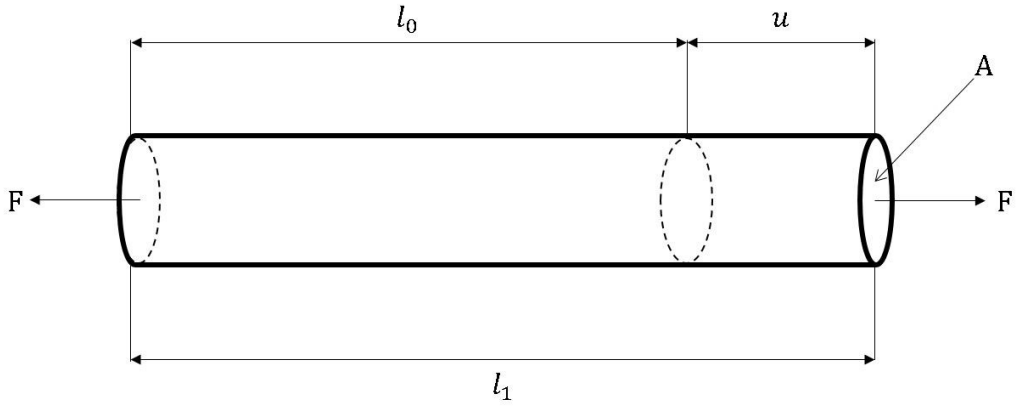

Figure 5–2 Non-linear elastic bar.

In order to analyse hyperelastic materials the conventional strain (ε) is often replaced by the so-called stretch (λ), which is defined by a quotient between the current (l_1) and the original (l_0) length [19]:

$$\lambda = \frac{l_1}{l_0} = \frac{l_0 + (l_1 - l_0)}{l_0} = \frac{l_0 + u}{l_0} = 1 + \varepsilon \tag{5.1}$$

The strain energy density is defined as a function, $W(\lambda)$, describing the strain energy density per undeformed volume of the bar.
The total strain energy, U, is thus expressed by multiplying $W(\lambda)$ with the undeformed volume [19]:

$$U = Al_0W(\lambda) \tag{5.2}$$

The incremental work done by the external force, F, should be equal to the increment in total strain energy. Hence, the energy balance is stated as [19]:

$$Fdu = dU \tag{5.3}$$

The increment in total strain energy can be expressed by the use of $W(\lambda)$ [19]:

$$dU = Al_0 \frac{dW(\lambda)}{d\lambda} d\lambda \tag{5.4}$$

The displacement increment can also be written in terms of stretch by using [19]:

$$\lambda = \frac{l_0 + u}{l_0} \Leftrightarrow u = (\lambda - 1)l_0 \tag{5.5}$$

Differentiating u gives [19]:

$$du = l_0 d\lambda. \tag{5.6}$$

Inserting them into the energy balance equation yields [19]:

$$Fl_0 d\lambda = Al_0 \frac{dW(\lambda)}{d\lambda} d\lambda \Leftrightarrow \frac{F}{A} = \frac{dW(\lambda)}{d\lambda} \Leftrightarrow \sigma_{nom} = \frac{dW(\lambda)}{d\lambda} \tag{5.7}$$

Based on this one-dimensional example, it is demonstrated that the stress can be obtained directly from the strain energy function. In a multi-axial case, the stresses are found in a similar manner from the strain energy density function. In that situation, the strain measured used is the left Cauchy-Green deformation tensor, $\boldsymbol{B}$.

A general assumption is that W depends on all of the components of the strain measure, giving [19]:

$$W = W(\boldsymbol{B}) \tag{5.8}$$

However, the state of deformation is fully determined by the principal stretches and the principal directions (n). In an isotropic material the three principal stretches are independent of the principal directions and consequently the strain energy density function can be written [19]:

$$W = W(\lambda_1, \lambda_2, \lambda_3, n_1, n_2, n_3) = W(\lambda_1, \lambda_2, \lambda_3) \tag{5.9}$$

In order to obtain the principal stretches it is necessary to find the roots of the characteristic polynomial of $\boldsymbol{B}$. Since it is easier to obtain the coefficients of the characteristic polynomial, instead of using the principal stretches we could therefore express W as function of the strain invariants, where J is the total volume ratio [19].

$$W = W(I_1, I_2, I_3) \tag{5.10}$$

$$\begin{cases} I_1 = tr(\boldsymbol{B}) = {\lambda_1}^2 + {\lambda_2}^2 + {\lambda_3}^2 \\ I_2 = \frac{1}{2}(tr(\boldsymbol{B})^2 - tr\,(\boldsymbol{B}^2)) = {\lambda_1}^2{\lambda_2}^2 + {\lambda_1}^2{\lambda_3}^2 + {\lambda_2}^2{\lambda_3}^2 \\ I_3 = \det(\boldsymbol{B}) = {\lambda_1}^2{\lambda_2}^2{\lambda_3}^2 = J^2 \end{cases} \tag{5.11}$$

For nearly incompressible materials, a more convenient set of invariants of $\boldsymbol{B}$ could be used, since the deviatoric (W_d) and the volumetric (W_v) terms of the strain energy function are split.

As a result, W_d is the strain energy necessary to change the shape and W_v is the strain energy necessary to change the volume, so under a pure volume change, I_1 and I_2 remain constant [19].

$$\begin{cases} \bar{I}_1 = J^{-\frac{2}{3}} I_1 \\ \bar{I}_2 = J^{-\frac{4}{3}} I_2 \\ \bar{I}_3 = \sqrt{\det(\boldsymbol{B})} = 1 \end{cases} \tag{5.12}$$

Therefore, the stress-strain law for an isotropic hyperelastic material could be derived from the strain energy density function considering an energy balance equation in the same way as in the initial example of the elastic bar [19].

The results are derived below [20]:

- Strain energy density in terms of I_1, I_2, I_3

$$\sigma_{ij} = \frac{2}{\sqrt{I_3}}\left[\left(\frac{\partial W}{\partial I_1} + I_1 \frac{\partial W}{\partial I_2}\right) B_{ij} - \frac{\partial W}{\partial I_2} B_{ik} B_{kj}\right] + 2\sqrt{I_3}\frac{\partial W}{\partial I_3}\delta_{ij} \tag{5.13}$$

- Strain energy density in terms of $\bar{I}_1, \bar{I}_2, J$

$$\begin{aligned} \sigma_{ij} = \frac{2}{J}\Bigg[\frac{1}{J^{2/3}}\left(\frac{\partial \bar{W}}{\partial \bar{I}_1} + \bar{I}_1 \frac{\partial \bar{W}}{\partial \bar{I}_2}\right) B_{ij} - \left(\bar{I}_1 \frac{\partial \bar{W}}{\partial \bar{I}_1} + 2\bar{I}_2 \frac{\partial \bar{W}}{\partial \bar{I}_2}\right)\frac{\delta_{ij}}{3} \\ - \frac{1}{J^{4/3}} \frac{\partial \bar{W}}{\partial \bar{I}_2} B_{ik} B_{kj}\Bigg] + \frac{\partial \bar{W}}{\partial J}\delta_{ij} \end{aligned} \tag{5.14}$$

- Strain energy density in terms of $\lambda_1, \lambda_2, \lambda_3$

$$\begin{aligned} \sigma_{ij} = \frac{\lambda_1}{\lambda_1\lambda_2\lambda_3}\frac{\partial \widetilde{W}}{\partial \lambda_1} b_i^{(1)} b_j^{(1)} + \frac{\lambda_2}{\lambda_1\lambda_2\lambda_3}\frac{\partial \widetilde{W}}{\partial \lambda_2} b_i^{(2)} b_j^{(2)} \\ + \frac{\lambda_3}{\lambda_1\lambda_2\lambda_3}\frac{\partial \widetilde{W}}{\partial \lambda_3} b_i^{(3)} b_j^{(3)} \end{aligned} \tag{5.15}$$

These stress-strain law are strongly non linear.

Let $\boldsymbol{b_1}, \boldsymbol{b_2}, \boldsymbol{b_3}$ denote three, mutually perpendicular unit eigenvectors of $\boldsymbol{B}$ [20].

Most of the hyperelastic constitutive models can be grouped in two broad categories: phenomenological and micromechanical models, see Figure 5–3. Since the physical significance of micro-mechanical material constants is often unclear, the use of phenomenological model is suggested [19].

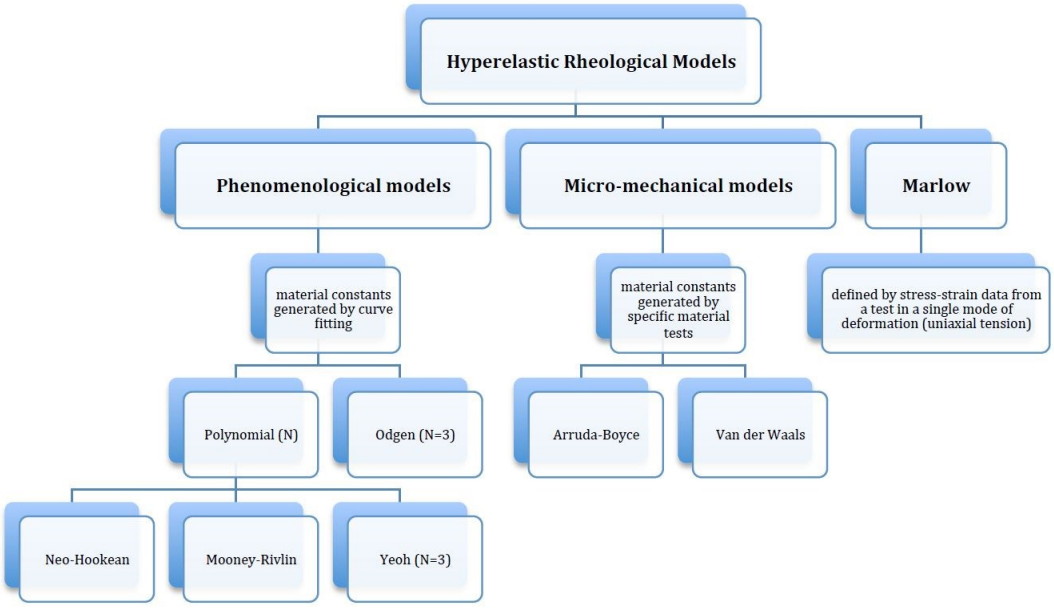

Figure 5–3 Hyperelastic constitutive models.

All hyperelastic models are based on the assumption of isotropic behavior throughout the deformation history [18].

5.3.1 FULL POLYNOMIAL MODEL

A general form of a strain energy density function, implemented not only in Abaqus but also in most of the finite element software's is the polynomial form, given by the following series expansion [18]:

$$\begin{aligned}\bar{W} &= \sum_{i+j=1}^{N} C_{ij}(\bar{I}_1 - 3)^i (\bar{I}_2 - 3)^j + \sum_{i=1}^{N} \frac{1}{D_i}(J_{el} - 1)^{2i} \\ &= \bar{W}_d(\bar{I}_1, \bar{I}_2) + \bar{W}_v(J_{el})\end{aligned} \tag{5.16}$$

Where C_{ij} and D_i are temperature-dependent material parameters, while J_{el} is the elastic volume ratio. The sum is formally written as a sum to infinity but, usually, only a few terms are considered [18]:

$$\begin{aligned}\bar{W} = {} & C_{10}(\bar{I}_1 - 3) + C_{01}(\bar{I}_2 - 3) + C_{20}(\bar{I}_1 - 3)^2 \\ & + C_{11}(\bar{I}_1 - 3)(\bar{I}_2 - 3) + C_{02}(\bar{I}_2 - 3)^2 \\ & + C_{30}(\bar{I}_1 - 3)^2 + C_{21}(\bar{I}_1 - 3)^2(\bar{I}_2 - 3) \\ & + C_{12}(\bar{I}_1 - 3)(\bar{I}_2 - 3)^2 + C_{03}(\bar{I}_2 - 3)^2 + \cdots \\ & + \sum_{i=1}^{N} \frac{1}{D_i}(J_{el} - 1)^{2i}\end{aligned} \tag{5.17}$$

Regardless of the value of N, the initial shear modulus (μ_0) and the initial bulk modulus (K_0) depend only on the polynomial coefficients of the first order ($N = 1$).

$$\mu_0 = 2(C_{10} + C_{01}) \tag{5.18}$$

$$K_0 = \frac{2}{D_1} \tag{5.19}$$

Only isotropic thermal expansion is permitted with the hyperelastic material model. The elastic volume ratio, J_{el}, relates the total volume ratio, J, and the thermal volume ratio, J_{th} [18]:

$$J_{el} = \frac{J}{J_{th}} \tag{5.20}$$

J_{th} is given by [18]:

$$J_{th} = (1 + \varepsilon_{th})^3 \tag{5.21}$$

Where ε_{th} is the linear thermal expansion strain.

5.3.2 NEO-HOOKEAN MODEL

Taking only the first term in the series yields to the Neo-Hooke form, which was first derived from statistical mechanics by considering the molecular structure of rubbers [18].

$$\bar{W} = C_{10}(\bar{I}_1 - 3) + \frac{1}{D_1}(J_{el} - 1)^2 \tag{5.22}$$

The initial shear modulus (μ_0) is given by [18]:

$$\mu_0 = 2C_{10} \tag{5.23}$$

While the initial bulk modulus (K_0) is given by the same relation (5.19).

5.3.3 MOONEY-RIVLIN MODEL

If only the linear terms in the deviatoric strain energy are retained $(N = 1)$, the Mooney-Rivlin is obtained [18]:

$$\bar{W} = C_{10}(\bar{I}_1 - 3) + C_{01}(\bar{I}_2 - 3) + \frac{1}{D_1}(J_{el} - 1)^2 \tag{5.24}$$

The Mooney-Rivlin form can be viewed as an extension of the Neo-Hookean form, where a term that depends on the second invariant of the left Cauchy-Green tensor is added. The initial shear modulus (μ_0) and the initial bulk modulus (K_0) is given by the same relation, respectively (5.18) and (5.19).

5.3.4 YEOH MODEL

By setting specific coefficients to zero, particular forms of the polynomial function could be obtained. The reduced polynomial form is obtained if all C_{ij} with $j \neq 0$ are set to zero. The Yeoh form is a special case of the reduced polynomial with $N = 3$ and it depends only on the first strain invariant [18].

$$\begin{aligned}\bar{W} = C_{10}(\bar{I}_1 - 3) + C_{20}(\bar{I}_1 - 3)^2 + C_{30}(\bar{I}_1 - 3)^3 + \frac{1}{D_1}(J_{el} - 1)^2 \\ + \frac{1}{D_2}(J_{el} - 1)^4 + \frac{1}{D_3}(J_{el} - 1)^6\end{aligned} \tag{5.25}$$

The initial shear modulus (μ_0) and the initial bulk modulus (K_0) is given by the same relation, respectively (5.23) and (5.19).

5.3.5 OGDEN MODEL

The Ogden model expresses the strain energy function in terms of principal stretches and it cannot be compared with the polynomial form, except for a specific choice of constants [18].

$$\widetilde{W} = \sum_{i=1}^{N} \frac{2\mu_i}{\alpha_i^2}\left(\bar{\lambda}_1^{\alpha_i} + \bar{\lambda}_2^{\alpha_i} + \bar{\lambda}_3^{\alpha_i} - 3\right) + \sum_{i=1}^{N} \frac{1}{D_i}(J_{el} - 1)^{2i} \qquad (5.26)$$

Where $\bar{\lambda}_i$ are the deviatoric principal stretches given by [18]:

$$\bar{\lambda}_i = J^{-\frac{1}{3}}\lambda_i \qquad (5.27)$$

While λ_i are the principal stretches and μ_i, α_i, D_i are temperature-dependent material parameters.

For $N = 1$ and $\alpha_1 = 2$ the Neo-Hook model is obtained and for $N = 2$, $\alpha_1 = 2$ and $\alpha_2 = 2$ the Mooney-Rivlin model is obtained.

The initial bulk modulus, K_0, depends on D_1 as before and the initial shear modulus, μ_0, depends on all coefficients [18]:

$$\mu_0 = \sum_{i=1}^{N} \mu_i \qquad (5.28)$$

5.3.6 ARRUDA-BOYCE MODEL

The Arruda-Boyce potential depends only on the first invariant and it is based on statistical mechanics [18].

$$\bar{W} = \mu\left\{\frac{1}{2}(\bar{I}_1 - 3) + \frac{1}{20\lambda_m^2}\left(\bar{I}_1{}^2 - 9\right) + \frac{11}{1050\lambda_m^4}\left(\bar{I}_1{}^3 - 27\right) + \frac{19}{7000\lambda_m^6}\left(\bar{I}_1{}^4 - 81\right) + \frac{519}{673750\lambda_m^8}\left(\bar{I}_1{}^5 - 243\right)\right\} + \frac{1}{D}\left(\frac{J_{el}{}^2 - 1}{2} - \ln J_{el}\right) \quad (5.29)$$

Where λ_m is the locking stretch, which is the stretch at which stress starts to increase without limit. If λ_m tends to infinite, the Arruda-Boyce form becomes the Neo-Hookean form.

The initial shear modulus, (μ_0), is related to (μ) with the expression [18]:

$$\mu_0 = \mu\left(1 + \frac{3}{5\lambda_m^2} + \frac{99}{175\lambda_m^4} + \frac{513}{875\lambda_m^6} + \frac{42039}{67375\lambda_m^8}\right) \quad (5.30)$$

The initial bulk modulus is related to D with the expression [18]:

$$K_0 = \frac{2}{D} \quad (5.31)$$

5.3.7 VAN DER WAALS MODEL

The Van der Waals potential, also known as the Kilian model, has the following form [18]:

$$\bar{W} = \mu\left\{-(\lambda_m^2 - 3)[\ln(1-\eta) + \eta] - \frac{2}{3}a\left(\frac{\tilde{I}-3}{2}\right)^{\frac{3}{2}}\right\} + \frac{1}{D}\left(\frac{{J_{el}}^2 - 1}{2} - \ln J_{el}\right) \tag{5.32}$$

Where

$$\tilde{I} = (1-\beta)\bar{I}_1 + \beta\bar{I}_2 \tag{5.33}$$

And

$$\eta = \sqrt{\frac{\tilde{I}-3}{\lambda_m^2 - 3}} \tag{5.34}$$

Here, a is the global interaction parameter, β is an invariant mixture parameter and D governs the compressibility.
The initial shear modulus (μ_0) is given by [18]:

$$\mu_0 = \mu \tag{5.35}$$

While the initial bulk modulus is related to D with the same expression (5.31).
In contrast to the Arruda-Boyce model the mathematical structure of the Van der Waals potential is such that the strain energy tends to infinity as the locking stretch is reached.

Thus, stretches larger than the locking stretch cannot be used in the Van der Waals potential.

5.3.8 MARLOW MODEL

The form of the Marlow strain energy potential is [18]:

$$\bar{W} = \bar{W}_d(\bar{I}_1) + \bar{W}_v(J_{el}) \tag{5.36}$$

The deviatoric part of the potential is defined by providing either uniaxial, equibiaxial, or planar test data; while the volumetric part is defined by providing the volumetric test data, defining the Poisson's ratio, or specifying the lateral strains together with the uniaxial, equibiaxial, or planar test data [18]. The Marlow model assumes that the strain energy potential is independent of the second deviatoric invariant $\bar{I}_2$. This model is defined by providing test data that define the deviatoric behavior, and, optionally, the volumetric behavior if compressibility must be taken into account. Abaqus will construct a strain energy potential that reproduces the test data exactly, as shown in Figure 5–4.

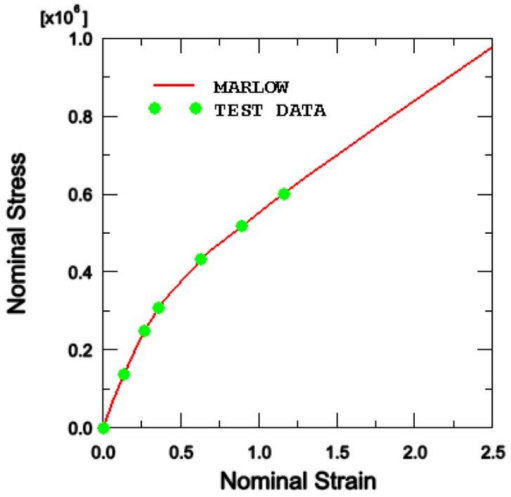

Figure 5–4 The results of the Marlow model with test data [18].

The interpolation and extrapolation of stress-strain data with the Marlow model is approximately linear for small and large strains. For intermediate strains in the range 0.1 to 1.0 a noticeable degree of nonlinearity may be observed in the interpolation/extrapolation with the Marlow model; for example, some nonlinearity is apparent between the 4th and 5th data points in Figure 5–4. To minimize undesirable nonlinearity, make sure that enough data points are specified in the intermediate strain range.

Generally, when data from multiple experimental tests are available (typically, this requires at least uniaxial and equibiaxial test data), the Ogden and Van der Waals forms are more accurate in fitting experimental results. If limited test data are available for calibration, the Arruda-Boyce, Van der Waals, Yeoh, or reduced polynomial forms provide reasonable behavior. When only one set of test data (uniaxial, equibiaxial, or planar test data) is available, the Marlow form is recommended. In this case a strain energy potential is constructed that will reproduce the test data exactly and that will have reasonable behavior in other deformation modes [18]. Figure 5–5 and Figure 5–6 are examples of how hyperelastic constitutive models reproduce the tested curve.

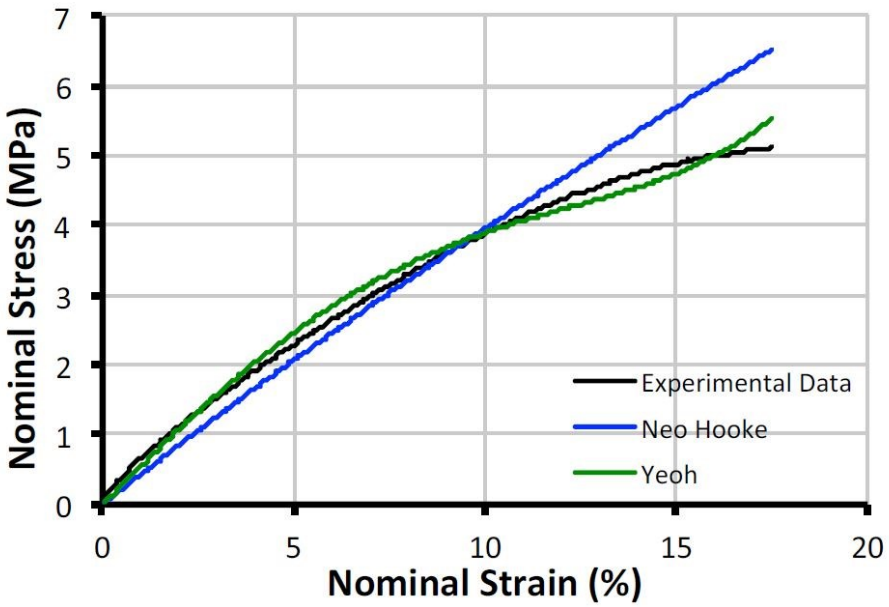

(a)

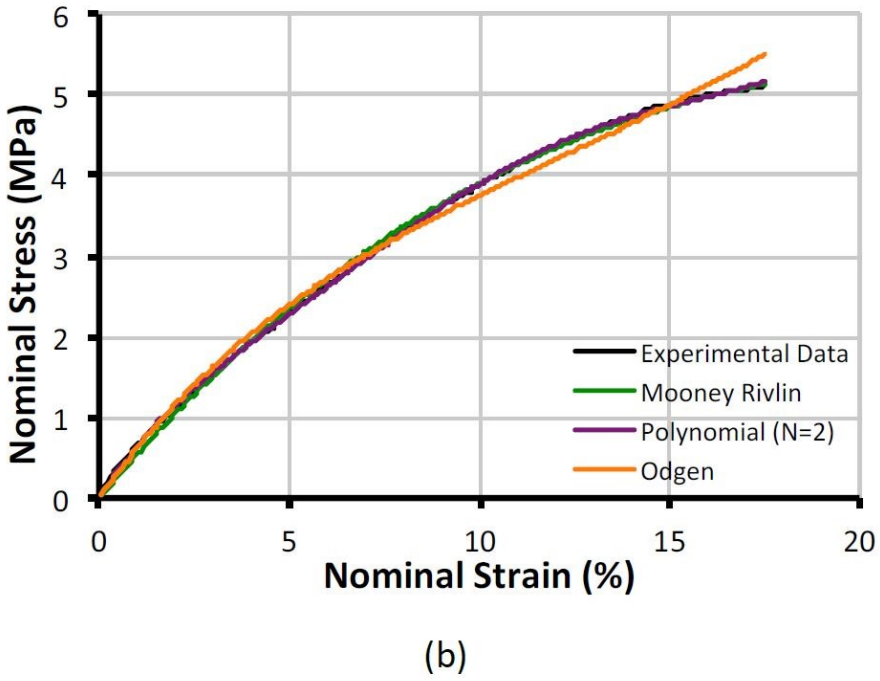

Figure 5–5 Numerical Fitting for the (a) reduced polynomial (b) polynomial and Ogden strain energy functions [19].

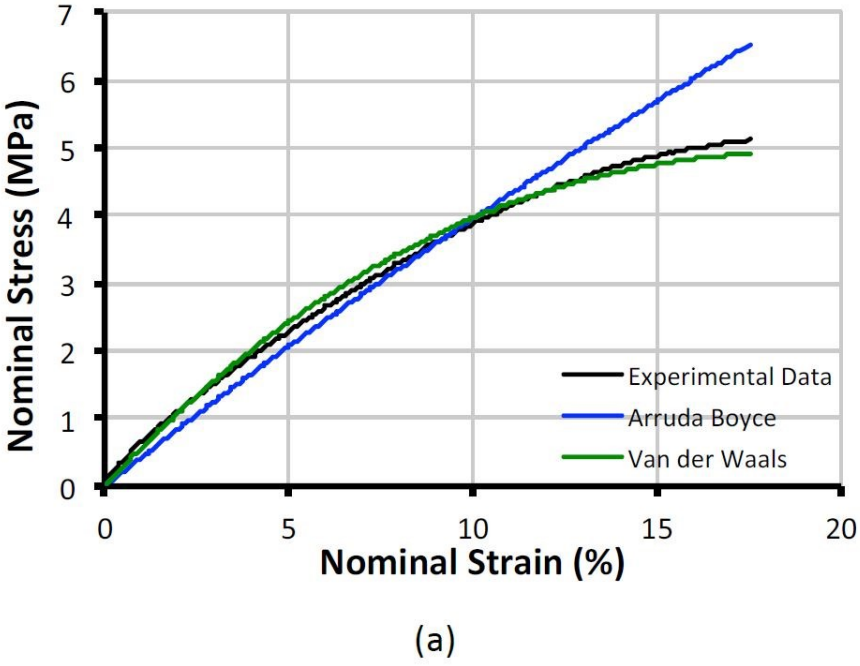

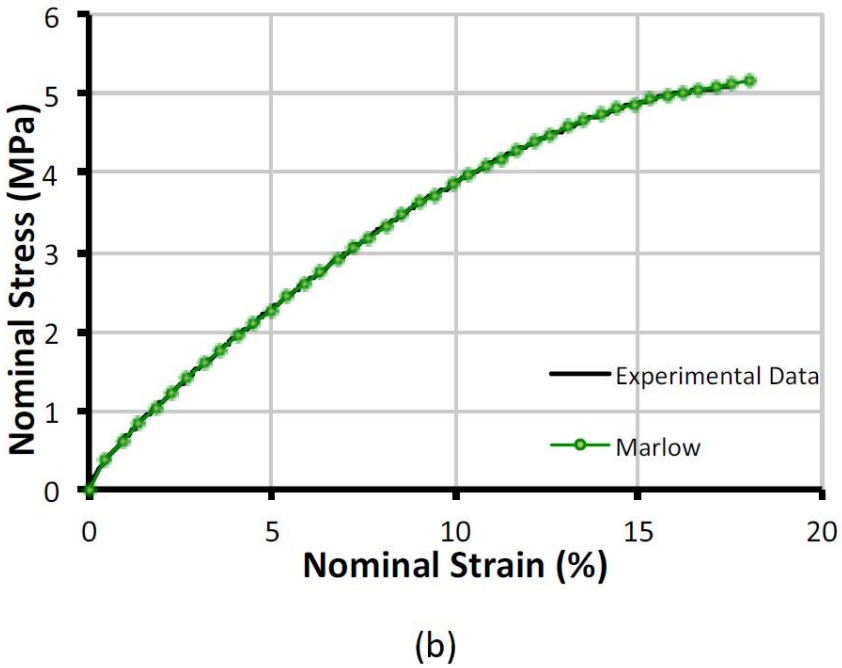

Figure 5–6 Numerical Fitting for the (a) Arruda-Boyce, Van der Waals and (b) Marlow strain energy functions [19].

Although hyperelastic constitutive models are the best models to reproduce the nonlinear behavior of these ones and the selection of a proper constitutive model remains an engineering challenge to be solved since the behavior of the material has a good fit with any hyperelastic model.

6 FULL SCALE IMPACT TEST

6.1 INTRODUCTION

This chapter shows the types of fishing devices and their iteration with the pipeline on the seabed. The fishing device induces a strong dynamic load to the pipeline, in particular the infill material used in the field joint area is designed to withstand at the dynamic load transferring as little as possible to the pipe.
The field joint coating is subjected to resistance checks by an impact test that simulates the interference between the fishing device and the pipe.
Therefore, the phases necessary to the coating of the field joint area and the impact test are showed below.

6.2 INTERFERENCE BETWEEN TRAWL GEAR AND PIPELINE

Fishing activities such as bottom trawling shall be considered for offshore pipelines for two main reasons:

1) Possible hazard and inconvenience to the fishermen in case of trawl gear hooking to the pipeline, and
2) Possible hazard to the integrity of the pipeline due to loads from the trawl gear.

Equipment used for bottom trawling can expose a pipeline to substantial loads that may damage it. Such load is associated with the instantaneous impact and the subsequent pull-over as the trawl gear hits and is dragged over the pipeline. In addition, hooking of trawl equipment may impose considerable loading to the pipeline [21].
Typical trawl gears are illustrated in Figure 6–1 to Figure 6–3.

Figure 6–1 shows a typical otter trawl. The otter trawl board holds the trawl net open by hydrodynamic forces. Such trawl boards are dragged along the seabed and may represent a hazard to the pipeline [21]. In beam trawling, a transverse steel beam is used to keep the net open as shown in Figure 6–2. Beam shoes are mounted at each end of the beam and represent a substantial hazard to pipelines due to their sharp edges and large kinetic energy.

In twin trawling the clump weight shown in Figure 6–3 has a mass typically in the range of 2 to 9 tonnes, and can cause larger impact energy and pull-over loads than trawl boards.

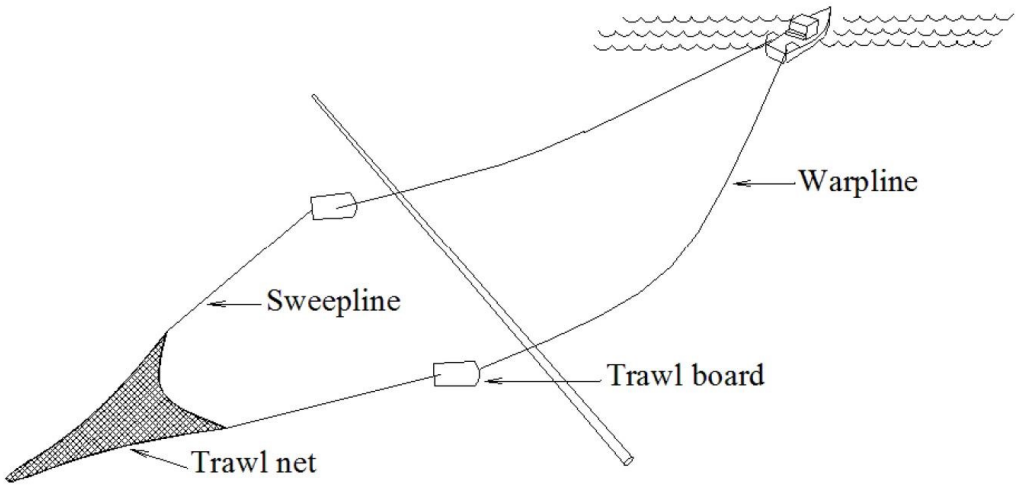

Figure 6–1 Typical otter trawl gear crossing a pipeline [21].

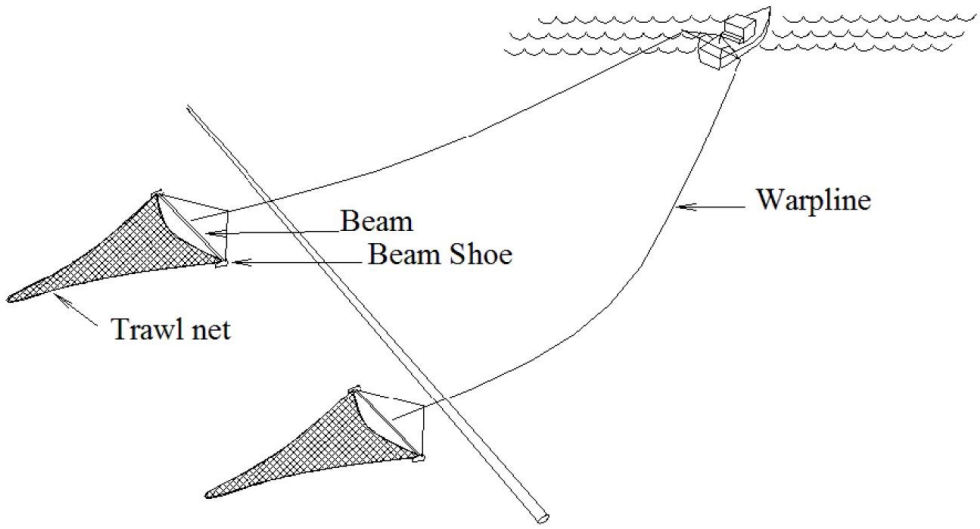

Figure 6–2 Typical beam trawl gear crossing a pipeline [21].

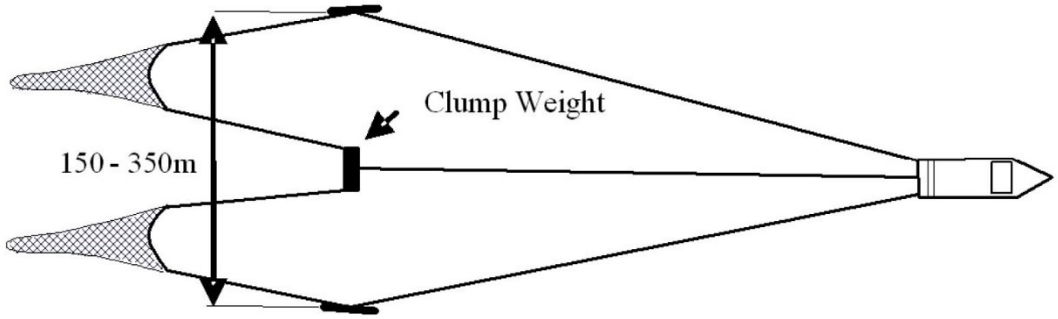

Figure 6–3 Typical twin trawling with clump-weight [21].

Several designs are used, ranging from a clump of chain to spherical or cylindrical rollers. Twin trawling with clump weight is currently not used for industrial trawling, and is hence only relevant in consumption trawl areas

Traditionally, pipelines are protected against trawl impact by coating, gravel or burial. As such protection is expensive, there is a need for improvement with respect to design methods and rules for trawl gear interference [21].

6.3 COATING IMPACT TESTING

The offshore pipeline are design to withstand to dynamics loads due to trawl gear through a external coating in CWC (see paragraph 3.4) and a field joint coating with infill material (see paragraph 3.5 and chapter 4).
In particular, the pipeline subjected testing has the following characteristics:

Description	Unit	30″ Oil Export Pipeline
		Offshore
		3LPE+CWC
Length of Pipe	[m]	6
Pipe Material	[-]	DNV-SAWL-450
Pipe Steel ID	[mm]	685.8
WT	[mm]	38.1
External Anticorrosion Coating	[-]	3LPE
Anticorrosion Thickness	[mm]	4.2
Anticorrosion Cutback	[mm]	150 -0/+20
Concrete Coating Thickness	[mm]	50
Concrete Coating Cutback	[mm]	370 -0/+20
Field Joint Coating & Infill Material	[-]	HSS+Solid PU
HSS Thickness	[mm]	≥1.5
Max Design Temp	[°C]	80

Table 6–1 Pipe properties.

To withstand impacts, particularly in the field joint coating area, specific materials are used to absorb and adequately release the impact energy, transferring as little as possible to the pipe.

In this thesis solid PU infill material is investigated, that is mixture of polyol and isocyanate. Full scale impact test are performed to characterize the behavior of these materials.

The test is divided into two macro phases:

1) Application of a complete field joint coating systems;
2) Impact test on field joint coating.

A complete FJC system was applied to a 6 meter CWC with the following application:

a) Blast cleaning of the steel (Figure 6–4);
b) Manual preheat of steel using propane torches (Figure 6–5);
c) Manual application of HSS using propane torches (Figure 6–6);
d) Application of bubble wrap around the ends of the joint (Figure 6–7);
e) Injection of solid PU into the preheated mould using propane torches (Figure 6–8);
f) Completed field joint coating (Figure 6–9).

Figure 6–4 Blast cleaning.

Figure 6–5 Preheat.

Figure 6–6 HSS application.

Figure 6–7 Bubble wrap application.

Figure 6–8 Mould application.

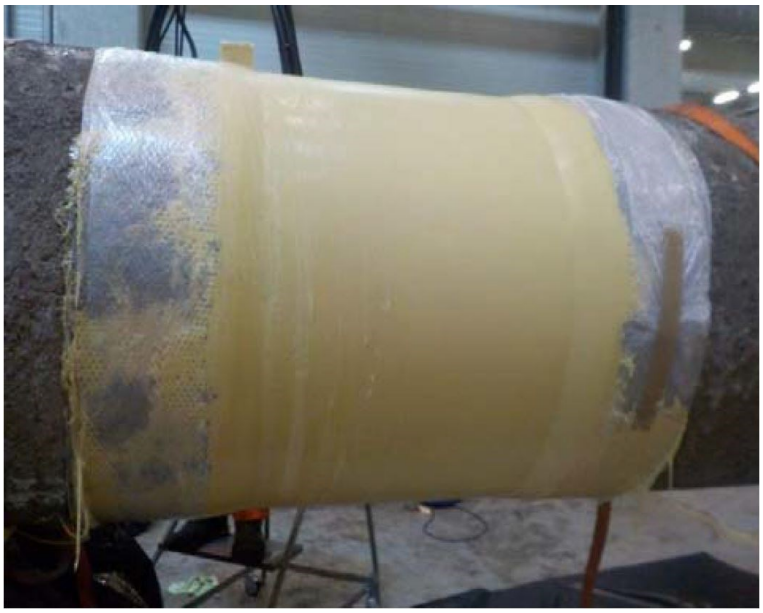

Figure 6–9 Complete FJC with infill material.

Once the field joint coating is completed, it passes to its test.

Full scale impact test consists in dropping a mass of 2.15 tons from a given height to guarantee an energy of 9500 J (see Figure 6–10).

A single 9500 J impact is given at the center of the field joint coating.

The height is determined from definition of potential energy (E_p):

$$E_p = mgh \Leftrightarrow h = \frac{E_p}{mg} = \frac{9500\ [J]}{2150\ [Kg] \cdot 9.81\ \left[\frac{m}{s^2}\right]} = 0.450\ [m] \qquad (6.1)$$

The field joint coating is subsequently inspected for analyzing the footprint depth released by the impact or the presence of any damage.

The results obtained from the test showed (see Figure 6–11):

- Absence of damage to the field joint coating;
- Depth of the footprint of about 2 mm.

Figure 6–10 Impact machine.

Figure 6–11 Footprint due to impact test.

7 FEA ANALYSES

7.1 INTRODUCTION

In this chapter is exposed the Abaqus software used to implemented the full scale impact test to the finite elements, using the basic data.
The development of the FE model is obtained considering the same geometries, loads and constrains used during impact test. In particular, it shows the assumptions, simplifications and the methodology necessary to reproduce faithfully the full scale impact test to the finite elements. Finally is exposed the analysis setup procedure and the post-processing of the FEA results.

7.2 ABAQUS

Finite element analysis (FEA) has been performed to faithfully reproduce the full scale impact test using the Abaqus software.
Abaqus FEA (formerly Abaqus) is a software suite for finite element analysis and computer-aided engineering. The name and logo of this software are based on the abacus calculation tool.
The Abaqus products use the open-source scripting language Python for scripting and customization.
Abaqus is used in the automotive, aerospace, and industrial products industries.
The product is popular with non-academic and research institutions in engineering due to the wide material modeling capability, and the program's ability to be customized, for example, users can define their own material models so that new materials could

also be simulated in Abaqus. Abaqus also provides a good collection of multiphysics capabilities, such as coupled acoustic-structural, piezoelectric, and structural-pore capabilities, making it attractive for production-level simulations where multiple fields need to be coupled [22].

Abaqus was initially designed to address non-linear physical behavior; as a result, the package has an extensive range of material models such as elastomeric (rubberlike) and hyperelastic (soft tissue) material capabilities.

Every complete finite-element analysis consists of 3 separate stages (see Figure 7–1):

1) *Pre-processing* or *modeling*: This stage involves creating an input file which contains an engineer's design for a finite-element analyzer (also called "solver").
2) *Processing* or *finite element analysis*: This stage produces an output visual file.
3) *Post-processing* or generating report, image, animation, etc. from the output file: This stage is a visual rendering stage.

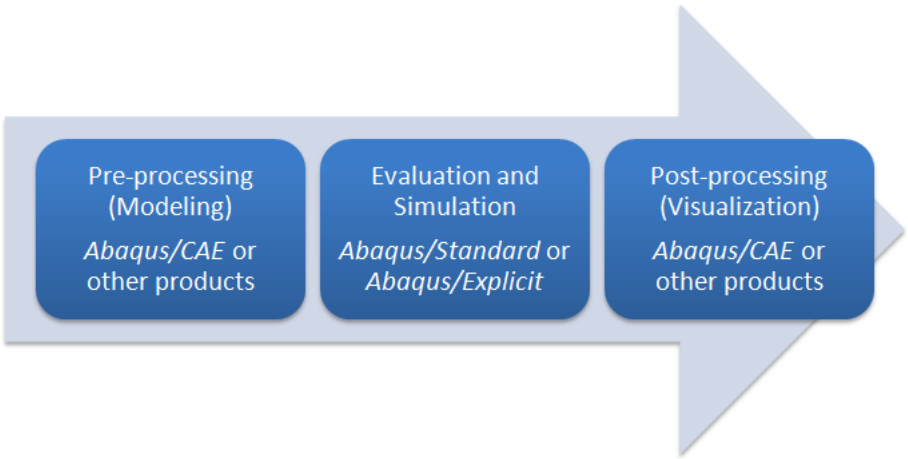

Figure 7–1 Three separate stages for a complete finite element analysis [22].

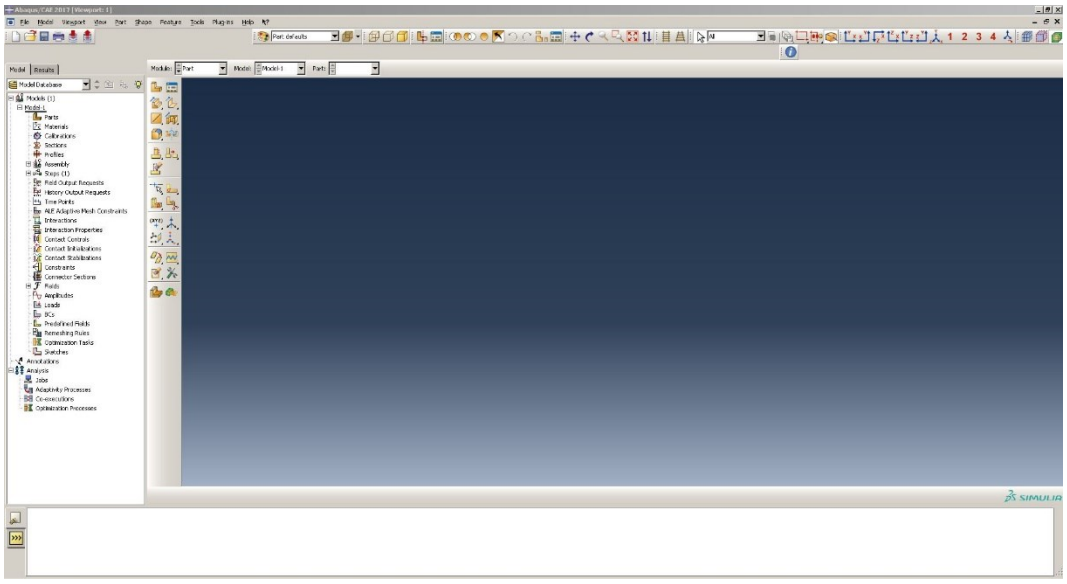

Figure 7–2 Screenshot of Abaqus/CAE 2017.

7.3 BASIC DATA

The basic data used to simulate the full scale impact test with Abaqus are summarized as follows. In particular they are reported:

- Pipeline material data;
- Field joint coating geometry;
- Infill material data;
- Full scale impact test results;

This data are necessary for reproduce faithfully the same conditions the full scale impact test.

7.3.1 PIPELINE MATERIAL DATA

Data for the 30” Oil Export pipeline are given in Table 7–1. Material properties are summarized in Table 7–2.

Item	Unit	Oil Export Pipeline
Nominal Diameter	[″]	30
Steel OD	[mm]	762
Wall Thickness	[mm]	38.1
Steel Material	[-]	DNV-450
Fabrication Method	[-]	SAWL
Corrosion Allowance	[mm]	0
Total OD Including Coating	[mm]	862

Table 7–1 30″ Oil Export pipeline.

Characteristics	Unit	DNV-450-SAWL
Density	[kg/m^3]	7850
Young's Modulus	[MPa]	$2.07 \cdot 10^5$
SMYS at 20°C	[MPa]	450
SMTS at 20°C	[MPa]	535
De-rated Yield Stress at 80°C	[MPa]	432
De-rated Tensile Stress at 80°C	[MPa]	517
Thermal Coefficient of Expansion	[°C^{-1}]	$11.7 \cdot 10^{-6}$
Poisson' s Ratio	[-]	0.3
External Corrosion Coating	[mm]	4.2
Concrete Weight Coating	[-]	50 mm concrete, density 2250 Kg/m^3, Young's Modulus 35000 MPa, Poisson's Ratio 0.15

Table 7–2 Material characteristics for DNV-450-SAWL.

When an engineering stress-strain curve is unavailable, the following approach might be consider as an alternative, that is the stress-strain of ferritic steels is derived from yield/proof strength, tensile strength and uniform elongation using the following method [23]:

$$\varepsilon = \frac{\sigma}{E} + \frac{A_r \sigma_y}{E}\left(\frac{\sigma}{\sigma_y}\right)^n \tag{7.1}$$

Where:

- ε is the total strain;
- σ is the stress;
- E is elastic modulus;
- A_r is a coefficient (Equation (7.2));
- σ_y is the yield strength;
- n is the strain hardening exponent (Equation (7.3)).

$$A_r = \frac{E\varepsilon_y}{\sigma_y} - 1 \tag{7.2}$$

$$n = \frac{\log[(E\varepsilon_u/\sigma_u) - 1] - \log\left[\left(E\varepsilon_y/\sigma_y\right) - 1\right]}{\log\left(\sigma_u/\sigma_y\right)} + 1 \tag{7.3}$$

Where:

- ε_y is the yield strain (total strain at which at σ_y is determined);
- σ_u is the ultimate tensile strength;
- ε_u is the uniform elongation strain at ultimate tensile strength.

If ε_u is not available, a value of 5% can be assumed [23].

An alternative to equation (7.3) is to derive the strain hardening exponent from the fallowing equation [23]:

$$N = \frac{1}{n} = 0.3\left(1 - \frac{\sigma_y}{\sigma_u}\right) \tag{7.4}$$

Equation (7.4) was derived from ferritic steel with yield/proof strengths in the range 300-1000 MPa and $0.65 < \sigma_y/\sigma_u < 0.95$. This is a lower bound estimate so underestimates the true hardening behaviour of the material, i.e. underestimates N [23]. True stress, σ_t, and true strain, ε_t, can be determined from engineering stress, σ, and strain, ε, as follows [23]:

$$\sigma_t = \sigma(1 + \varepsilon) \tag{7.5}$$

$$\varepsilon_t = \log(1 + \varepsilon) \tag{7.6}$$

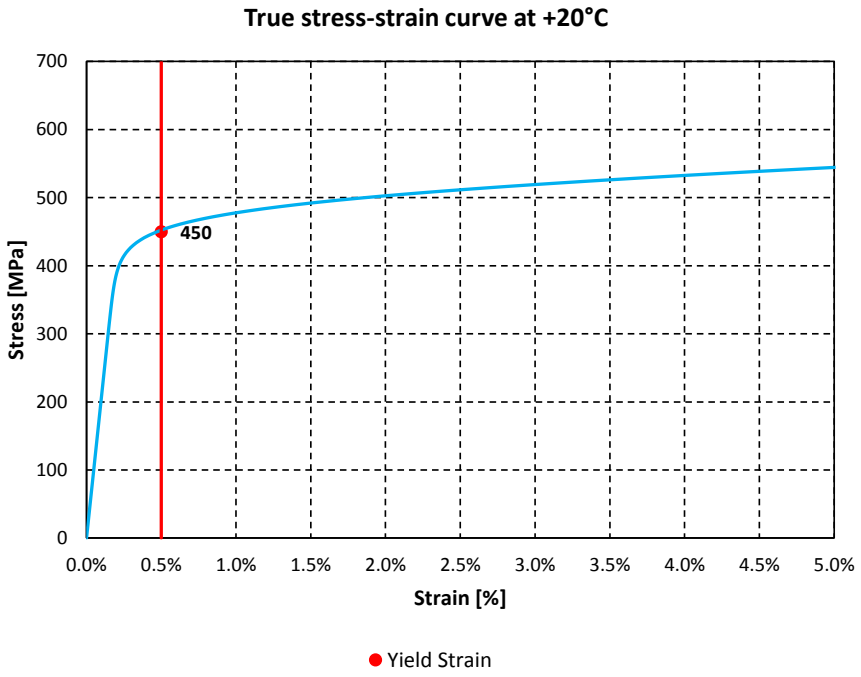

Figure 7–3 Curve of the pipeline material DNV-450.

7.3.2 FIELD JOINT COATING GEOMETRY

Detailed about field joint coating geometry are reported in Figure 7–4 and Figure 7–5.

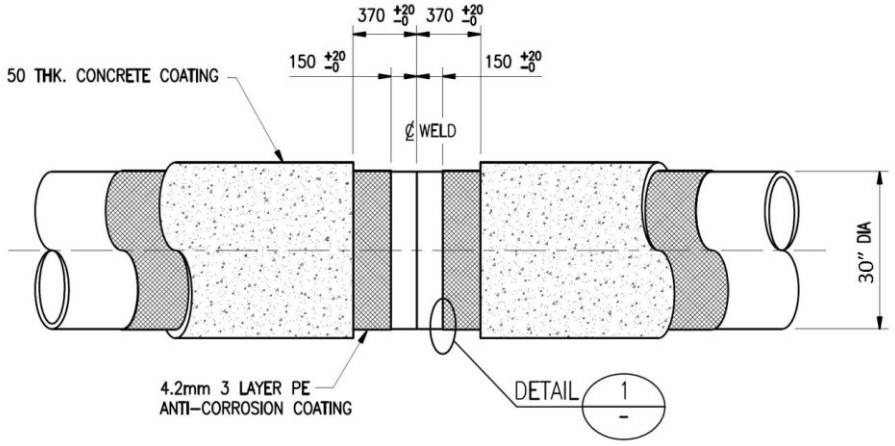

Figure 7–4 Coating initial arrangement.

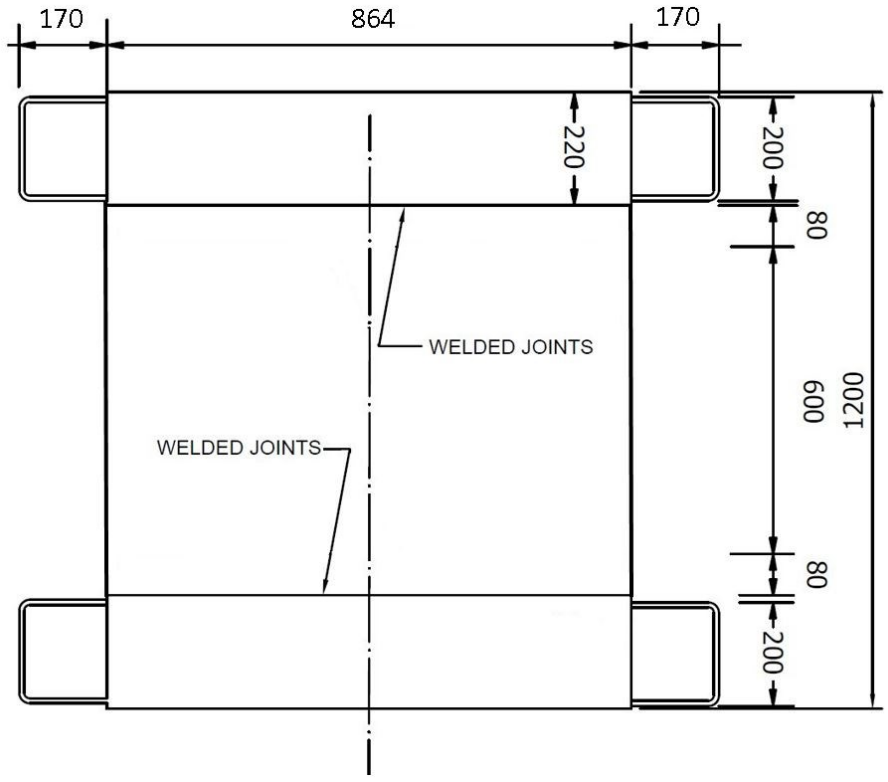

Figure 7–5 Field joint coating 30" ─ Mould details.

7.3.3 INFILL MATERIAL DATA

Several tensile and compression tests were performed on solid PU at various temperatures ranging from +20°C to 80°C, and all testing conditions were in accordance with ASTM D695-15 [24].

Since the impact test has been performed at room temperature, compressive testing results at 20°C have been considered more representative for FEA simulation.

The various compression tests results of solid PU showed different characteristics both in the elastic modulus and in the resistance characteristics, i.e. yield between 8-40 MPa, ultimate between 200-230 MPa and modulus of elasticity between 255-2000 MPa.

The Figure 7–6 shows the stress-strain material curves obtained during testing.

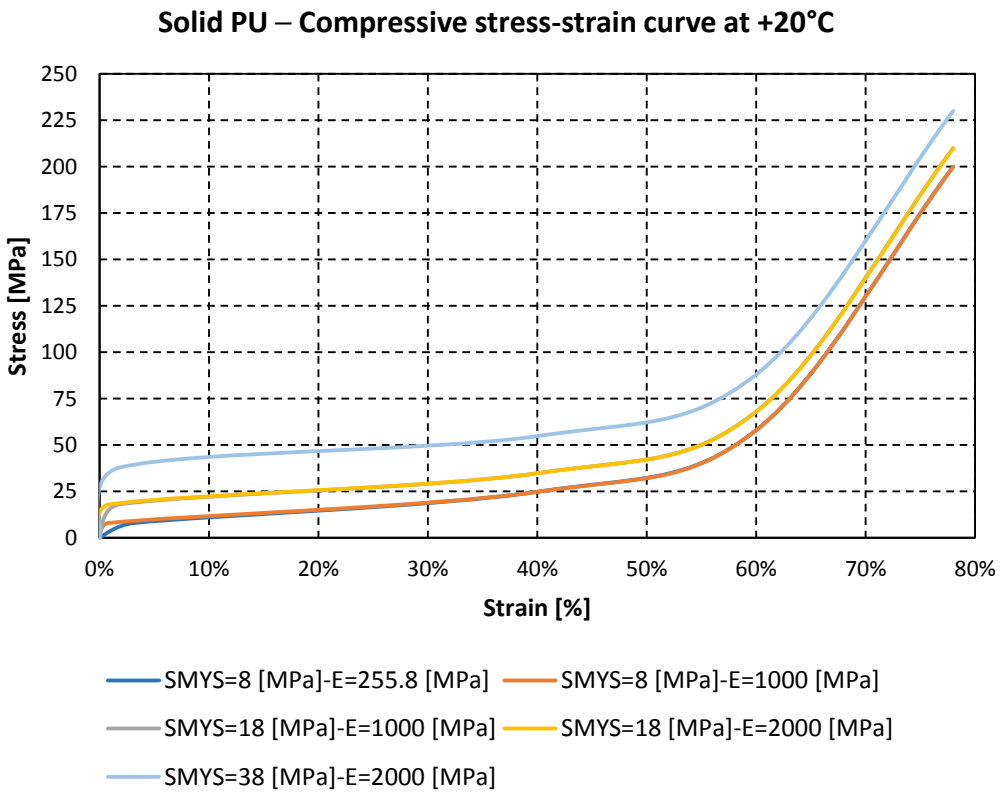

Figure 7–6 Curves of the infill material ─ ASTM D695-15.

The Figure 7–7 shows the samples, while Figure 7–8 shows the compression machine used for the test.

Figure 7–7 Compression test samples.

Figure 7–8 Compression test.

7.3.4 FULL SCALE IMPACT TEST RESULTS

A single impact in the central area of the field joint coating shows the following (see paragraph 6.3):

- Absence of damage to the field joint coating;
- Depth of the footprint of about 2 mm.

All the basic data are necessary to implement the finite element model of the full scale impact test.

7.4 FINITE ELEMENT MODEL DESCRIPTION

A 3-D finite element model has been developed with the aim to reproduce the interaction between pipeline and fishing devices.

The objective of the FEM analysis is to define the representative material model of solid polyurethane (infill material) to obtain the same footprint depth of test of about 2 mm.

A 3-D finite element model of the full scale impact test was implemented in Abaqus considering the same geometries and constraint conditions of the real test.

In the Figure 7–9 and Figure 7–10 shows the equipment used for the test.

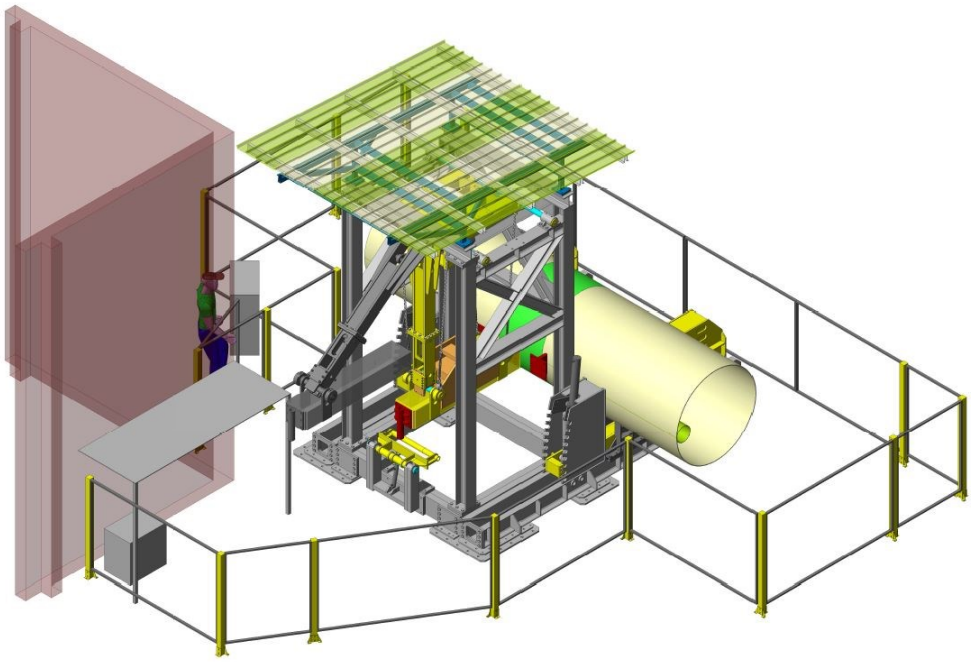

Figure 7–9 Equipment used for the test ─ Back view.

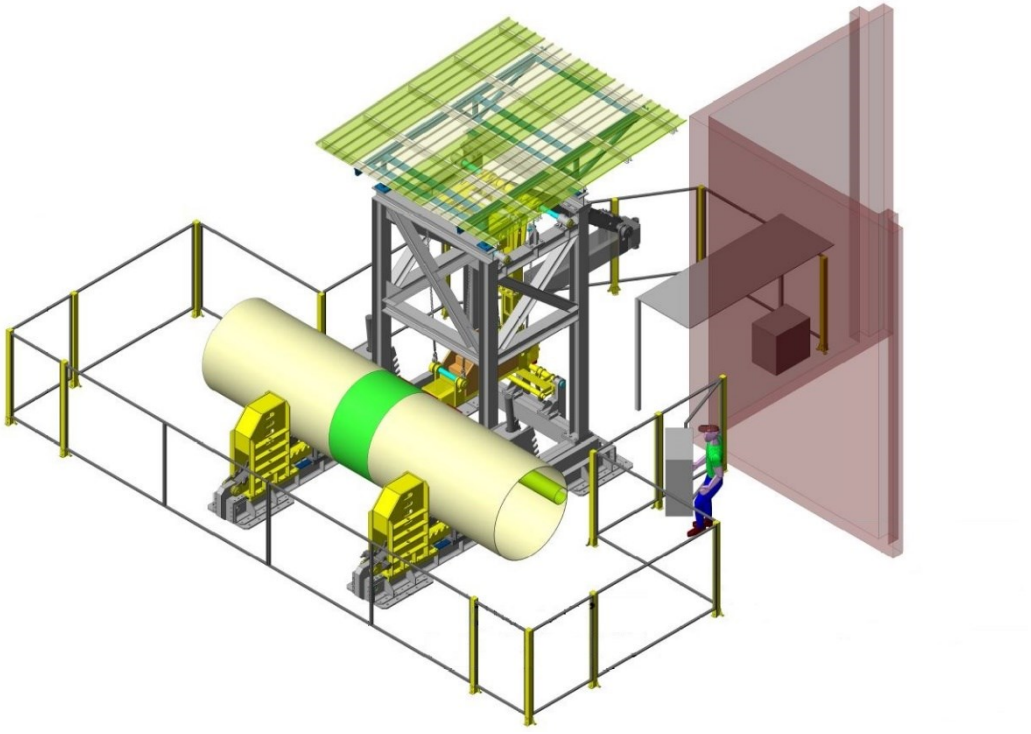

Figure 7–10 Equipment used for the test ─ Front view.

The pipe is hinged at 1.5 m from the ends and receives an impact of 9500 J in the middle of the field joint coating. They are conservatively neglected the two sections of pipe of 1.5 m starting from the hinges.
The load and constraint configuration is shows in the Figure 7–11 below:

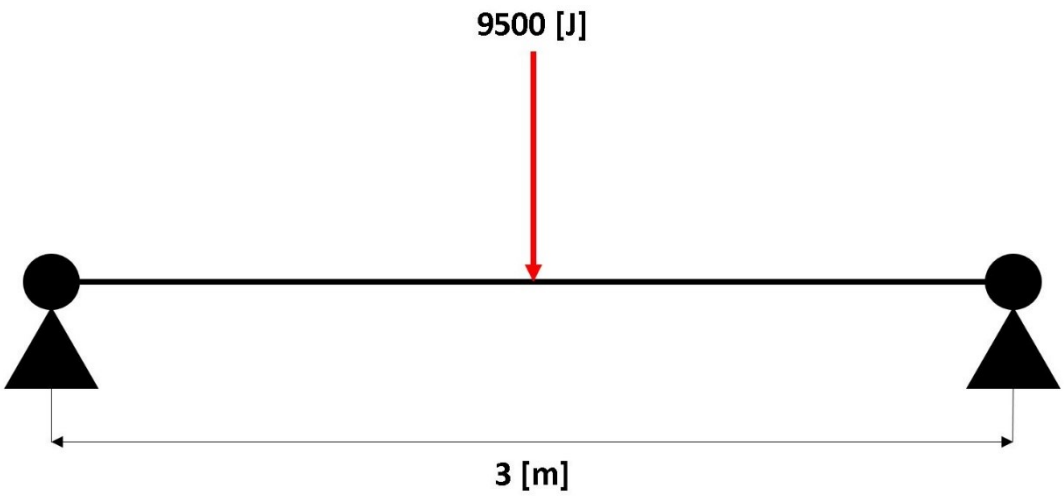

Figure 7–11 Simplified impact scheme.

For implemented the FE model the following assumptions are considering:

- Isotropic materials;
- The hammer, modelled as rigid body;
- Concrete weight coating, modelled as elastic material;
- Pipe, modelled as deformable body (see subparagraph 7.3.1);
- Impact in y direction rather than in x direction as in reality;
- Hammer free to move only in the y direction;
- HSS conservatively neglected;
- External anticorrosion coating conservatively neglected;
- Perfectly tie pipe-concrete and pipe-infill surfaces;
- Constraints at the end of the pipe modeled as hinges;
- Symmetric finite element model.

HSS and external corrosion coating are neglected because there aren't subject to damage (see paragraph 6.3).

For the pipe, CWC, infill material and hammer, classical brick elements have been used (C3D8R elements, see Figure 7–12).

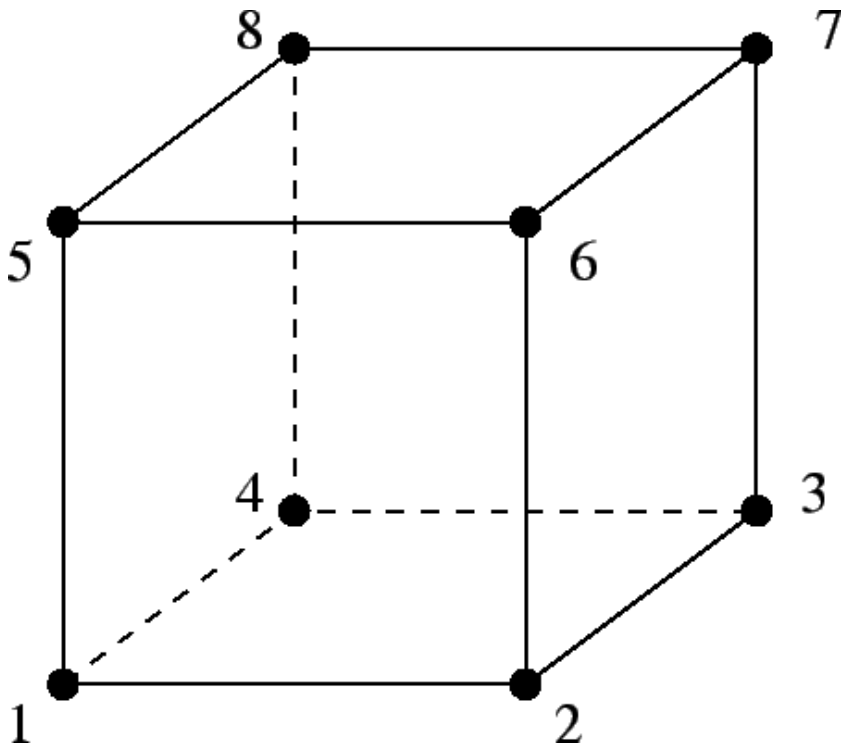

Figure 7–12 C3D8R elements.

From the Figure 7–13 and Figure 7–14 is possible to notice how the pipe and the external coating have a coarser mesh, while more dense in the impact area on the field joint.

The Figure 7–15 summarizes the type of elements, number of elements and number of nodes adopted in FE model.

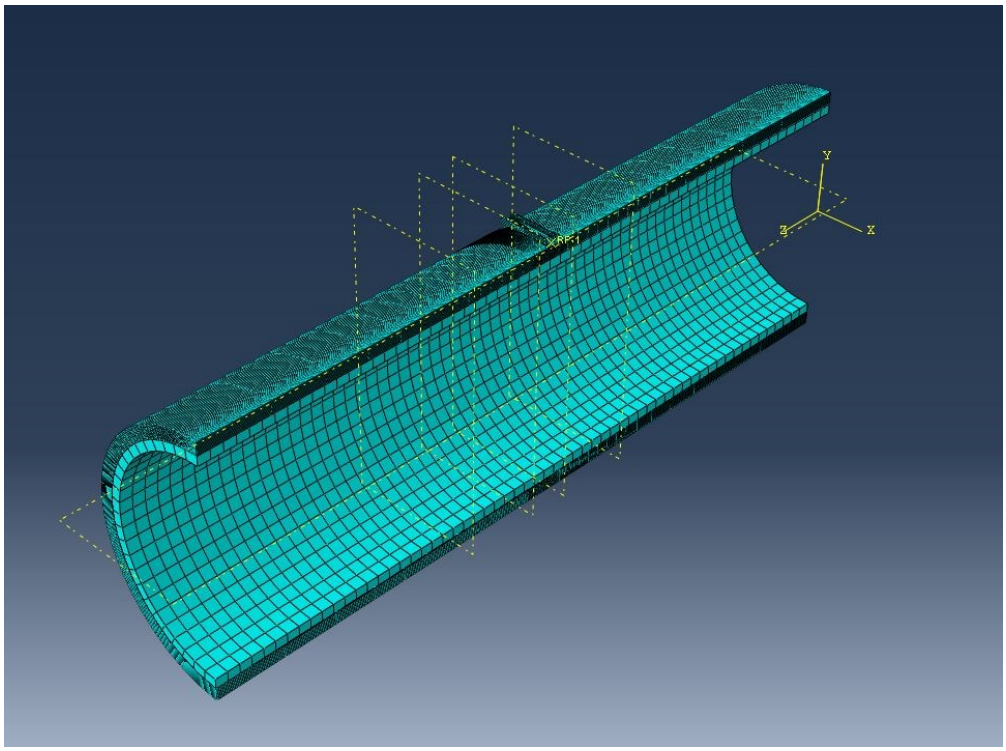

Figure 7–13 Finite element model with C3D8R elements.

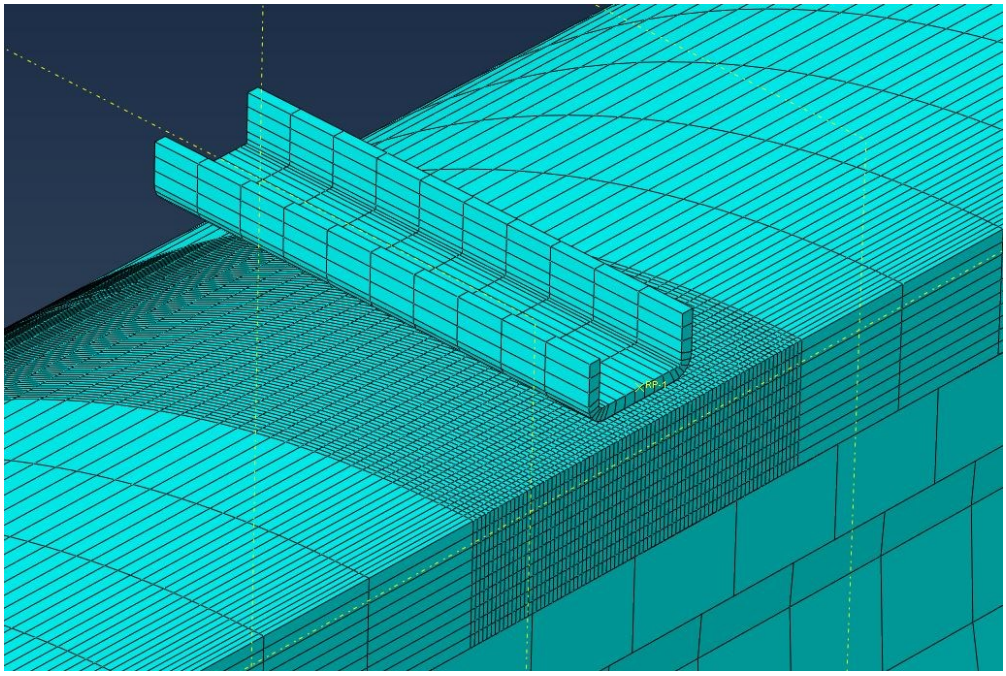

Figure 7–14 C3D8R elements more dense in impact zone.

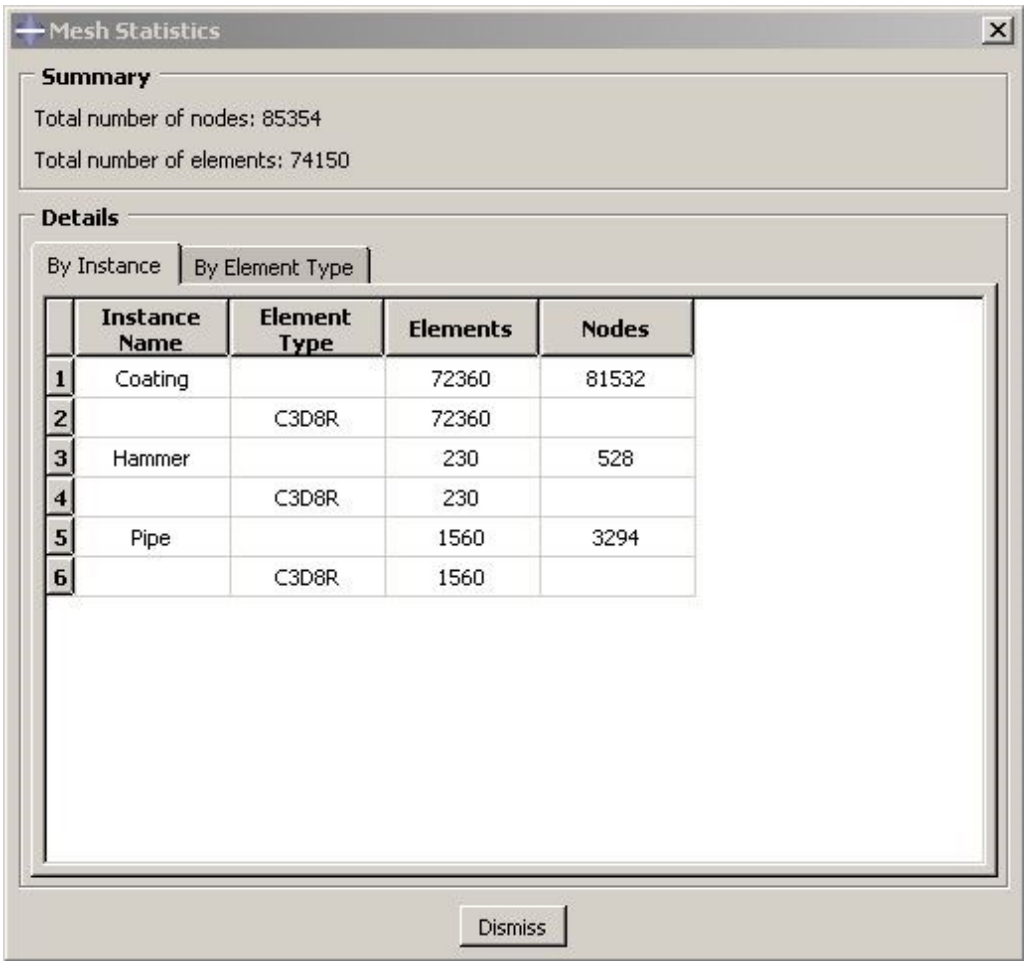

	Instance Name	Element Type	Elements	Nodes
1	Coating		72360	81532
2		C3D8R	72360	
3	Hammer		230	528
4		C3D8R	230	
5	Pipe		1560	3294
6		C3D8R	1560	

Figure 7–15 Mesh statistics.

7.5 FINITE ELEMENT MODEL CALIBRATION AND VALIDATION

Finite element results have been calibrated and validated considering different materials models for the solid PU. The solid PU used for the field joint coating infill material is a polymeric material that typically has a purely elastic behavior compared to the plastic one. In particular, both a Elastic-Plastic and a Hyperelastic-Plastic material models have been investigated during the FE model development. The latter has been selected as the most appropriate to simulate the permanent deformation generated during the impact with strain energy potential per unit of volume Marlow (see subparagraph 5.3.8).

The substantial difference between the two models is in the elastic field, in fact, the first has a linear behavior, while the second has a non-linear type.

To definite the Hyperelastic-Plastic behaviour of PU, compressive material test results have been considering (see Figure 7–6).

In particular, the plastic curve was calibrated by shifting the elastic deformation limit for a single stress-strain curve. Subsequently, a validation of the material model is obtained by setting the elastic deformation limit and varying the characteristics of the materials in the range observed by the tests.

The Figure 7–16 and Figure 7–17 shows the definition of the materials for the FE model:

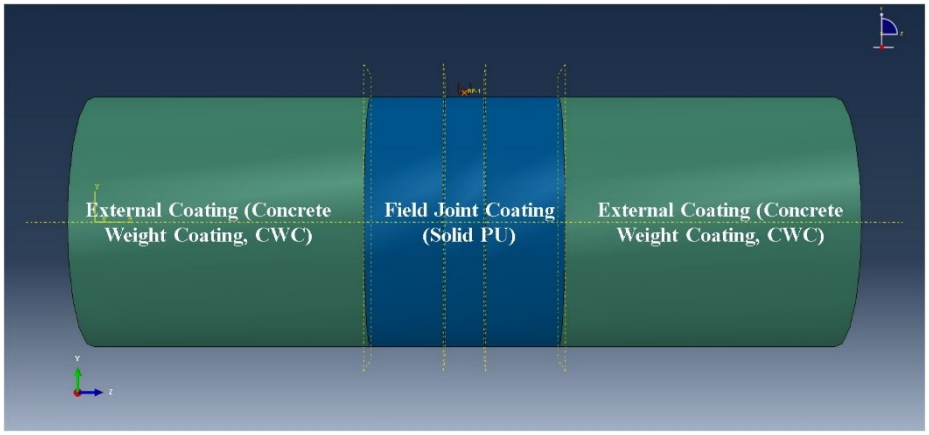

Figure 7–16 Definition of materials in Abaqus for CWC and solid PU.

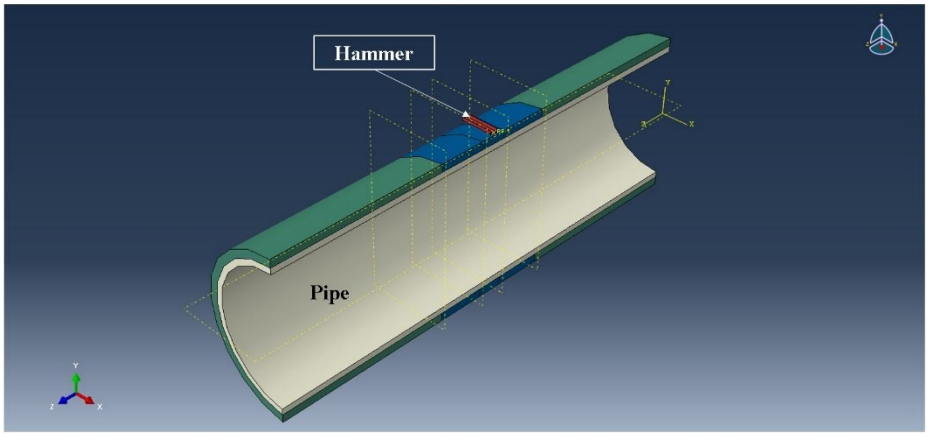

Figure 7–17 Definition of materials in Abaqus for the pipe and hammer.

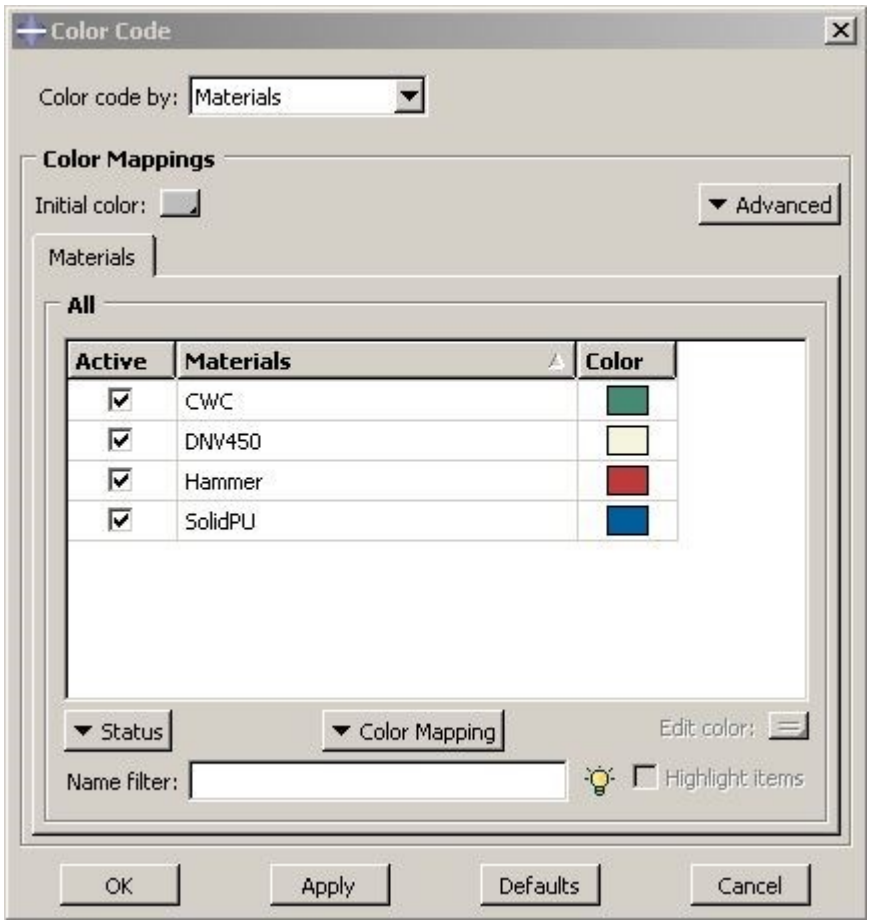

Figure 7–18 Color code of the materials.

The Figure 7–18 above summarizes the colors of the materials defined for the FE model.

7.6 BOUNDARY CONDITIONS AND INTERACTION

For the finite element model calibration, half pipe has been modelled and symmetry boundary condition have been applied (see Figure 7–19).

The hammer is used to transfer kinetic energy to the solid PU being free to move along the y direction only with set speed U2 (see Figure 7–21). The ram mass and its initial velocity have been assigned to achieve the target impact energy of 9.5 kJ.

The impact energy of 9500 J in Abaqus was defined by assigning to the hammer mass a certain initial velocity derived from the definition of kinetic energy.

For a symmetrical model the volumes, masses and energy are half compared to a complete model, consequently the hammer will have a mass of 1.075 t and the impact energy will be 4750 J

The hammer (rigid body see Figure 7–24) was modeled in the FEA with a reduced volume compared to the actual volume of the test, therefore to assign it the correct mass the density was increased to obtain the value of 1.075 t:

$$\rho = \frac{m}{V} = \frac{1.075\ [t]}{84177\ [mm^3]} = 1.27707E-05\left[\frac{t}{mm^3}\right] \tag{7.7}$$

Subsequently the hammer speed was calculated in order to guarantee a kinetic energy of 4750 J according to the relation:

$$E_k = \frac{1}{2}mv^2 \Leftrightarrow v = \sqrt{\frac{2E_k}{m}} = \sqrt{\frac{2 \cdot 4750 \cdot (1000)^2\left[\frac{kg \cdot mm^2}{s^2}\right]}{1075\ [kg]}} = 2972.7\left[\frac{mm}{s}\right] \tag{7.8}$$

Where:

- ρ is density of hammer;
- m is mass of hammer;

- V is volume of hammer;
- E_k is kinetic energy.

For the finite element model calibration, the coating surfaces (both concrete and PU) have been fully fixed to the pipeline surface (tie interaction see Figure 7–22) and a continuous mesh is used for concrete-PU, while the ends of the pipe are hinged (see Figure 7–20). The interaction between hammer and infill material is modelled as surface to surface with friction coefficient of 0.25 (see Figure 7–23).

These assumptions is in compliance to full scale impact test results.

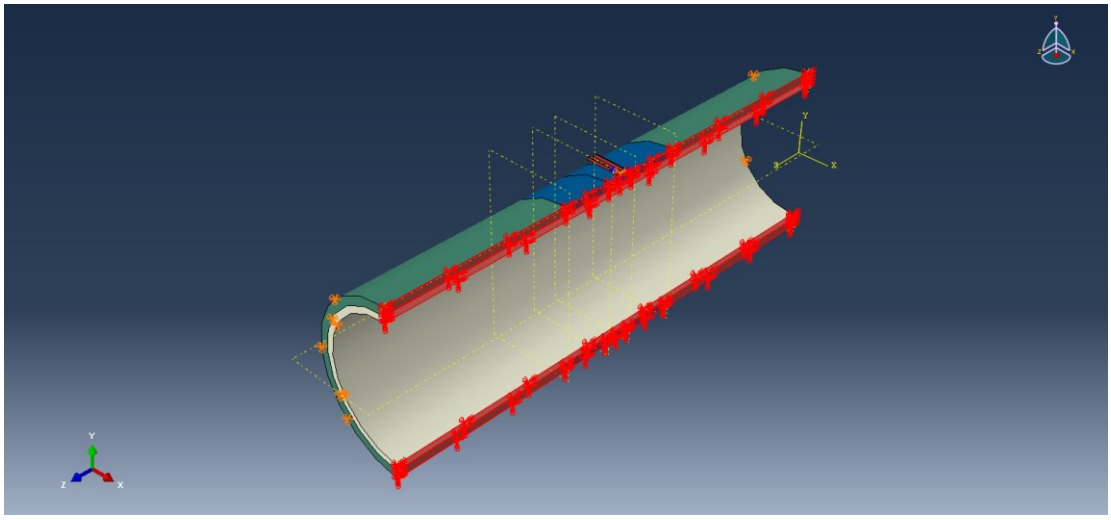

Figure 7–19 Boundary conditions — Symmetry about a plane X (U1=UR2=UR3=0).

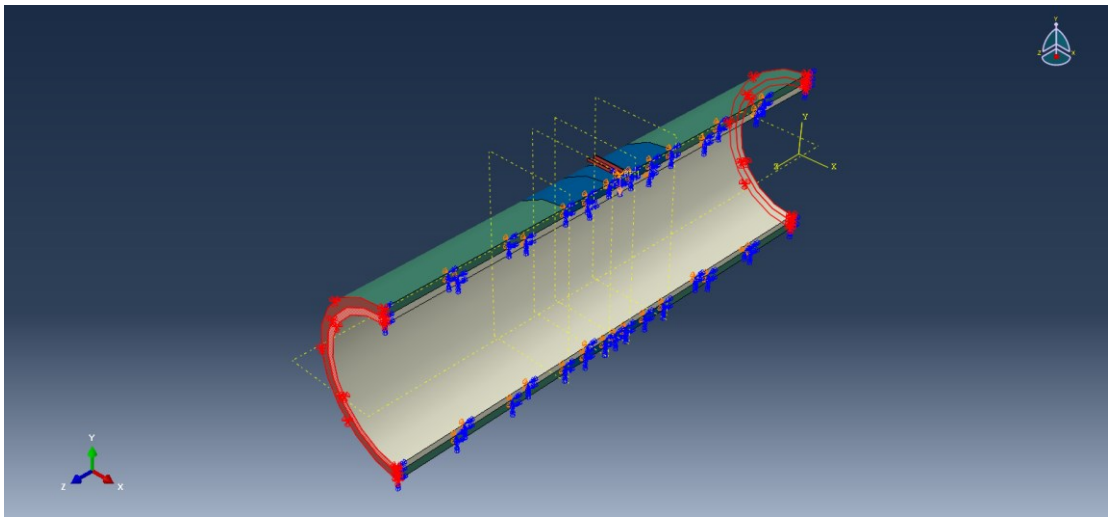

Figure 7–20 Boundary conditions ─ Pipe displacement U1=U2=U3=0.

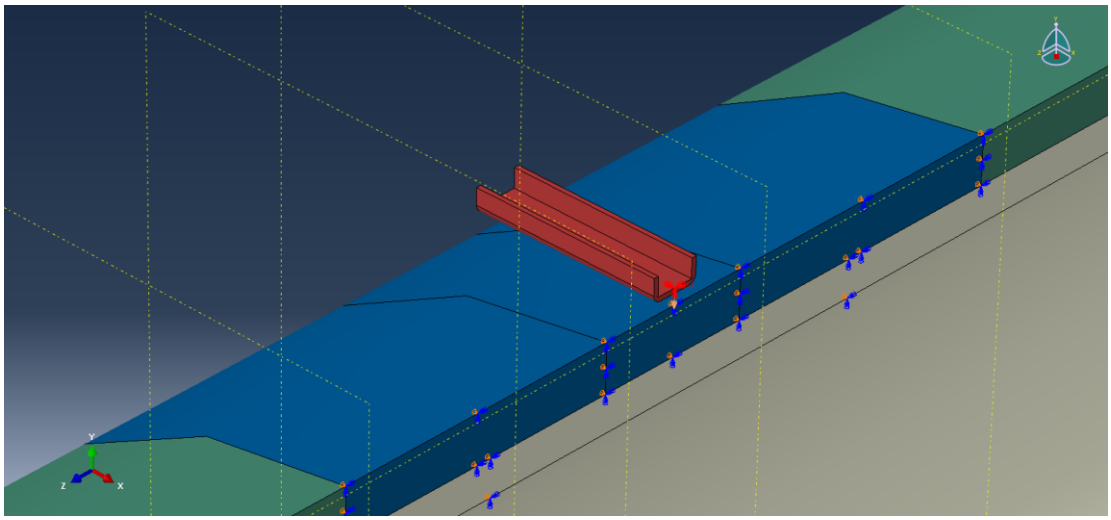

Figure 7–21 Boundary conditions ─ Hammer displacement and rotation U1=U3=UR1=UR2=UR3=0 respectively.

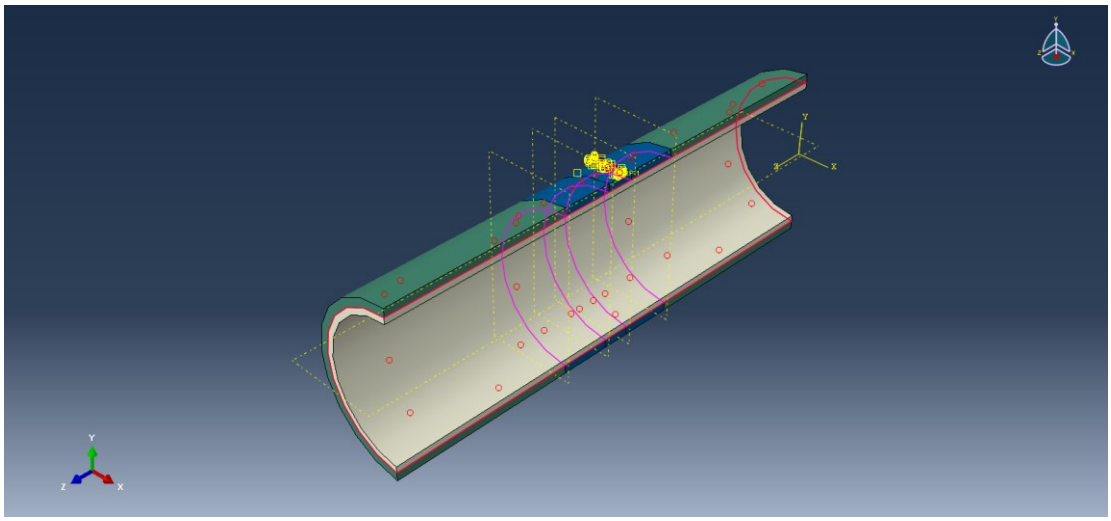

Figure 7–22 Interaction ─ Tie between pipe-concrete and pipe-infill material.

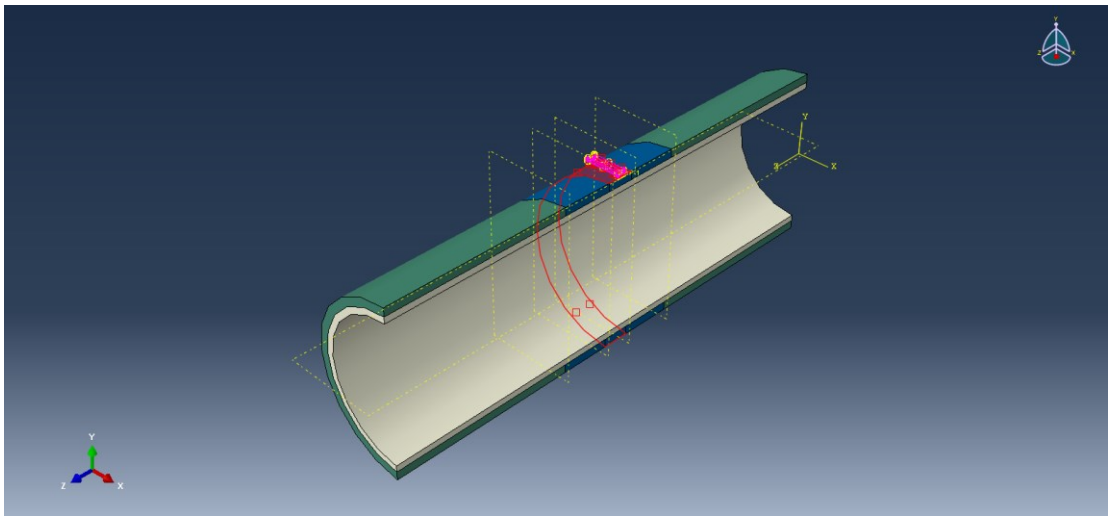

Figure 7–23 Interaction ─ Surface to surface contact between hammer and infill material.

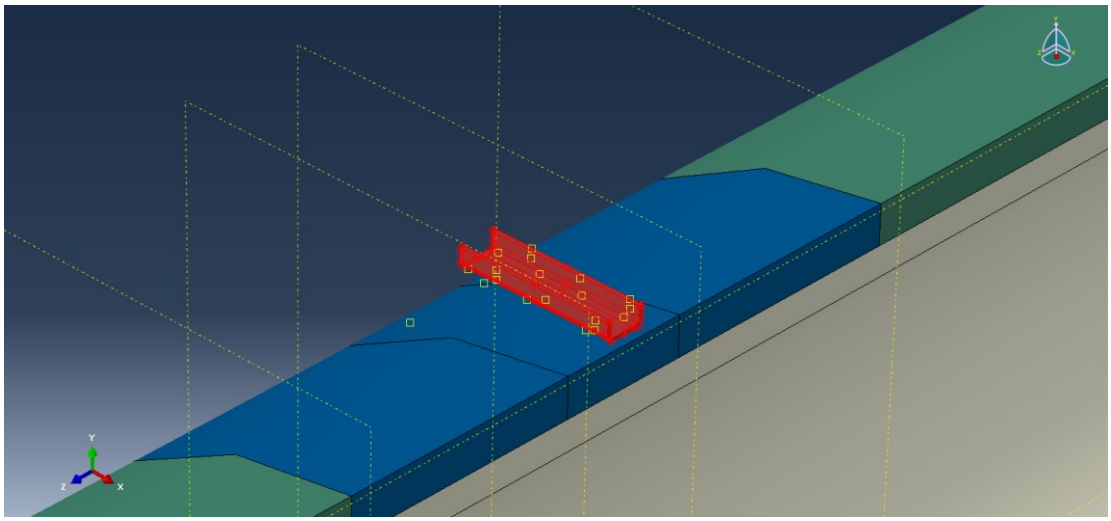

Figure 7–24 Interaction ─ Rigid body.

7.7 ANALYSIS SETUP PROCEDURE

FEM analysis are performed with Abaqus explicit solver. The hammer has been initially positioned, at a distance of 11.49 mm from the impact surface. This positioning is sufficient to analyze the full impact in a time of 0.05 s (see Figure 7–25).

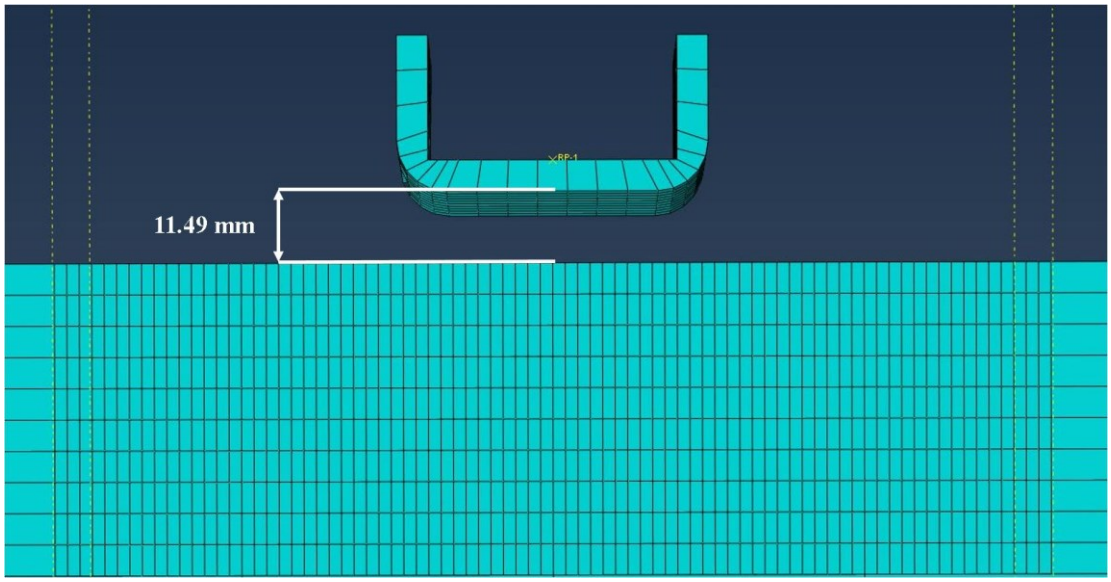

Figure 7–25 Initial condition of the hammer.

7.8 POST-PROCESSING

During the full scale impact test the measured parameter has been the depth of the footprint released by the impact. For the finite element model calibration and validation the footprint depth has been analyzed and compared with the laboratory test.

In the finite element model, the depth of the footprint was defined by analyzing the displacement of the node in the middle of the solid PU, since the area having the highest value as show in Figure 7–26.

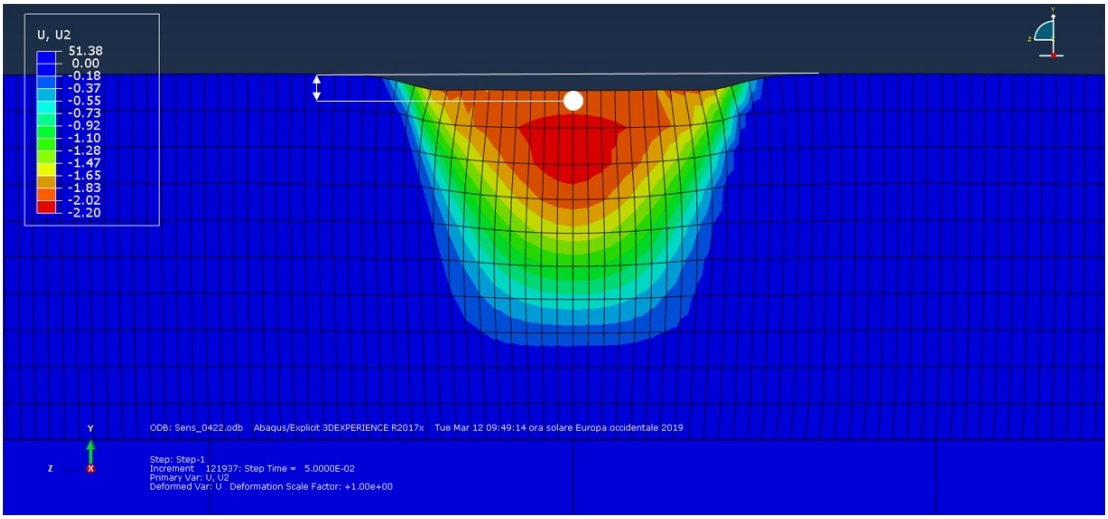

Figure 7–26 Displacement post-processing.

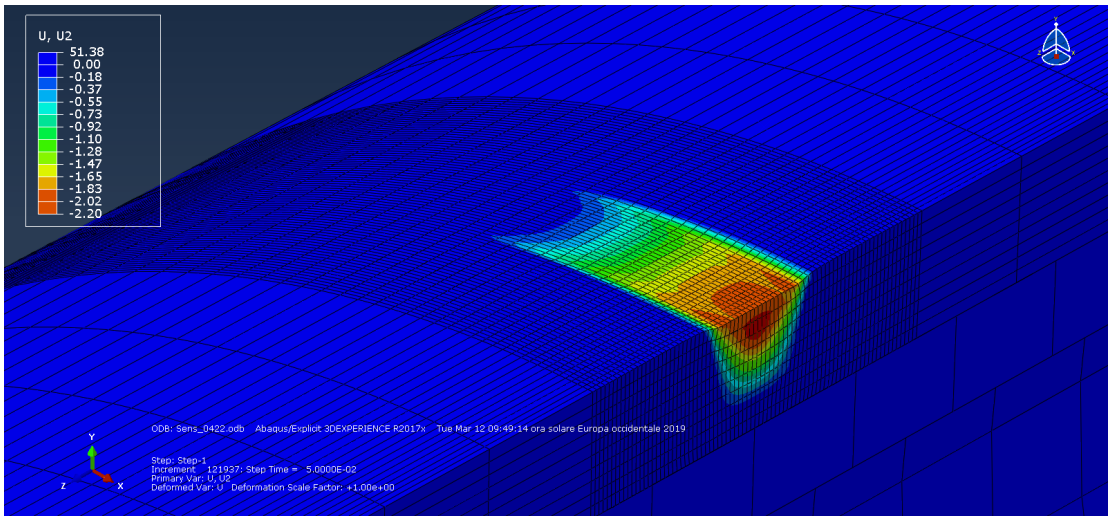

Figure 7–27 Footprint to the finite elements.

Furthermore, the follow quantities have been calculated:

- Pipe internal energy;
- Solid PU internal energy;
- Concrete internal energy;
- Total energy (i.e. sum of the individual energies shown above);
- Hammer return energy.

Figure 7–28 shows two different footprints obtained by full scale impact test and FEA respectively.

Figure 7–28 Comparison between the footprint of the impact test with the footprint to the finite elements.

8 COMPARISON OF TEST VS. FEA

8.1 INTRODUCTION

This chapter exposes the calibration of solid polyurethane used such as infill material of the field joint coating, in particular the results of the calibration.
Moreover are showed the results of the energy analysis using the hyperelastic-plastic material models. This is very important to understand if the solid PU can be used as a protective barrier to the pipe against the impacts due to by fishing device.

8.2 FEM CALIBRATION RESULTS

For the FE model calibration, two different models of the solid PU have been investigated during the finite element model development. In particular, elastic-plastic and hyperelastic-plastic models are adopted.

8.2.1 ELASTO-PLASTIC MODEL CALIBRATION

The stress-strain curve obtained from compression test (see subparagraph 7.3.3) have elastic-plastic law, i.e. the elastic behaviour.
The calibration has initially been performed by several attempts varying the mechanical characteristics (i.e. SMYS, Young's Modulus and SMTS) in the range of variation observed during the compression test (SMYS 8-40 MPa, SMTS 200-230 MPa and Young's Modulus 255-2000 MPa).

Figure 8–1 shows the results of the first set of analyses. This variation has not been sufficient to guarantee the 2 mm footprint, so the analyses have proceeded to further increase the properties to obtain a 2 mm footprint.

From the results (see Figure 8–2 and Figure 8–3) it is clear that the elastic-plastic model is not representative of solid polyurethane, because to reach the convergence of about 2 mm of footprint, a resistance increase of about 100 MPa is required which is absolutely outside the range of the tested properties of solid polyurethane.

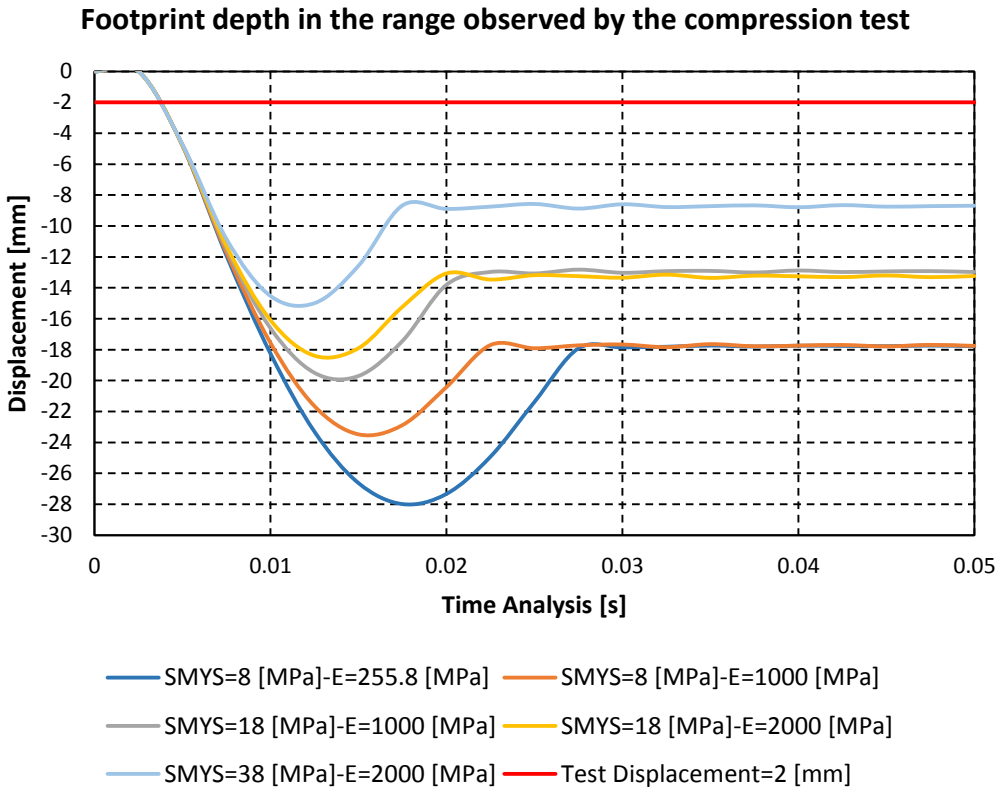

Figure 8–1 Displacement for elastic-plastic model.

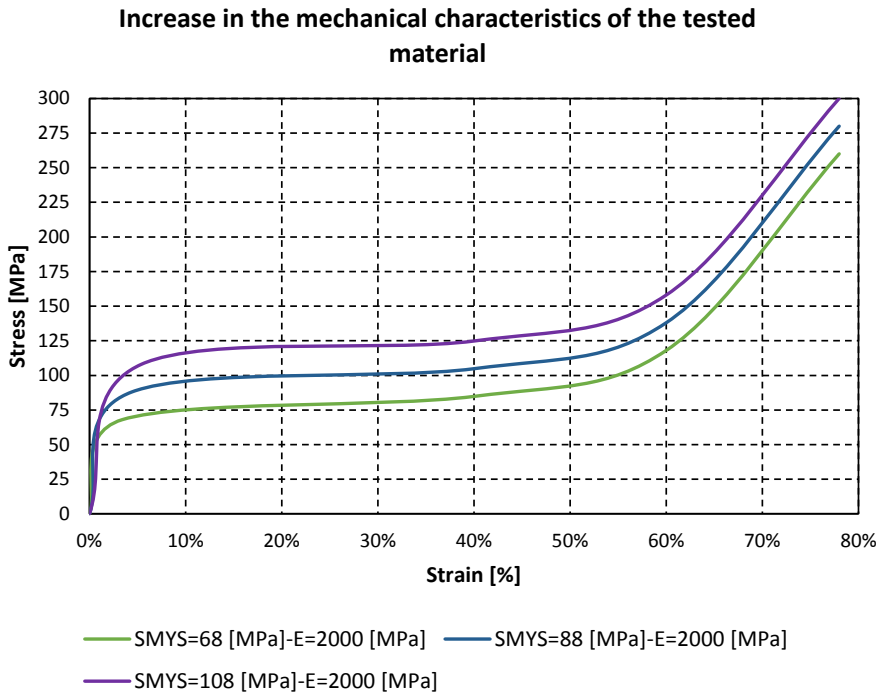

Figure 8–2 Increase of the stress-strain curves of the material tested.

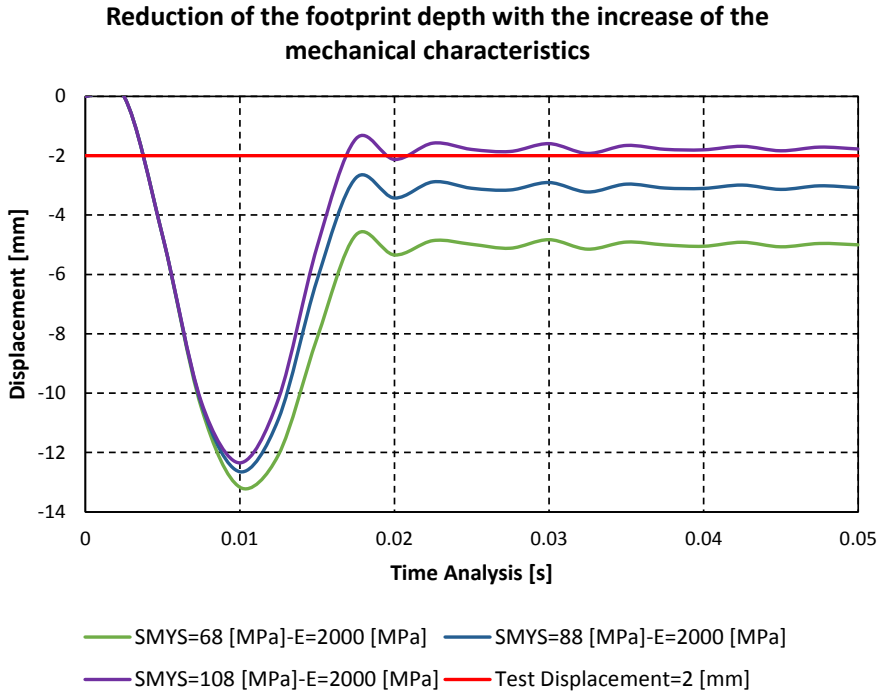

Figure 8–3 Displacement for increased stress-strain curves.

8.2.2 HYPERELASTIC-PLASTIC MODEL CALIBRATION

The hyperelastic-plastic material model has been investigated for the finite element model calibration. The hyperelastic material has a non-linear elastic behavior, this feature allows to obtain a wider elastic strain field than a typical linear elastic material. The calibration was performed on a single stress-strain curve varying by attempts the elastic deformation limit, which identifies the end of the elastic field and the beginning of the plastic field (see Figure 8–4).

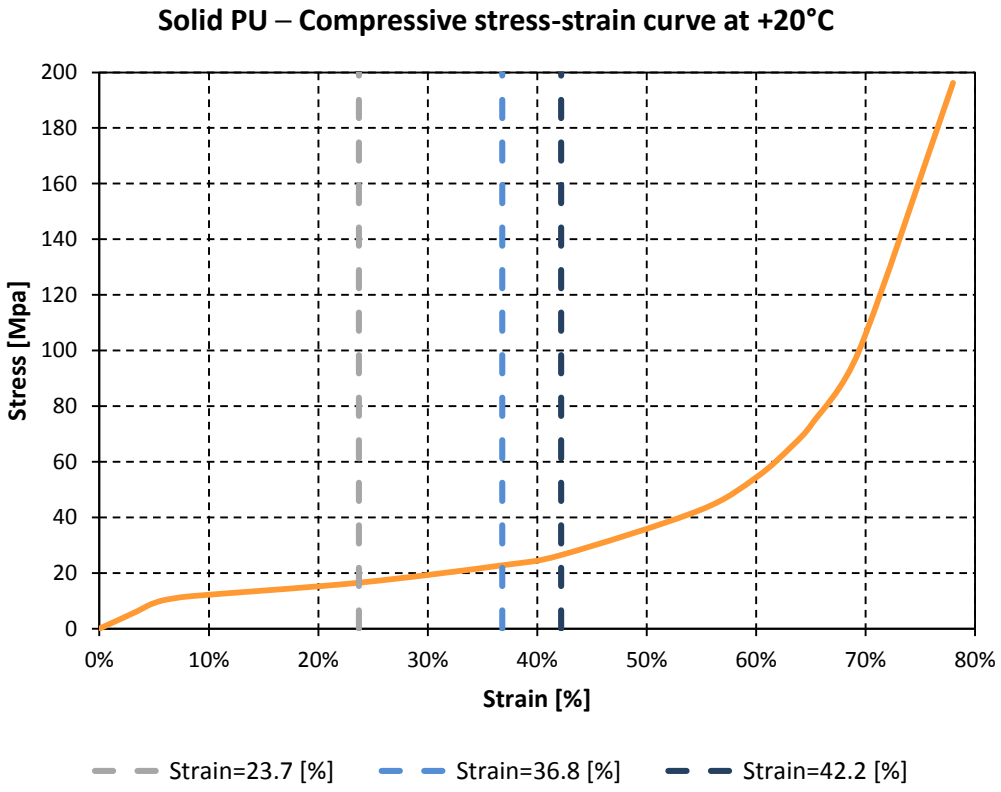

Figure 8–4 Increase of the elastic strain limit for hyperelastic-plastic model.

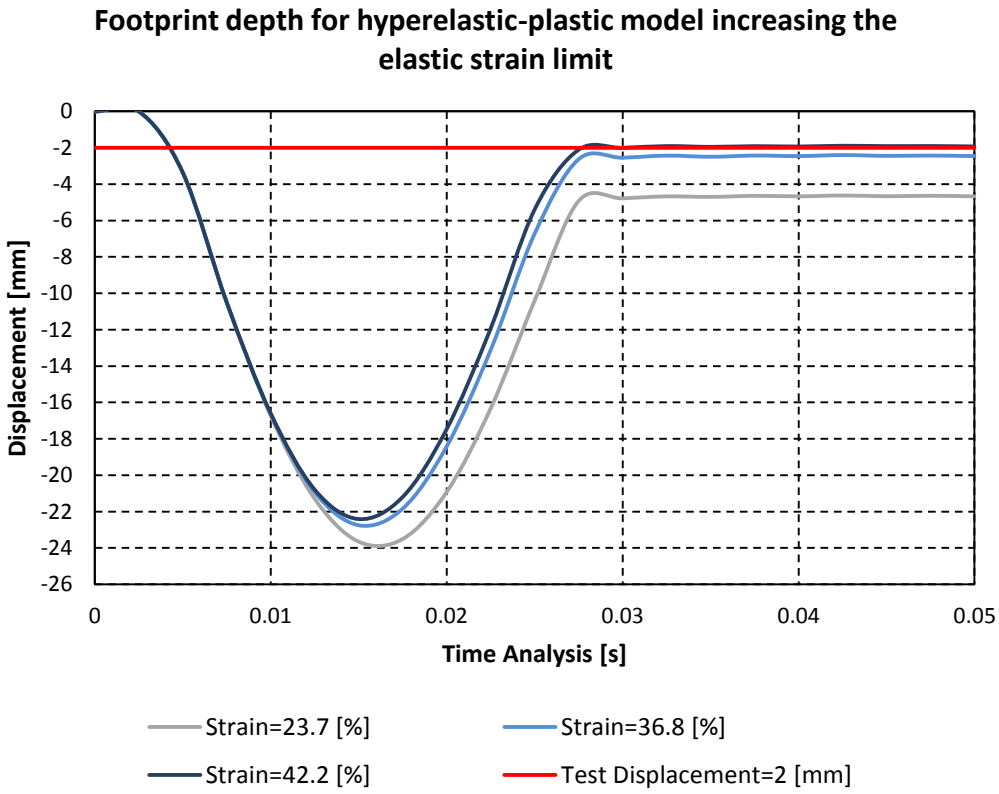

Figure 8–5 Displacement for hyperelastic-plastic model.

The absolute convergence of 2 mm is obtained with an elastic stain limit of 42.2% (see Figure 8–5).

Therefore, this model is representative of solid polyurethane, since the characteristics of the tested curve have not been changed.

Another possible calibration scenario, using hyperelastic-plastic model, can be analyzed fixing an elastic strain limit and increasing the material properties in the range of variations measured during testing. To carry out this calibration a strain limit of 20% has been fixed (see Figure 8–6) an the material yield have been increased from to 15 to 35 MPa. By this calibration option, the convergence target of 2 mm has been easily obtained with a material yield of 35 MPa (see Figure 8–7). In conclusion, the results showed that the hyperelastic-plastic model can be considered representative of the solid PU.

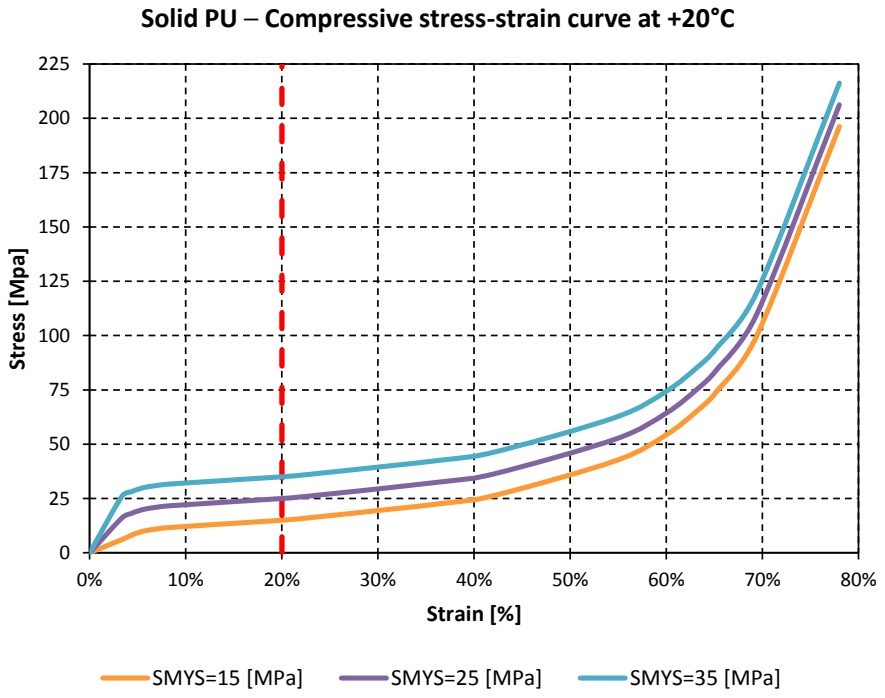

Figure 8–6 Strass-strain curves in the observed range by compression test.

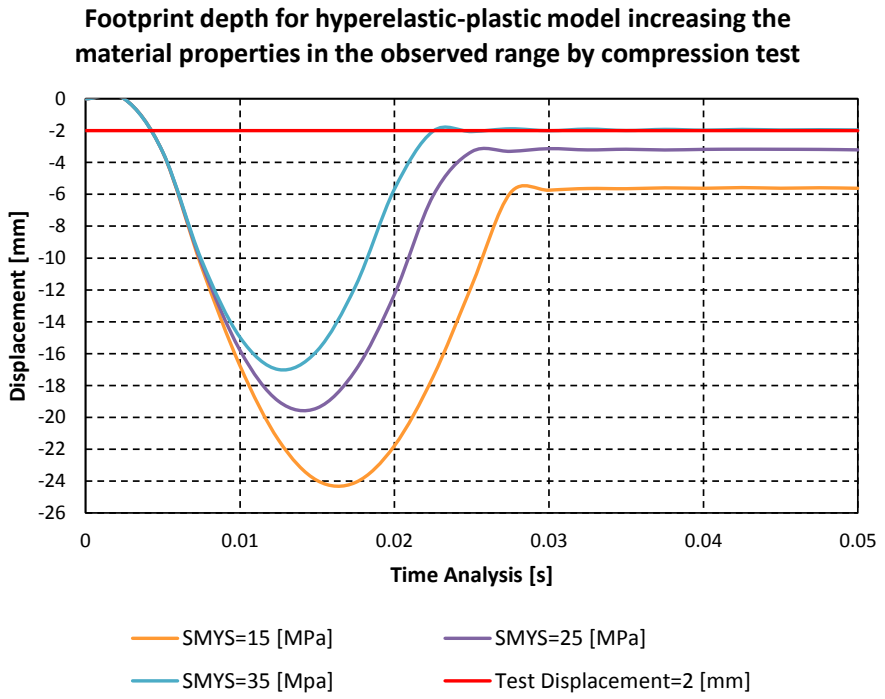

Figure 8–7 Displacement in the observed range by compression test.

8.3 ENERGY RESULTS

An important and interesting analysis is that to investigate the energy absorbed/released during the impact.

This is very important to understand if the solid PU can be reasonable used as a pipe protection barrier against the impacts. For this reason it is useful to investigate the kinetic and potential energy of all components of the model i.e. solid PU, CWC, pipe. The energy analysis has been performed using the hyperelastic-plastic material model show in previous subparagraph 8.2.2.

All graphs show an inflection point in the first analysis steps, fallowed by a maximum (or minimum) point and a second inflection point. The first inflection point is the initial contact between hammer and solid PU and once the maximum (or minimum) point is exceeded, the hammer returns back ending the contact in the second inflection point.

In fact the graphs of the kinetic energy of the hammer (see Figure 8–11 and Figure 8–15) and of the displacements (see Figure 8–5 and Figure 8–7) are mirrored with respect to those of the potential energy (see Figure 8–8, Figure 8–9, Figure 8–10, Figure 8–12, Figure 8–13 and Figure 8–14).

The total time of impact is of about 0.02 seconds, it can be seen in all figures below.

In this time the peach of internal energy increases for all components. In particular the Figure 8–8 shows that the total impact energy (9380 J) is absorbed of 84.22% from solid PU (7900 J), 14% from pipe (1313.78 J) and the rest 1.78% is dissipated in the model. An important results is that only 14% of the impact energy is passed to the pipe, therefore the solid PU can be considered a good barrier to protect the pipe.

Increasing the elastic strain limit (see Figure 8–9 and Figure 8–10), the energy absorbed from the pipe increases to 17.5 % and 19.24 % respectively. In any case a good margin of protection is still guaranteed. Figure 8–11 shows the kinetic energy of the hammer, in particular the difference between the maximum value of the total energy curve (see Figure 8–8, Figure 8–9 and Figure 8–10) and total residual energy is equal to residual energy of the hammer.

Increasing the elastic strain limit, the residual energy of the hammer increases. This demonstrate that the solid PU is a good barrier to protect the pipe.

Figure 8–12, Figure 8–13, Figure 8–14, Figure 8–15 show the results of the second set of analyses.

The maximum value of the impact energy (9370 J) is absorbed of 84.84% (7950 J) from solid PU, 13.34% from pipe (1250 J) and the rest 1.82% is dissipated in the model (see Figure 8–12). Increasing the material properties in the range observed by compression test (see Figure 8–13 and Figure 8–14), the energy absorbed from the pipe increases to 15.86% and 18.25% respectively.

The results show a few percent points less than the first set of analyses, therefore the solid PU can be considered a good barrier to protect the pipe.

The residual energy of the hammer increasing with increases of the material properties (see Figure 8–15) of equal value to the difference between the maximum value of the total energy (see Figure 8–12, Figure 8–13 and Figure 8–14) and the total residual energy.

The above is due to the increase in resilience, i.e. the area subtended to the elastic field of the stress- strain curve (see Figure 8–4 and Figure 8–6).

Resilience is defined as the ability of a material to absorb energy in the form of elastic deformation and then return it once unloaded. This consideration is valid for all set of analyses.

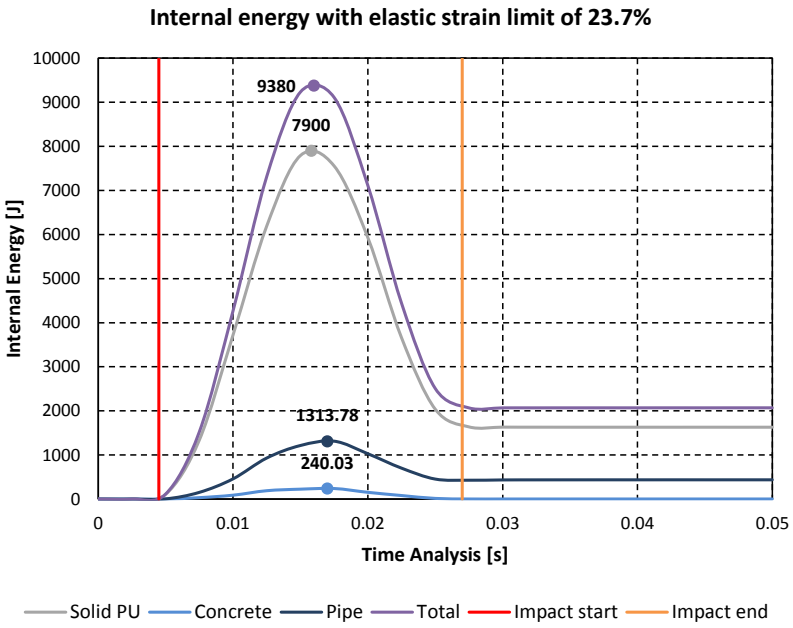

Figure 8–8 Internal energy as a function of time analysis for a hyperelastic-plastic model with elastic strain limit of 23.7%.

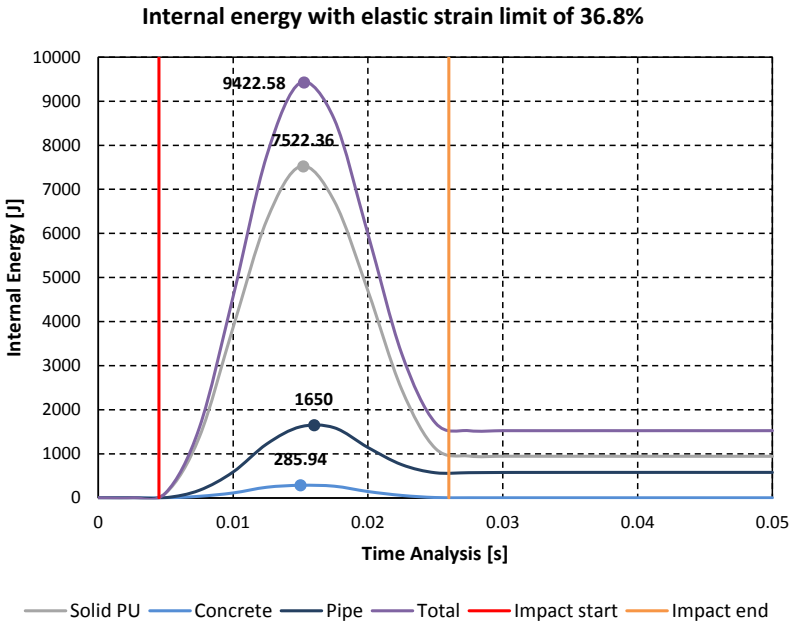

Figure 8–9 Internal energy as a function of time analysis for a hyperelastic-plastic model with elastic strain limit of 36.8%.

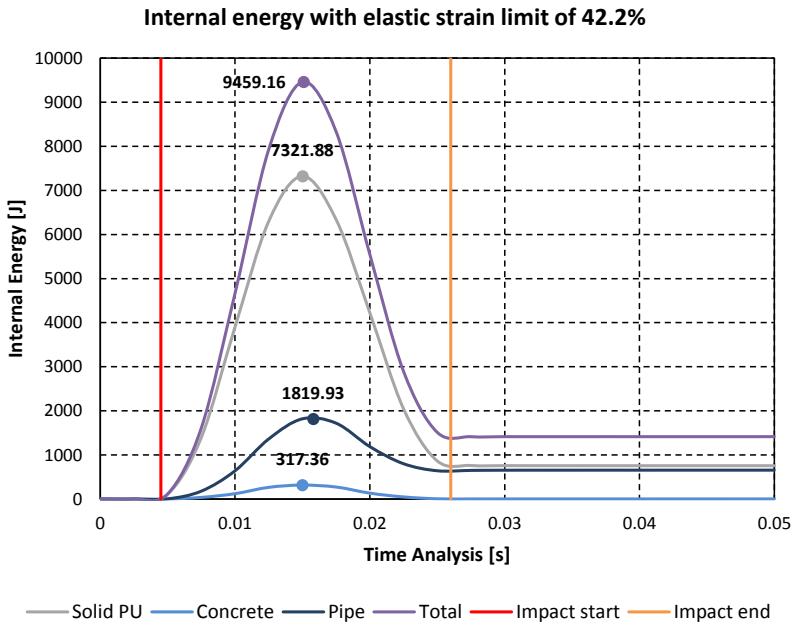

Figure 8–10 Internal energy as a function of time analysis for a hyperelastic-plastic model with elastic strain limit of 42.2%.

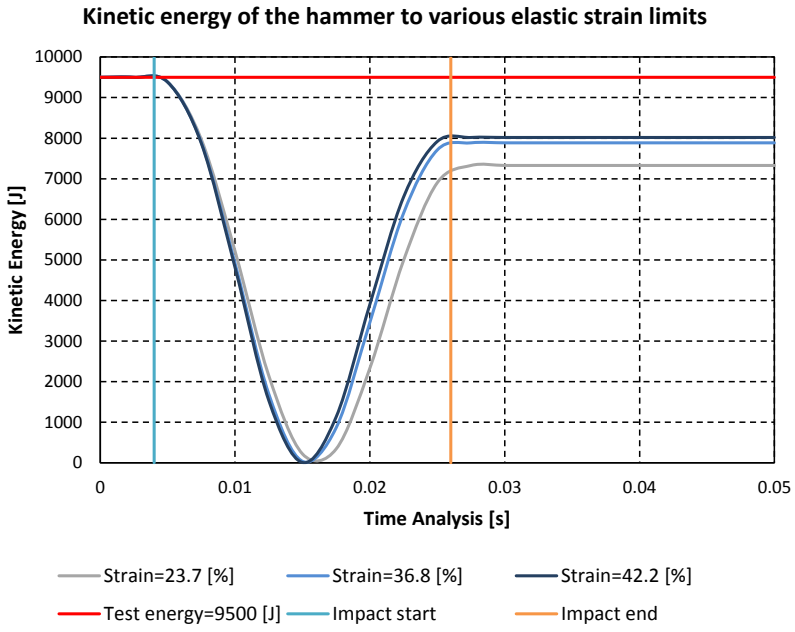

Figure 8–11 Kinetic energy as a function of time analysis for a hyperelastic-plastic model to various elastic strain limit.

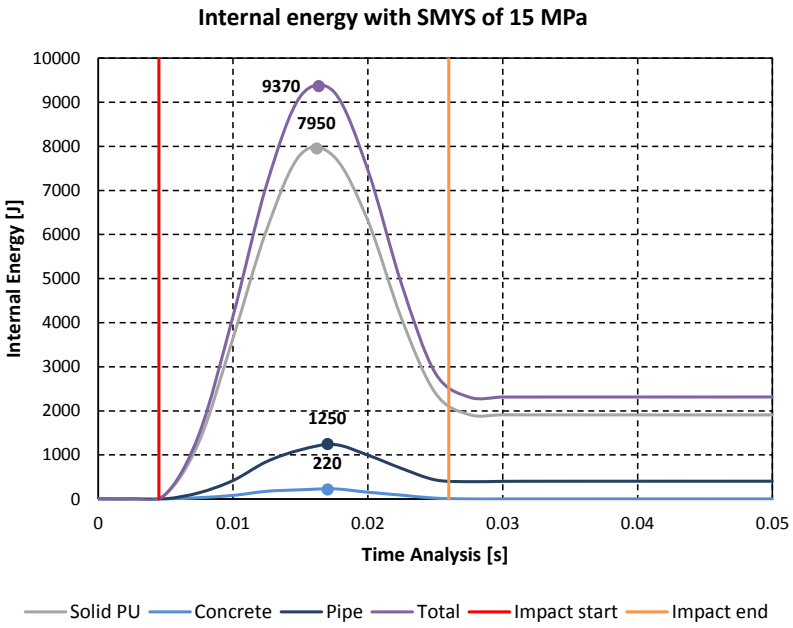

Figure 8–12 Internal energy as a function of time analysis for a hyperelastic-plastic model with SMYS of 15 MPa.

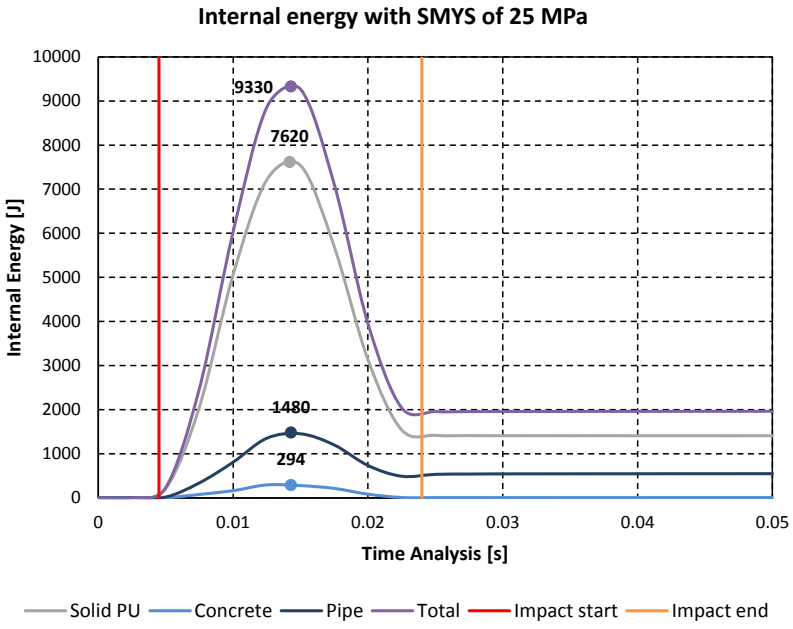

Figure 8–13 Internal energy as a function of time analysis for a hyperelastic-plastic model with SMYS of 25MPa.

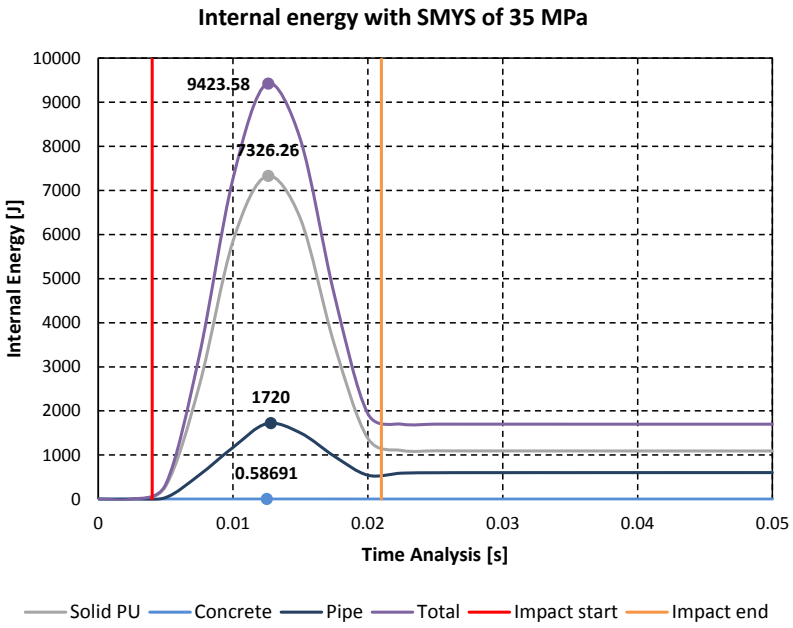

Figure 8–14 Internal energy as a function of time analysis for a hyperelastic-plastic model with SMYS of 35 MPa.

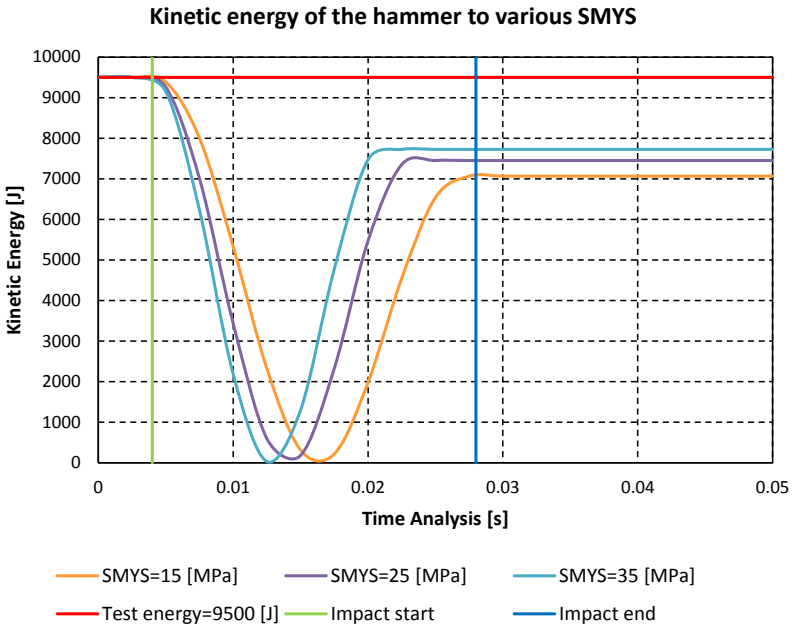

Figure 8–15 Kinetic energy as a function of time analysis for a hyperelastic-plastic model to various SMYS.

9 CONCLUSIONS

During the development of the finite element model two models of solid polyurethane material were taken into account for its calibration and validation.

In particular, both elastic-plastic and hyperelastic-plastic models have been investigated during finite element model development.

The finite element analysis results showed that the elastic-plastic material model is not representative of solid PU, while the hyperelastic-plastic material model resulted as the most appropriate to represent the solid PU. Indeed the absolute convergence of 2 mm of the footprint depth was easily obtained keeping the tested material properties with a definition of a elastic strain limit of 42.2%.

Another important result has been got from energy analysis, which shows that the solid PU can be considered a good protection again impact, because only a range 13-19% of the total impact energy is transmitted to the pipe.

In conclusion, this finite element model can be adopted with an elastic strain limit of 42.2% to extend the finite element analysis scenarios and then to analyze the behavior under operational load of the offshore pipelines that is not easy to test in the laboratory.

BIBLIOGRAPHY

[1] M. Carnaroli, S-lay Pipeline Installation from Low to Hight Depth, Ancona: Università Politecnica delle Marche, 2012-2013.

[2] A. C. P. a. R. A. King, Subsea Pipeline Engineering, USA: PennWell, 2008.

[3] Det Norske Veritas, "DNVGL-RP-F106," May 2017. [Online]. Available: https://www.dnvgl.com/oilgas/download/dnvgl-rp-f106-factory-applied-external-pipeline-coatings-for-corrosion-control.html. [Accessed 18 March 2019].

[4] N. Fatmala, "Subsea Pipeline Engineering," 17 February 2016. [Online]. Available: http://nfatmala.blogspot.com/2016/02/anti-corrosion-coating-for-subsea.html. [Accessed 18 March 2019].

[5] SHAWCOR, "Fusion Bonded Epoxy Coating," [Online]. Available: https://www.shawcor.com/pipe-coating-solutions/products/fbe. [Accessed 18 March 2019].

[6] ISO, Petroleum and natural gas industries-External coatings for buried or submerged pipelines used in pipeline transportation systems-Part 2: Single layer fusion-bonded epoxy coatings, 2014.

[7] SHAWCOR, "3-Layer Polyethylene Coating," [Online]. Available: https://www.shawcor.com/pipe-coating-solutions/products/3lpe. [Accessed 18 March 2019].

[8] ISO, Petroleum and natural gas industries-External coatings for buried or submerged pipelines used in pipeline transportation systems-Part1: Polyolefin coatings (3-layer PE and 3-layer PP), 2011.

[9] SHAWCOR, "3-Layer Polypropylene Coating," [Online]. Available: https://www.shawcor.com/pipe-coating-solutions/products/3lpp. [Accessed 19 March 2019].

[10] Det Norske Veritas, "DNVGL-ST-F101," October 2017. [Online]. Available: https://www.dnvgl.com/oilgas/download/dnvgl-st-f101-submarine-pipeline-systems.html. [Accessed 18 March 2019].

[11] SHAWCOR, "HeviCote®," [Online]. Available: https://www.shawcor.com/pipe-coating-solutions/products/hevicote. [Accessed 18 March 2019].

[12] SHAWCOR, "Compression Coat™," [Online]. Available: https://www.shawcor.com/pipe-coating-solutions/products/compression-coat. [Accessed 04 March 2019].

[13] Det Norske Veritas, "DNVGL-RP-F102," August 2017. [Online]. Available: https://www.dnvgl.com/oilgas/download/dnvgl-rp-f102-pipeline-field-joint-coating-and-field-repair-of-linepipe-coating.html. [Accessed 18 March 2019].

[14] ISO, Petroleum and natural gas industries-External coatings for buried or submerged pipelines used in pipeline transportation systems-Part 3: Field joint coatings, 2008.

[15] PIPELINE INDUCTION HEAT, "INJECTION MOLDED POLYURETHANE (IMPU)," [Online]. Available: http://www.pipelineinductionheat.com/applications/injection-molded-polyurethane-impu. [Accessed 18 March 2019].

[16] PIPELINE INDUCTION HEAT, "POLYURETHANE FOAM INFILL," [Online]. Available: http://www.pipelineinductionheat.com/applications/polyurethane-foam-infill-puf. [Accessed 18 March 2019].

[17] Brunel University London, [Online]. Available: http://people.brunel.ac.uk/~eesrgat/research/pdf_phd/root02a.pdf. [Accessed 28 March 2019].

[18] Simulia, "Abaqus Analysis User's Guide," 2014. [Online]. Available: https://www.sharcnet.ca/Software/Abaqus/6.14.2/v6.14/books/usb/default.htm?startat=pt05ch22s05abm07.html. [Accessed 07 August 2019].

[19] C. Bedon, Numerical modelling of a structural adhesive, Trieste: University of Trieste, 2015.

[20] A. F. Bower, "Applied Mechanics of Solids," [Online]. Available: http://solidmechanics.org/Text/Chapter3_5/Chapter3_5.php. [Accessed 07 August 2019].

[21] Det Norske Veritas, "DNVGL-RP-F111," May 2017. [Online]. Available: https://www.dnvgl.com/oilgas/download/dnvgl-rp-f111-interference-between-trawl-gear-and-pipelines.html. [Accessed 09 August 2019].

[22] Wikipedia, "Abaqus," [Online]. Available: https://en.wikipedia.org/wiki/Abaqus. [Accessed 03 June 2019].

[23] B. Standard, Guide to methods for assessing the acceptability of flaws in metallic structures, BSI Standards Publication, 2013.

[24] ASTM D695-15, Standard Test Method for Compressive Properties of Rigid Plastics, American Society for Testing and Materials.

Francesca,

ti scrivo quello che penso di Mattia ed è un mio personale giudizio in base a quello che ho potuto constatare in questi mesi dal punto di vista caratteriale, comportamentale, operativo e dei risultati ottenuti.

Mattia è un ragazzo umile, educato, abituato a fare sacrifici e ad impegnarsi a pieno in quello che fa, entrava in ufficio alle 8:00 del mattino e usciva quasi sempre alle 20:00 di sera. Il modo con cui ha operato è strettamente legato al suo metodo di studio universitario, che spesso si è rivelato molto rigoroso, pignolo e finalizzato a voler capire in maniera approfondita quello che sta facendo, entrando spesso in dettagli, forse anche eccessivi per una tesi, che lo hanno portato a rallentare i tempi di stesura.

Dal punto di vista comportamentale, il suo modo di mostrare eccessiva fiducia in se stesso deriva probabilmente dalla predominante conoscenza teorica di base rispetto a quella pratica, ciononostante ho sempre notato una grande umiltà nel comprendere i suoi errori e nel cercare tenacemente la risposta giusta ai quesiti tecnici che gli sottoponevo.

Dal punto di vista operativo (analisi FEA) ho dovuto aiutarlo nella fase iniziale di introduzione al software ABAQUS di cui non aveva alcuna conoscenza. In poco tempo è riuscito a mettere a punto il modello dinamico e a risolvere i vari problemi di convergenza, considera che spesso questa fase richiede molto tempo (vedi Simulia che per JSP ha richiesto 2 mesi solo per calibrare il modello) anche per l'elevato numero di simulazioni che ha dovuto lanciare.

Dal punto di vista dei risultati, credo che il modello finale che ha impostato sia molto più efficiente e realistico di quello fatto sul progetto JSP, introducendo concetti più intuitivi di calibrazione del Solid PU con modello iperelastico. Attualmente grazie anche ai risultati della sua tesi abbiamo acquisito delle buone basi per affrontare in

modo più concreto il problema delle cricche sul solid PU visto che ormai sappiamo come caratterizzarlo (considerando che per noi questo era un materiale assolutamente sconosciuto).

Saluti.

Angelo